



**US Army Corps
of Engineers®**
Engineer Research and
Development Center

ERDC
INNOVATIVE SOLUTIONS
for a safer, better world

Interaction between Brash Ice and Boat Propulsion Systems

Kevin L. Haskins, Zoe R. Courville, Devinder Singh Sodhi,
Jesse M. Stanley, Leonard J. Zabilansky, and Jason M. Story

February 2014



The US Army Engineer Research and Development Center (ERDC) solves the nation's toughest engineering and environmental challenges. ERDC develops innovative solutions in civil and military engineering, geospatial sciences, water resources, and environmental sciences for the Army, the Department of Defense, civilian agencies, and our nation's public good. Find out more at www.erdclibrary.army.mil.

To search for other technical reports published by ERDC, visit the ERDC online library at <http://acwc.sdp.sirsi.net/client/default>.

Interaction between Brash Ice and Boat Propulsion Systems

Leonard J. Zabilansky, Devinder Singh Sodhi, Jesse M. Stanley,
and Zoe R. Courville

*Cold Regions Research and Engineering Laboratory
US Army Engineer Research and Development Center
72 Lyme Road
Hanover, NH 03755*

Kevin L. Haskins

*Geotechnical and Structural Laboratory
US Army Engineer Research and Development Center
3909 Halls Ferry Road
Vicksburg, MS 39180*

Jason M. Story

*US Coast Guard Research and Development Center
1 Chelsea Street
New London, CT 06320*

Final report

Approved for public release; distribution is unlimited.

Prepared for US Coast Guard Research and Development Center
New London, CT 06320

Under Project 6204, Arctic Craft Project

Monitored by Cold Regions Research and Engineering Laboratory
US Army Engineer Research and Development Center
72 Lyme Road, Hanover, NH 03755

Abstract

Increased interest and ship traffic in ice-covered Arctic waters necessitates the determination of the range of conditions in which current, small non-ice-hardened vessels can operate and the best operating procedures in ice-covered conditions. A series of tests in varying brash ice thickness conditions were conducted at a range of speeds in the CRREL test basin using a model craft with shrouded and open propellers as well as an intake pumping propulsion system. Results from the testing indicate that boats operating in brash ice fields should operate at slow speeds (9 kilometers per hour) to prevent increased strain on the outboard motors and possible damage to the propulsion system. Waterjet impellers appear to have greater protection from brash ice than an outboard propulsion system. It was thought that the shrouds would protect the propellers from ice impacts, which they may have done, but a secondary effect was that the brash ice caught inside the shroud area could not be forced away by the propellers as could be done in the open-propeller tests. This could mean that shrouds may still offer protection to the propellers but in a different configuration than the one tested.

DISCLAIMER: The contents of this report are not to be used for advertising, publication, or promotional purposes. Citation of trade names does not constitute an official endorsement or approval of the use of such commercial products. All product names and trademarks cited are the property of their respective owners. The findings of this report are not to be construed as an official Department of the Army position unless so designated by other authorized documents.

DESTROY THIS REPORT WHEN NO LONGER NEEDED. DO NOT RETURN IT TO THE ORIGINATOR.

Contents

Abstract	ii
Figures and Tables	iv
Preface	vi
Unit Conversion Factors	vii
1 Introduction	1
2 Background	2
3 Methodology	4
Overview	4
Boat Model	7
Propulsion systems	8
Test Setup.....	12
Test Matrix	12
Data Acquisition/Instrumentation.....	15
<i>Data Acquisition</i>	15
<i>Instrumentation</i>	15
<i>Video</i>	17
Ice conditions	18
4 Results	20
Open Outboard Propellers	24
Outboard Propellers with Shrouds	26
Waterjet Intake System	30
5 Conclusions and Recommendations	34
6 Future Research	37
References	38
Appendix A: Open-Propellers Plots	39
Appendix B: Shrouded-Propellers Plots	51
Appendix C: Waterjet Intake System Plots	68
Report Documentation Page	

Figures and Tables

Figures

Figure 1. Picture of front view of boat attached to carriage; right side of carriage is the instrumentation cabin.	5
Figure 2. Left picture–bumpers retracted; right picture–bumpers deployed.	5
Figure 3. Carriage pushers being used to break up ice sheet	6
Figure 4. Breaking up ice chunks to smaller pieces; yellow carriage also used to reconsolidate channel after a test run.	6
Figure 5. DTMB model boat #5631 used for testing.	7
Figure 6. US Coast Guard Response Boat-Small (RB-S II) (picture from USCG webpage).	8
Figure 7. US Coast Guard Response Boat-Medium (RB-M) (picture from USCG webpage).	8
Figure 8. DTMB-provided, scale-model outboard propulsion system (propeller and motor removed).	9
Figure 9. Plexiglas shroud that surrounds the outboard propeller.	10
Figure 10. Thrust comparison between outboard and waterjet intake system at a given propeller rotation.	11
Figure 11. Model's waterjet intake system.	12
Figure 12. Installed simplified induction system.	13
Figure 13. View of the boat model's stern with the waterjet intake system installed.	13
Figure 14. Boat connection to carriage.	14
Figure 15. Sensors mounted to the boat.	16
Figure 16. Encoder locations for outboard (left) and waterjet intake system (right) tests.	16
Figure 17. Location of underwater camera fixture and a screen shot from video.	17
Figure 18. Above-water camera locations for waterjet intake system tests.	18
Figure 19. Brash ice fragment used during testing.	19
Figure 20. Modified yard stick used to measure brash ice field thickness.	19
Figure 21. Plots of carriage speed and position (top 0.8 ms^{-1} , middle 1.3 ms^{-1} , bottom 1.8 ms^{-1}).	20
Figure 22. Carriage speed of 0.8 ms^{-1} speed in open water with shrouded propeller.	21
Figure 23. Open propellers in 102 mm of ice at carriage speed of 0.8 ms^{-1}	22
Figure 24. Grams software output for open propellers in 102 mm of ice at carriage speed of 0.8 ms^{-1}	23
Figure 25. Plot of force data in open water, motors not spinning, and a carriage speed of 1.8 ms^{-1}	24
Figure 26. Plot of average current for open, outboard propellers.	25
Figure 27. Plot of standard deviation for open, outboard propeller current.	26
Figure 28. Plot of the number of impacts on open propellers at various carriage speeds.	27
Figure 29. Plot of mean area under a spike at various carriage speeds.	27
Figure 30. Plot of average current for open, outboard propellers.	28

Figure 31. Plot of standard deviation for open, outboard propeller current.	29
Figure 32. Plot of the number impacts on propellers at various carriage speeds.	29
Figure 33. Plot of mean area under a spike at various carriage speeds.	30
Figure 34. Plot of average current for waterjet intake system.	31
Figure 35. Plot of standard deviation for waterjet intake system current.	32
Figure 36. Plot of the number impacts on propellers at various carriage speeds.	32
Figure 37. Plot of mean area under a spike at various carriage speeds.	33
Figure 38. Ramping up of motor current that may be caused either by a trapped piece of brash ice or the propellers milling an ice piece.	34
Figure 39. Possible revised shroud.....	35

Tables

Table 1. Outboard test matrix.	14
Table 2. Outboards-with-shrouds test matrix.....	14
Table 3. Waterjet intake system test matrix.....	14
Table 4. Open outboard propellers average current and standard deviation.....	25
Table 5. Shrouded outboard propellers' average current and standard deviation.	28
Table 6. Waterjet intake system average current and standard deviation.....	31

Preface

This study was conducted for the US Coast Guard Research and Development Center under the Arctic Craft Project Number 6204. Jason Story served as the technical monitor. For his contribution, appreciation is expressed to Andrew Krauss of the Navy's Carderock Division, Naval Surface Warfare Center in West Bethesda, Maryland.

The Engineering Resources Branch (RV-E) of the US Army Engineer Research and Development Center, Cold Regions Research and Engineer Laboratory (ERDC-CRREL) performed the work. At the time of publication, Jared Oren was Chief, CEERD-RV-E. The Deputy Director of ERDC-CRREL was Dr. Lance Hansen, and the Director was Dr. Robert Davis.

COL Jeffrey J. Eckstein was the Commander of ERDC, and Dr. Jeffery P. Holland was the Director.

Unit Conversion Factors

Multiply	By	To Obtain
cubic feet	0.02831685	cubic meters
cubic inches	1.6387064 E-05	cubic meters
cubic yards	0.7645549	cubic meters
degrees Fahrenheit	$(F-32)/1.8$	degrees Celsius
feet	0.3048	meters
foot-pounds force	1.355818	joules
gallons (US liquid)	3.785412 E-03	cubic meters
inches	0.0254	meters
knots	0.5144444	meters per second
miles (nautical)	1,852	meters
miles (US statute)	1,609.347	meters
miles per hour	0.44704	meters per second
pounds (force)	4.448222	newtons
pounds (force) per square foot	47.88026	pascals
pounds (force) per square inch	6.894757	kilopascals
quarts (US liquid)	9.463529 E-04	cubic meters
square feet	0.09290304	square meters
square inches	6.4516 E-04	square meters
square miles	2.589998 E+06	square meters
square yards	0.8361274	square meters
yards	0.9144	meters

1 Introduction

The recent historically unprecedented retreat of the Arctic ice cap has resulted in a surge of interest in using Arctic waters for direct shipping routes, military operations, mineral exploration and extraction, and tourism opportunities. With increased vessel traffic and active mineral extraction in the Arctic, the possibility of a major disaster occurring is dramatically increased. At the same time, the current availability of US Coast Guard (USCG) assets capable of operating in the harsh, ice-covered waters of the Arctic is low, according to the US Coast Guard Arctic Strategic Approach (COMDTINST 16003.1 of 26 April 2011).

In order to be able to respond rapidly to emergency situations in the waters north of the Alaskan coast, the USCG plans to operate small vessels that are not designed to break ice but may be capable of operating in the presence of brash ice. The Arctic presents a unique challenge to USCG operations with cold temperatures, a range of ice conditions, and a lack of infrastructure to support small-craft operations.

To develop future craft capable of operating in the Arctic, it is important to determine the range of operating conditions for current craft, especially the small craft generally employed by the USCG, as well as the performance of possible modifications to current craft. The research presented here examines the range of speed and brash ice conditions (i.e., thickness) in which a conventional, propeller-driven small craft can operate effectively, as well as tests the efficacy of an outboard propeller shroud and waterjet intake system to reduce the amount of ice impacts under those conditions. Shrouds are currently used in industry to improve efficiency and protect outboard propeller systems in shallow water. Since they offer protection to the propellers, a series of tests was conducted to determine if a simple shroud design could protect the propellers of the model from ice impacts.

2 Background

Ice conditions in the Arctic present one of the most challenging impediments to operations. Ice thicknesses and properties (e.g., hardness) vary temporally and spatially with changing meteorological conditions and underlying bed topography and sea states. Of particular interest is brash ice, which represents an accumulation of floating ice comprised of small ice fragments approximately 2 meters (m) or smaller in diameter. Brash ice is formed from the wreckage of other forms of ice and is commonly encountered in coastal regions, in regions where pressure ridges have collapsed, or between two colliding floes. The brash ice can consist of a variety of different ice forms including frazil ice (grown during freeze-up), floe ice, or pack ice.

One of the most important factors in the operation of small craft in ice-covered waters is propeller-to-ice interaction. The impact of ice on propellers not only threatens the integrity of the propulsion system but also decreases efficiency as higher torque is needed to produce the required thrust (Riska 2011). The interaction is complex due to high strain rates caused by high propeller blade tip velocities, the complexity of the flow around the propeller, and the randomness of the ice pieces that impact the propeller (Wang et al. 2007). Operation of small craft in ice-covered waters has been studied experimentally through model-scale and full-scale tests as well as computer modeling (Re and Veitch 2007; Sampson et al. 2009). Research on the interaction of ice with propellers has historically concentrated on contact loads between propeller blades and ice. Ducts, shrouds, or nozzles are used on open-water tugs and Arctic supply vessels and offer protection for propeller blades. The potential for clogging with such adaptations does exist in thick and deformed ice conditions such as encountered in rafted or ridged ice. The use of a shroud-protected propeller has been investigated and shown to minimize the impact of large pieces of ice on the propellers but can also lead to prolonged non-contact loads from cavitation (Laskow 1988; Walker et al. 1997).

The use of waterjets in ice-covered waters shows promise but has not been thoroughly researched. Waterjet intake systems (impellers) are usually well protected and draw water from below the ship's hull, which helps reduce impacts by ice pieces at the surface. Grates on the waterjet intake

keep large pieces of impeller-damaging ice out of the waterjet intake tunnel. Waterjets are currently being operated in the Arctic successfully.

To develop future craft capable of operating in the Arctic, it is important to determine the range of conditions current craft, especially the small craft generally employed by the USCG, can operate in as well as the performance of possible modifications to current craft. The research presented here examines the range of speed and brash ice conditions (i.e., thickness) in which a conventional, propeller-driven small craft can operate effectively as well as tests the use of shrouds and waterjets in a range of speeds and ice conditions.

3 Methodology

Overview

The scale model testing was conducted at the Ice Engineering Facility located within the CRREL laboratory. The tests were conducted in the test basin, which is a refrigerated room with a sunken basin that is 42.7 m long, 9.1 m wide and 2.4 m deep. The room temperature can be chilled to -29 °C. This room was primarily built to conduct model testing of ships and structures in various ice conditions. A rail and carriage system spans the width of the tank and is used to either push ice against structures or pull models through the length of the basin. There is an attached prep-tank that can be isolated from the main basin area. The temperature in this area can be maintained above freezing so that models can be attached to the carriage prior to testing. The carriage uses a computer-controlled drive system that allows the researcher means to control the velocity as the carriage travels the length of the track. The initial ramp-up time, travel speed, and deceleration rate are controlled from the carriage computer. The current maximum speed of the carriage is 1.8 ms⁻¹. A control cabin is mounted on the carriage where the carriage controls are maintained. The cabin is heated and allows space for the data acquisition equipment to reside. The carriage with its control cabin is shown in Figure 1.

The testing required three different scaled thicknesses of brash ice to be evaluated against each propulsion system. The depth of the brash ice tested was 102, 127, and 152 millimeters (mm). Typically, a 102 mm thick ice sheet requires 72 hr to freeze, and thicker ice requires an exponential increase in time to grow. To reduce the number of ice sheets that would have to be grown, a timber bumper system was placed along both sides of the test basin. This system allowed the 102 mm thick brash ice field to be consolidated to a 127 and 152 mm thick brash ice by reducing its width. This was accomplished by moving the timber bumpers away from the wall. Pictures of the bumpers retracted and deployed are shown in Figure 2.

The test basin was filled with 946,353 liters (L) of saline water (10 parts per million (ppm)). The saline solution was cooled to freezing point using the combination of sub-freezing air temperature and air bubbler on the floor of the tank to prevent thermal stratification of the water. To grow the ice sheet, the room temperature was brought to -12 °C. A fine mist of fresh water was

Figure 1. Picture of front view of boat attached to carriage; right side of carriage is the instrumentation cabin.



Figure 2. Left picture–bumpers retracted; right picture–bumpers deployed.



sprayed over the saline water to *seed* an ice sheet. This freshwater crystal served as a nucleating particle for the ice crystal and subsequently the formation of uniform ice sheet of small grain size. Immediately after seeding the ice sheet, the room temperature was dropped to $-23\text{ }^{\circ}\text{C}$. The room temperature was maintained at $-23\text{ }^{\circ}\text{C}$ for a pre-calculated number of hours. For a 102 mm ice sheet, this requires 2–3 days. Because the propulsion systems were being tested in brash ice having low strength, the room temperature was increased to $2\text{ }^{\circ}\text{C}$ after growing the ice sheet to the required thickness. Additionally, the test basin's perimeter heat was turned on to melt the edge of the ice sheet from the concrete wall. Approximately one day was allowed to temper the ice sheet to the required strength. To create the brash ice field, the sheet was broken up using the ice pushers on the front of the carriage (Figure 3). Any remaining large pieces were then broken up manually (Figure 4) so that no pieces in the main channel were

greater than 152 mm × 152 mm × 102 mm. Prior to any subsequent test, the ice was manually redistributed for the nominal brush thickness, particularly along the centerline of the tank.

Figure 3. Carriage pushers being used to break up ice sheet



Figure 4. Breaking up ice chunks to smaller pieces; yellow carriage also used to reconsolidate channel after a test run.



Boat Model

The boat used for all of the tests came from the Navy's David Taylor Model Basin (DTMB) within the Carderock Division of the Naval Surface Warfare Center. The model's length was 3 m with a beam of 0.68 m (Figure 5). The 5631 hull from Carderock was originally used in resistance experiments to evaluate a systematic series of models based on the USCG 14 m Motor Lifeboat (MLB) hull design (Metcalf et al. 2005).

Figure 5. DTMB model boat #5631 used for testing.



The 5631 hull is not a scale model of any existing Coast Guard craft. It was modified in a number of ways from the MLB hull form including a 20-degree deadrise at the transom and a re-faired hull bottom. For these tests, hull 5631 would be outfitted with propulsion system configurations similar to existing Coast Guard boats. The outboard propulsion system configuration for shrouded and open propellers tests is comparable to active duty Coast Guard vessels like the Response Boat–Small II (RB-S II). The RB-S II is a multi-mission boat typically used for search and rescue and law enforcement activities. This boat (Figure 6) is 8.7 m long with a beam of 2.6 m. Two 250 horsepower (hp), 4-stroke outboard engines are used to power the full-scale boat. Froude Scaling was used for comparing geometric similarity of the scaled model. The scale for the model boat compared to the RB-S II is 0.35 in length only (not in beam).

A comparable active duty Coast Guard vessel that uses a waterjet propulsion system is the Response Boat Medium (RB-M). The RB-M (Figure 7) is a 13.7 m-long, 2.6 m-beam boat. This boat is propelled by two Rolls Royce FF 375s waterjets, each connected to an MTU Detroit Diesel 825 hp engine. For comparison, the scale for the model compared to the RB-M is 0.22 in length (not in beam).

Figure 6. US Coast Guard Response Boat-Small (RB-S II) (picture from USCG webpage).



Figure 7. US Coast Guard Response Boat-Medium (RB-M) (picture from USCG webpage).



Propulsion systems

The DTMB model boat came equipped with two scale-model outboard engine lower units mounted to the stern of the boat. The model outboard system is shown in Figure 8 with the propeller and motors not installed. These outboards represented $\frac{1}{4}$ -scale, Yamaha 250 hp engines. The motors that drive the outboard propellers are computer controlled. The motor to the propeller shaft had a 2:1 gear ratio through a belt-and-pulley

system. A revolution rate of 6,000 degrees per second (deg/sec) for the motor was selected for all tests. This would equate to a 12,000 deg/sec for the propeller or 2,000 revolutions per minute (rpm) (scale). Also, each propeller can be individually controlled and rotated in the correct direction for the use of right-handed or left-handed propellers.

Figure 8. DTMB-provided, scale-model outboard propulsion system (propeller and motor removed).



During pre-experiment testing, several different revolution rates were investigated: 1000, 2000, 3000, 4000, and 6000 deg/sec. During the original DTMB testing, a rate of 4,000 deg/sec was used, which matched thrust-to-drag resistance, but with a Carderock representative on site, it was agreed to use the greater 6000 deg/sec for this testing to generate the greatest amount of thrust in the ice field without causing harm to the motors and drive system. It was decided that more thrust would be needed to overcome the ice loads on the boat than what was originally seen in the open-water tests conducted at DTMB.

The outboard propulsion tests were conducted in two ways: open and shrouded propellers. Shrouded propellers are used in industry (depending on vessel use) to improve thrust and to protect the propellers. This series of testing was performed to see if shrouds could protect the propellers from ice impacts. For the model testing, a simple, clear Plexiglas shroud (Figure 9) was built to be installed around each of the outboards' propellers. Clear Plexiglas was used so underwater cameras could better capture the ice/shroud/propeller interaction during testing. The use of cameras provided a viewpoint to observe the interaction of the ice and the shroud regarding whether the shrouds were actually protecting the propellers or if ice would become trapped at the entrance of the shroud area.

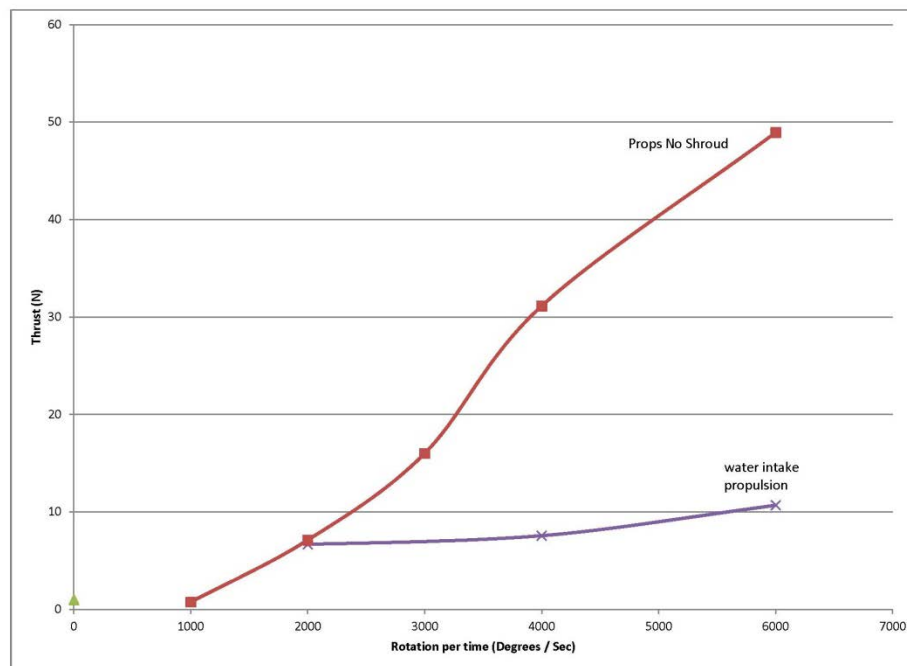
Figure 9. Plexiglas shroud that surrounds the outboard propeller.



It was decided early on that the flow and thrust mechanics of a full scale waterjet would be difficult to scale down. Due to the complexity of construction, proprietary design, and difficulty of correctly achieving accurate flow characteristic at the model scale, a simplistic approach was taken for the model waterjet intake system. It was decided that the goal of the waterjet testing would be to approximate the waterjet intake and develop a flow through it to see if the waterjet was ingesting any ice. The ingestion of ice into the water intake tunnel is a function of the flow of ice and water along the vessel's hull. The model testing would show, visually and by the motor current draw, if ice were being ingested. This would not provide any insight whether a real world waterjet intake system draws ice into the intake tunnel. For these reasons, a clear Plexiglas box was created that housed the propeller and shaft. The clear box allowed for easy viewing and video recording during the tests and visual indication if the water-intake opening or tunnel became clogged with ice. The same motors and drive set up was

used so that the current draw on the motor was recorded. Using this simplified intake system, these tests could not be compared to either the shrouded or open-propeller tests because there was very little thrust developed. The thrust forces using the propeller housed in the waterjet intake system was shown to be five times lower than the thrust developed by the outboard propulsion system. A graph of thrust versus motor revolutions per sec for the two propulsion systems is shown in Figure 10.

Figure 10. Thrust comparison between outboard and waterjet intake system at a given propeller rotation.



The model's waterjet intake system is shown in Figure 11. It was decided that the square corners would be adequate for the test and that rounding the corners would not improve the system enough for the loss of visibility through the Plexiglas. It also made it easier to build the system and seal it from water intrusion to the boat. The propulsion propeller was mounted mid-way between the end of the cut in the bottom of the boat and the stern (approximately 76.2 mm from the stern). The propeller was installed on a shaft that exited the tapered front face of the Plexiglas box and connected to drive gear. The same motors and gears used in the scale model outboard propulsion system were used in the waterjet intake system. The motors were mounted in a horizontal position, and a longer belt (twice the length of the ones used in the outboard setup) drove the propellers.

Figure 11. Model's waterjet intake system.

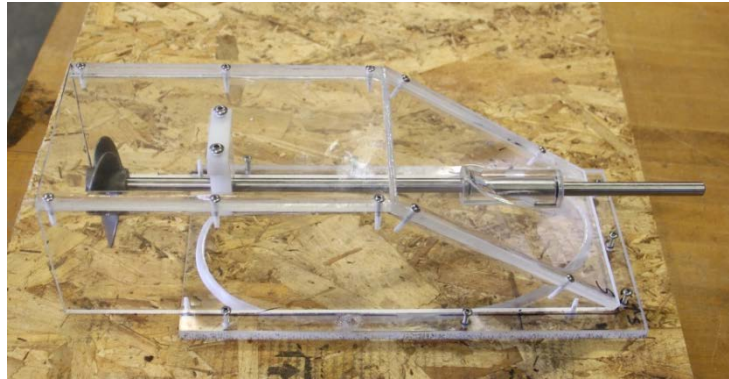


Figure 12 shows a plan view of the motors, gears, and the Plexiglas intake. Figure 13 shows the stern of the boat of the completed system. The same motor rotation of 6,000 deg/sec was used during the waterjet intake system tests.

Test Setup

The boat model for all tests was attached to the carriage in the same manner. An aluminum bracket was clamped to the structural support beam of the blue carriage frame. A six-axis load cell was bolted to the bracket. A mounting plate was then placed between the linear bearing and the load cell. The vertical post of the linear bearing was attached to the gimbal tow post. The gimbal system was pre-installed in the model from DTMB. The connection of the model to the carriage is shown in Figure 14.

Test Matrix

For each of the three propulsion systems (outboard, outboard with shroud, and waterjet intake), there were three test runs at speeds of 1.8, 1.3, and 0.8 ms^{-1} . Additionally, three different thickness of brash ice field were used (102, 127, and 152 mm).

The test matrices follow (Tables 1, 2, and 3).

Figure 12. Installed simplified induction system.



Figure 13. View of the boat model's stern with the waterjet intake system installed.



Figure 14. Boat connection to carriage.

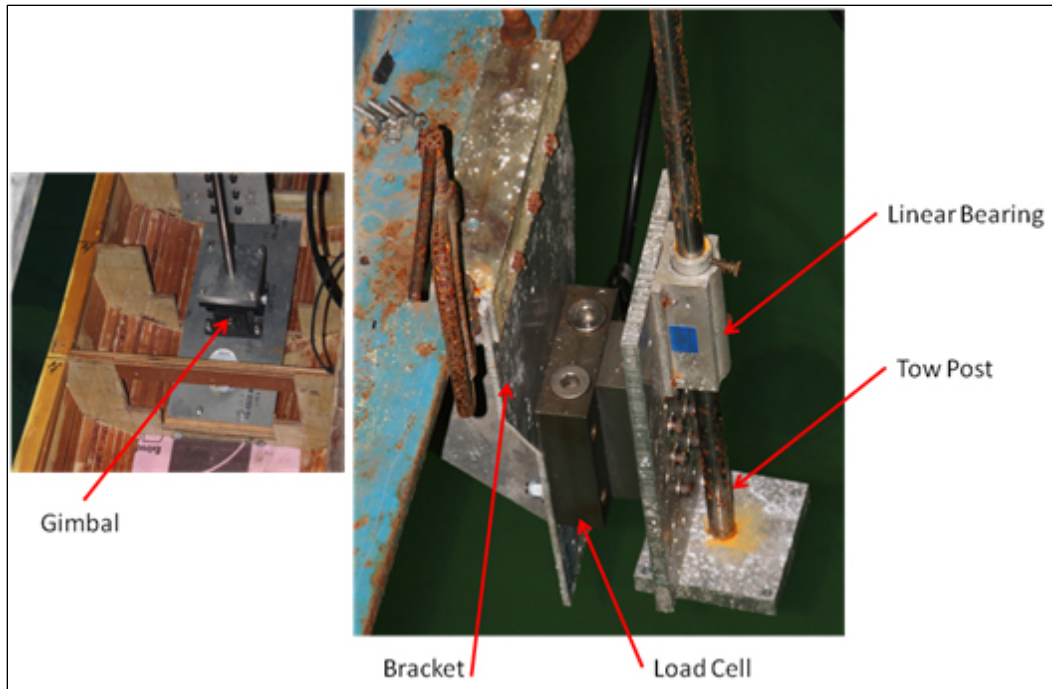


Table 1. Outboard test matrix.

Scale Factor = 0.35 (2.85)	Thickness of Brash Ice (full-scale/model)		
	290 mm/ 102 mm	363 mm/ 127 mm	434 mm/ 152 mm
2.3 ms ⁻¹ (0.8 ms ⁻¹)	x	x	x
3.7 ms ⁻¹ (1.3 ms ⁻¹)	x	x	x
6.6 ms ⁻¹ (1.8 ms ⁻¹)	x	x	x

Table 2. Outboards-with-shrouds test matrix.

Scale Factor = 0.35 (2.85)	Thickness of Brash Ice (full-scale/model)		
	290 mm/ 102 mm	363 mm/ 127 mm	434 mm/ 152 mm
2.3 ms ⁻¹ (0.8 ms ⁻¹)	x	x	x
3.7 ms ⁻¹ (1.3 ms ⁻¹)	x	x	x
6.6 ms ⁻¹ (1.8 ms ⁻¹)	x	x	x

Table 3. Waterjet intake system test matrix.

Scale Factor = 0.22 (4.55)	Thickness of Brash Ice (full-scale/model)		
	464 mm/ 102 mm	578 mm/ 127 mm	692 mm/ 152 mm
3.6 ms ⁻¹ (0.8 ms ⁻¹)	x	x	x
5.9 ms ⁻¹ (1.3 ms ⁻¹)	x	x	x
8.2 ms ⁻¹ (1.8 ms ⁻¹)	x	x	x

Data Acquisition/Instrumentation

Data Acquisition

An Astro-Med Inc. TMX portable Data recorder was used to capture all the data during the tests. This system provides a color display allowing for real-time viewing and data playback. The sampling frequency was 5,000 samples/sec. A low-pass, 500 Hz Butterworth filter was used by the TMX system during acquisition.

Instrumentation

The forces and the response of the scale model boat were collected using several sensors.

Heave was measured using an L-Gage Laser gauging sensor that had a range of 75 to 125 mm. The laser was positioned over the top of the vertical tow post. The laser beam was centered over the rod.

Horizontal force was measured using an Advanced Mechanical Technology Inc. (AMTI) underwater MC37 transducer. The range for loads in F_x , F_y , and F_z was 1,112 N; the range for moment in M_y and M_z was 85 N-M and M_x of 42 N-M. Only the horizontal force was recorded for these tests. The load cell was mounted between the linear bearing and the carriage mounting bracket. Positive force (F_x) is recorded as a load pushing on the bow of the boat towards the stern.

Pitch and roll of the boat was measured using a Measurement Specialties D-Series $\pm 30^\circ$ inclinometer. The inclinometer was secured to the aluminum plate directly in front of the gimbal. Positive pitch is recorded as bow up and negative pitch as stern up. Positive roll is with the starboard side of the boat up and negative as the port side up. The yaw rotation of the boat was limited so that the boat would track correctly down the centerline of the tank. Figure 15 shows locations of these three sensors.

An encoder was attached to each of the final drive shafts (one for each propeller), and they recorded the rotational position from 0 to 360 deg. The location of encoders used for outboard and waterjet intake system tests is shown in Figure 16.

Figure 15. Sensors mounted to the boat.

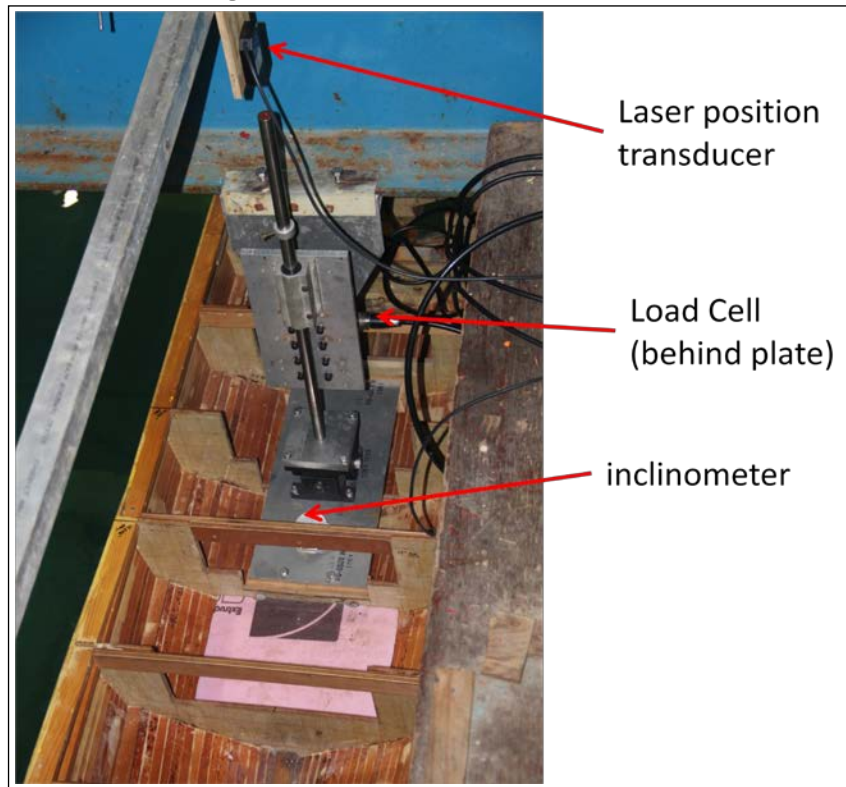
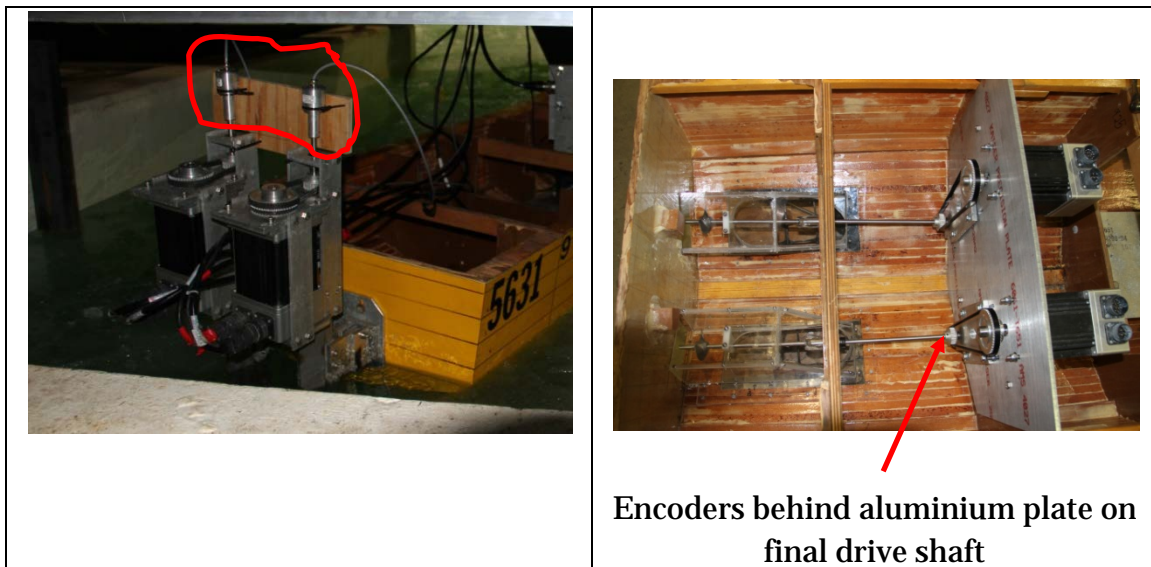


Figure 16. Encoder locations for outboard (left) and waterjet intake system (right) tests.



An Aerotech Soloist CP20 programmable drive amplifier paired with BM800E motors was used to drive the propulsion systems. The current was directly recorded by the data acquisition system as output by the amplifier in near real time. Positive current was recorded as the propeller spun counter clockwise. For the outboard tests, the port motor was spun

counterclockwise and the starboard motor clockwise. This was done because a right-hand and a left-hand propeller were installed to mimic the set up on the full-scale boat. For the water-intake propulsion system tests, two identical propellers were used and spun counterclockwise. The use of right-handed or left-handed propellers was not needed for the waterjet intake system because they were enclosed in the Plexiglas box.

Video

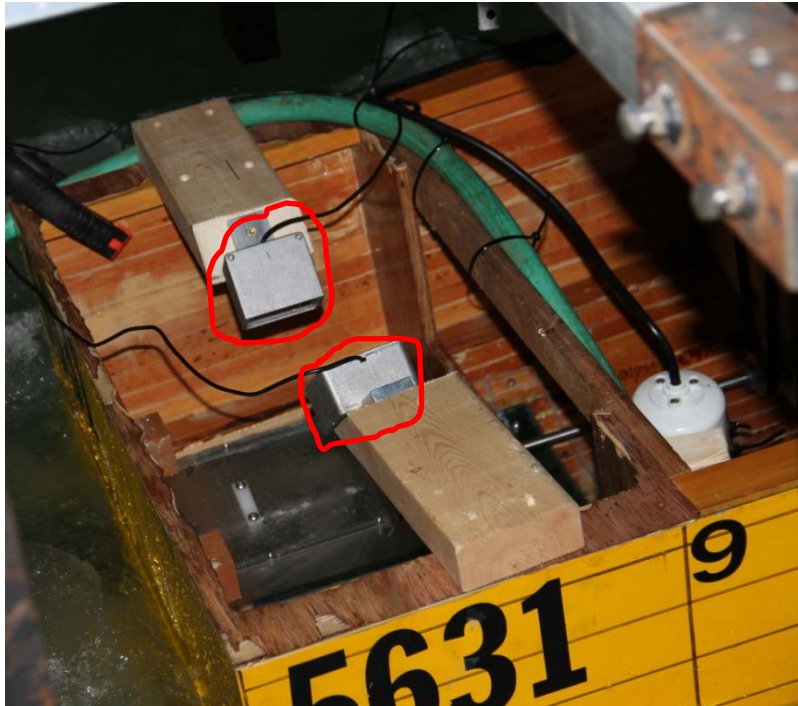
Underwater streaming video was taken using a Go-Pro camera encased in a waterproof fixture attached to the carriage. This video was recorded for all propulsion tests but was only useful for the outboard propulsion. Because the waterjet intake system was interior to the boat, no useful information could be gained. Location of the underwater camera is shown in Figure 17.

Figure 17. Location of underwater camera fixture and a screen shot from video.



Above-water video was taken only during the waterjet intake system tests. The clear Plexiglas water intake tunnel allowed for better viewing above water. A commercial off-the-shelf computer web camera encased in a water-resistant case was used to capture the video. Cameras were focused on the respective port and starboard water intake tunnels (Figure 18).

Figure 18. Above-water camera locations for waterjet intake system tests.



Ice conditions

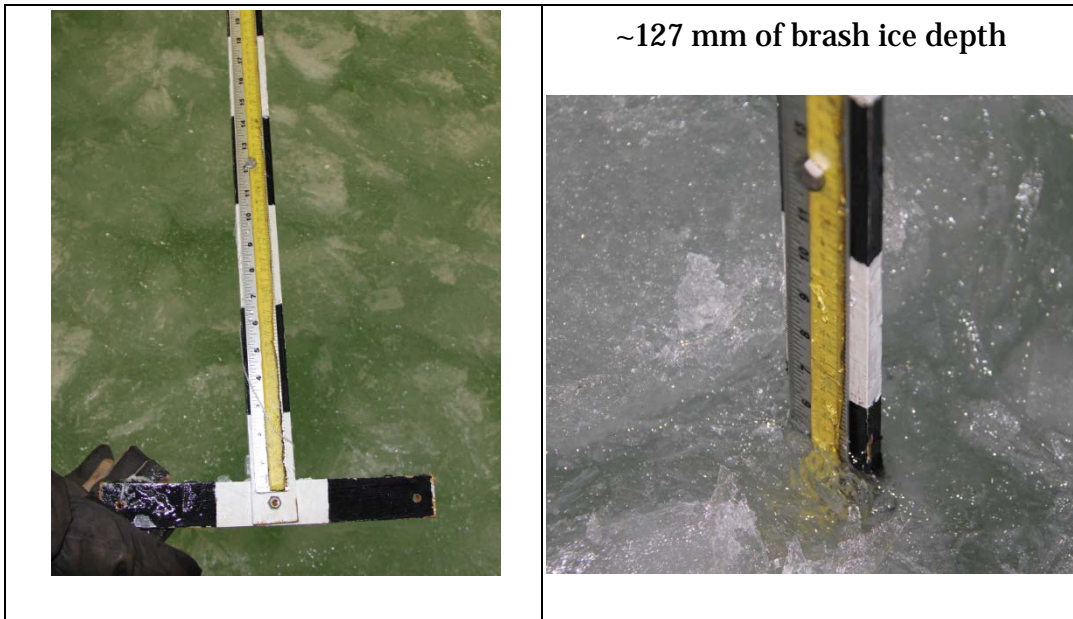
The test ice sheet is grown from saltwater using a methodology developed at CRREL by Hirayama (1983) for urea-doped water. The ice is grown in the test basin on the surface of an aqueous solution of water with a sub-freezing ambient temperature. The air temperature uniformity ensures that the resulting grown ice sheet has uniform thickness and mechanical properties. When the water temperature approaches the freezing temperature of the solution, the submerged bubblers used for mixing are stopped to allow the water to become calm. The ice sheet is then seeded with a mist of fine water spray at a temperature of approximately $-10\text{ }^{\circ}\text{C}$. The crystal sizes of the ice grown in this manner are approximately 2 mm at the top of the ice sheet and increase with depth, generally doubling in size for a typical ice-sheet thickness. The resulting ice sheet is then tempered by increasing the ambient room temperature above freezing for a prescribed time in order to obtain the desired ice-sheet strength. A picture of a brash ice fragment is shown in Figure 19.

The thickness of the brash ice was measured using the T scale pictured in Figure 20. The T scale was inserted below the ice, positioned at 90° , and gently pulled upward to contact the bottom of the rubble ice, noting the depth on the yellow scale.

Figure 19. Brash ice fragment used during testing.



Figure 20. Modified yard stick used to measure brash ice field thickness.

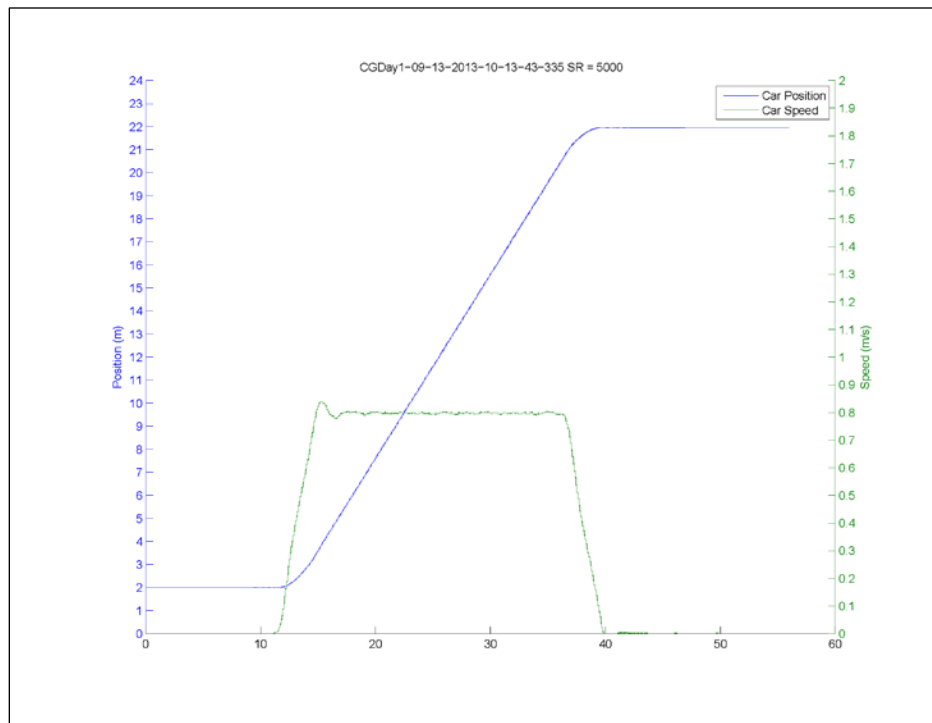


4 Results

The main focus of the testing was to determine the interaction of brash ice on propulsion systems. The different propulsion systems were tested at different carriage speeds and different brash ice field thicknesses. During each test, the rotation of the final drive, current draw by the motors, horizontal force, heave, pitch, roll, carriage speed, carriage position, and time were recorded.

Typical plots for different carriage speeds and positions are shown in Figure 21. For each test, the carriage start position was at the test basin's 2 m mark. The carriage moved a total distance of 20 m for each test and stopped at the test basin's 22 m mark. Because of the time required for the carriage to accelerate and decelerate (held constant across each test), the total time the model spent at the desired speed was reduced for increased model run speeds. All carriage speed plots can be found in Appendix A.

Figure 21. Plots of carriage speed and position (top 0.8 ms⁻¹, middle 1.3 ms⁻¹, bottom 1.8 ms⁻¹).



One piece of data thought to be important, with respect to propulsion system, was the change in motor current draw. It was expected that the current data would change when ice impacted or restricted flow of water to the propellers. The feed-back controllers for propeller motors maintain a specified rotational speed, and a change in current demonstrates a change of load on the motor to maintain that rotational speed. The baseline for the current profile at a particular speed is, therefore, the test run in open water at that speed. Figure 22 shows the open-water current profiles for a carriage speed of 0.8 ms^{-1} . Figure 23 shows the carriage being run at the same speed in a 102 mm brash ice field.

The spikes in the current data are an indication of the ice interaction with the propellers. All current plots can be found in Appendix A. To quantify the change in current due to ice and carriage speed, the average current and standard deviation were determined. This was calculated only for each test run from basin position marker 8 m to 18 m. The reason for this is that between the 8 m and 18 m locations, a constant velocity of the carriage was achieved for all tests.

Figure 22. Carriage speed of 0.8 ms^{-1} speed in open water with shrouded propeller.

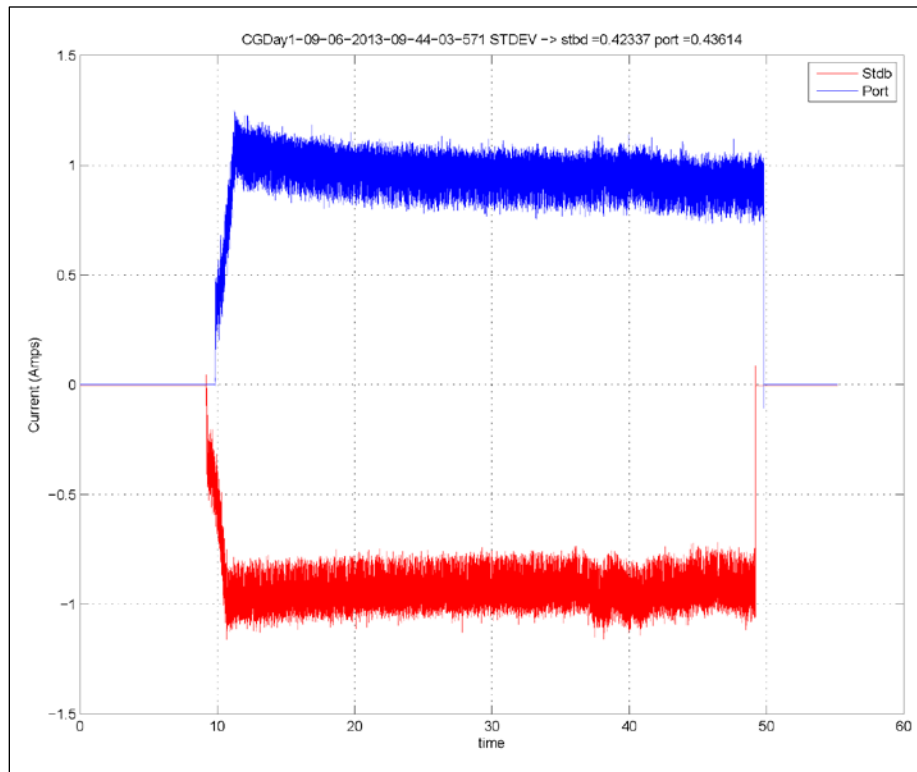
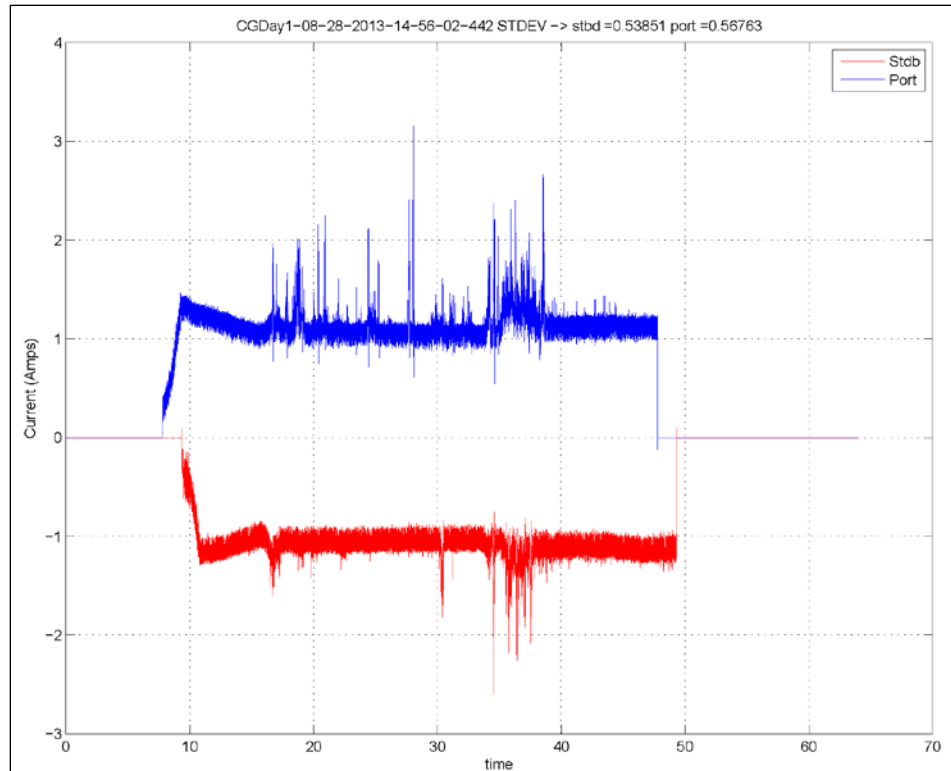


Figure 23. Open propellers in 102 mm of ice at carriage speed of 0.8 ms⁻¹.



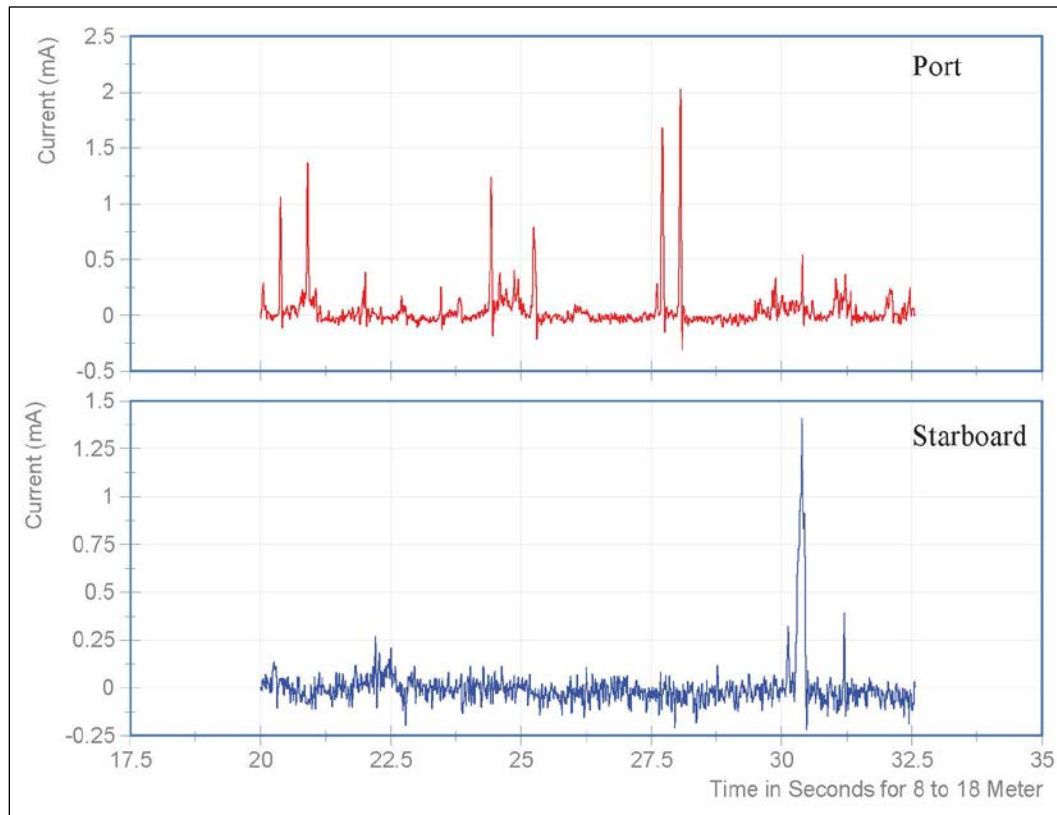
Additional post processing (using Matlab scripts) was performed on the current data. Current data was then uploaded into Grams/AI spectroscopy software (Thermo Electron Corp., v8.0) for post processing. Each current trace (for port and starboard motors) was baseline corrected, zeroed, and then Fourier smoothed.

Individual data traces were Fourier-transformed filtered and then reverse Fourier-transformed with the cut-off point for the filter set at 98%, which was found to provide optimum results. The smoothing process produced a trace from which individual peaks could be identified. Individual peaks were identified by noise-level edge detection (peak edges detected at the local minimum on either side of the peak) and retained if they met a minimum peak-height threshold (0.06) and area (0.0025). Values are expressed in terms of the y-axis units.

For the evaluation, the number of peaks identified was taken as the number of ice propeller interactions that occurred in a given run, peak height as the intensity of each interaction, and peak width as the duration of each interaction. For example, a sharp peak (narrow width) would represent a piece of ice quickly bouncing off the propeller, with the height of the peak indicating

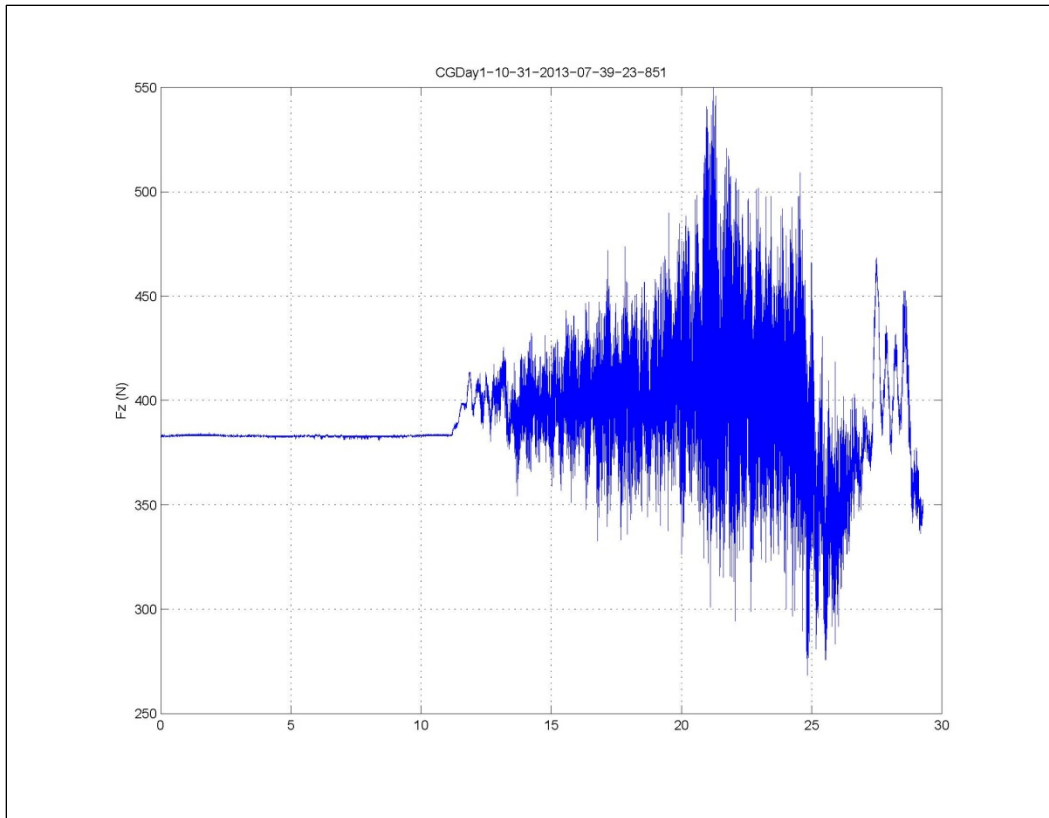
the intensity of the impact, presumably related to ice size (thickness). In contrast, a shallow, broad peak would represent an ice impact where the ice stayed in contact with the propeller for a longer time, possibly indicating multiple propeller blade impacts on the same ice block or series of ice blocks. An example plot of the output for the Grams software is shown in Figure 24.

Figure 24. Grams software output for open propellers in 102 mm of ice at carriage speed of 0.8 ms^{-1} .



The force data collected during the testing were found to be erroneous. The force data as shown in Figure 25 represent a typical force-versus-time plot that was recorded. The force would start out a very large value and then oscillate back and forth with an increasing band. This was unexpected and was even produced during open-water testing. It was anticipated that an increasing load would occur from start and would eventually stabilize during the tests. It is assumed that either the load cell used was faulty or there were some unknown, larger outside oscillating forces occurring.

Figure 25. Plot of force data in open water, motors not spinning, and a carriage speed of 1.8 ms^{-1} .



Also found during post processing, the laser used for heave measurement was inadequate for the ice-impact tests. In most tests the heave values were out of range. The laser selected had a range of $\pm 52 \text{ mm}$, which would have been more than adequate for open-water testing. It was expected that the model would push through the ice and not ride up onto the ice, which appears to be the case and the reason the laser range was inadequate.

During the tests, pitch and roll of the model boat were recorded. These data were not presented in the report because they did not provide information on the overall goal of the report to determine the interaction of brash ice on the propulsion system.

Open Outboard Propellers

Table 4 lists the average and the standard deviation of current data for three ice thicknesses and three carriage speeds. The data on current for port and starboard motors for each test are their own respective line because the starboard is spun in the clockwise (negative) direction as the port motor is spun in the counterclockwise (positive) direction. Computation of the

average and the standard deviation is done between positions 8 m and 18 m. The data for 152 mm ice field for carriage speeds of 0.8 m s⁻¹ and 1.3 m s⁻¹ were not useable and are not included in the tables.

Table 4. Open outboard propellers average current and standard deviation.

Ice Thickness	Carriage Speed	TestName-Feature	Avg	STDV
102 mm	0.8 ms ⁻¹	CGDay1-08-28-2013-14-56-02-442 Current_Port	1.1	0.14
	0.8 ms ⁻¹	CGDay1-08-28-2013-14-56-02-442 Current_Starboard	-1.07	0.07
	1.3 ms ⁻¹	CGDay1-08-28-2013-15-05-18-376 Current_Port	1.06	0.17
	1.3 ms ⁻¹	CGDay1-08-28-2013-15-05-18-376 Current_Starboard	-1.01	0.15
	1.8 ms ⁻¹	CGDay1-08-28-2013-15-14-35-439 Current_Port	1.11	0.34
	1.8 ms ⁻¹	CGDay1-08-28-2013-15-14-35-439 Current_Starboard	-1.02	0.31
127 mm	0.8 ms ⁻¹	CGDay1-08-28-2013-10-48-07-410 Current_Port	1.13	0.18
	0.8 ms ⁻¹	CGDay1-08-28-2013-10-48-07-410 Current_Starboard	-1.08	0.11
	1.3 ms ⁻¹	CGDAY1-08-28-2013-10-36-43-610 Current_Port	1.18	0.28
	1.3 ms ⁻¹	CGDAY1-08-28-2013-10-36-43-610 Current_Starboard	-1.07	0.23
	1.8 ms ⁻¹	CGDAY1-08-28-2013-10-25-37-393 Current_Port	1.21	0.35
	1.8 ms ⁻¹	CGDAY1-08-28-2013-10-25-37-393 Current_Starboard	-1.21	0.39
152 mm	1.8 ms ⁻¹	CGDAY1-08-28-2013-08-46-20-195 Current_Port	1.78	0.59
	1.8 ms ⁻¹	CGDAY1-08-28-2013-08-46-20-195 Current_Starboard	-1.59	0.72

Figure 26 plots the average current shown in Table 4. Figure 27 plots the standard deviation.

Figure 26. Plot of average current for open, outboard propellers.

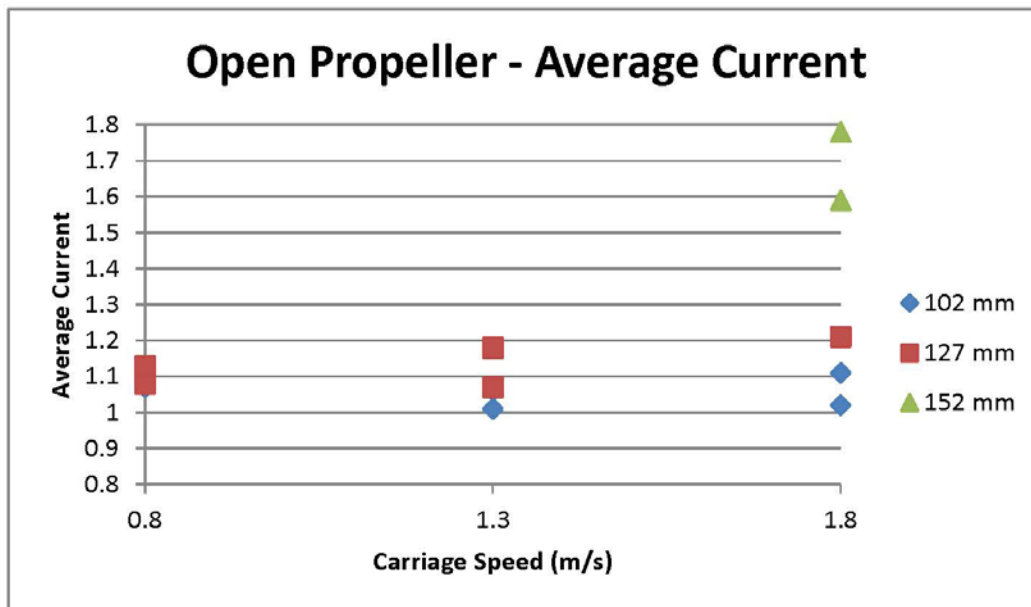
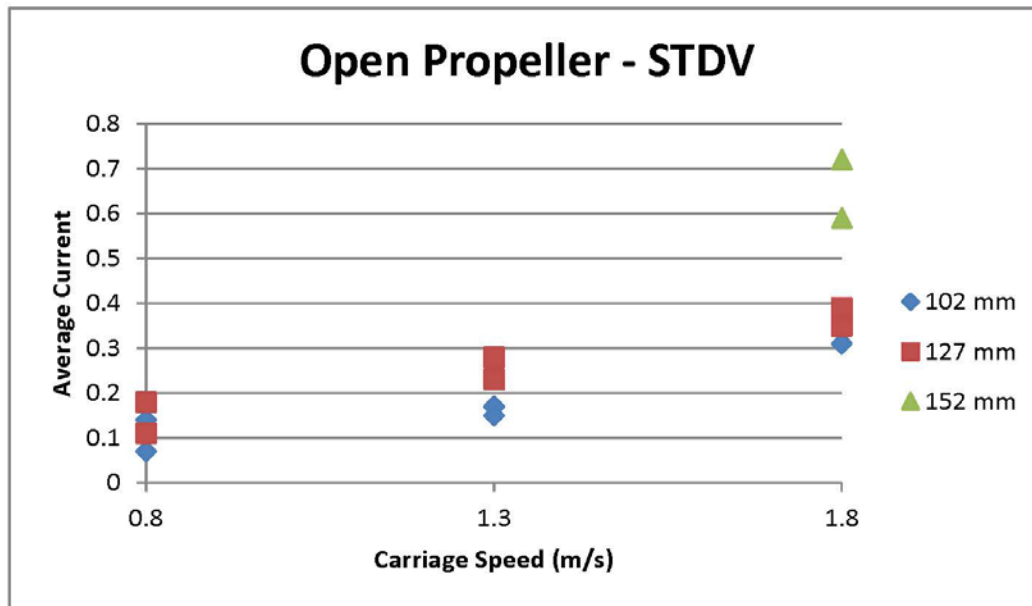


Figure 27. Plot of standard deviation for open, outboard propeller current.



From the standard deviation plot of the current data, there is an increase in the standard deviation value with increase in boat speed and thickness of brash ice. In other words, the faster the boat moves through an increasing ice field, the greater effect it has on the motors. This trend is attributed to increase in ice impacts on propellers with increase in boat speed and thickness of brash ice.

From the Grams software, a plot of the quantity of impacts is shown in Figure 28. The mean area under each peak is plotted in Figure 29.

Outboard Propellers with Shrouds

Table 5 lists the average and the standard deviation of the current data for tests with three ice thicknesses and three carriage speeds. (The port and starboard motor currents for each test are their own respective line because the starboard is spun in the clockwise (negative) direction as the port motor is spun in a counterclockwise (positive) direction.) The average and the standard deviation are calculated when carriage position was between 8 and 18 m at a constant speed. The data from the open water test (OW) at carriage speed of 1.8 m/s were not useable and are not included in the tables.

Figure 28. Plot of the number of impacts on open propellers at various carriage speeds.

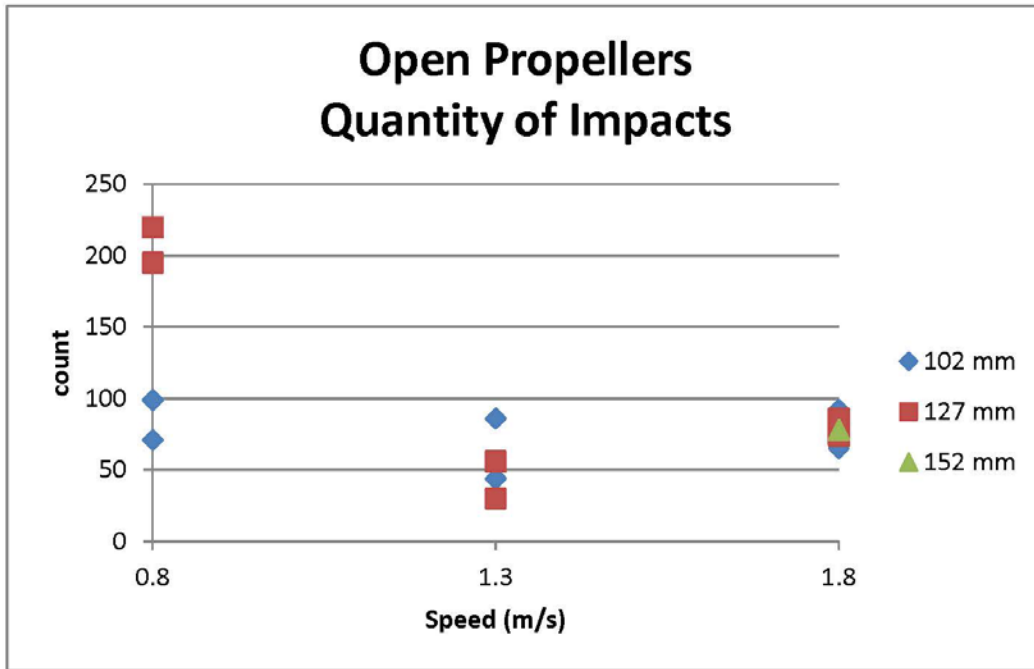


Figure 29. Plot of mean area under a spike at various carriage speeds.

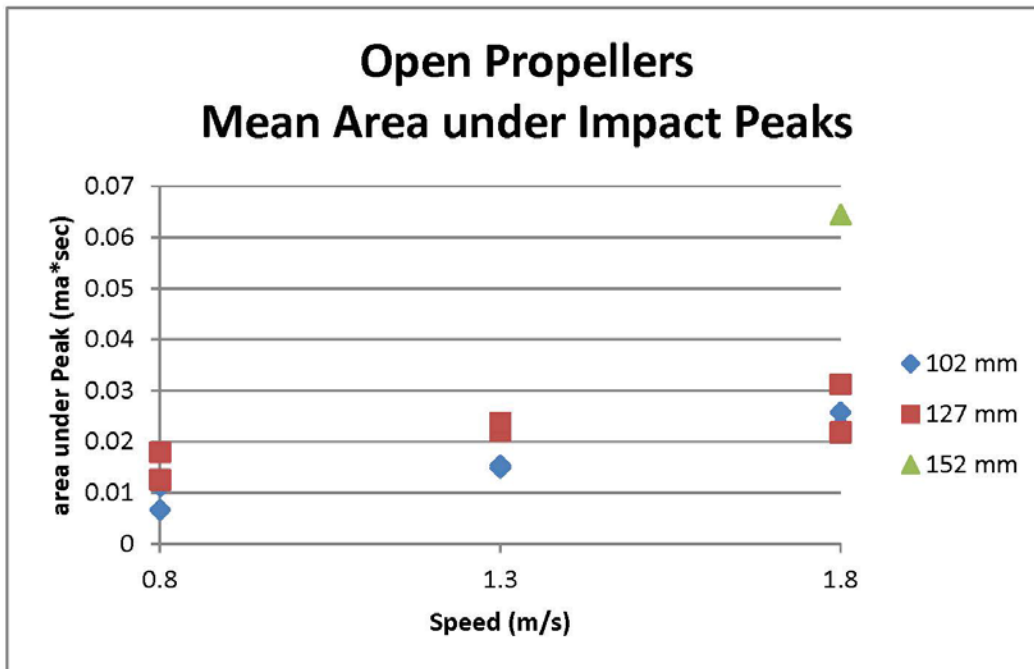


Table 5. Shrouded outboard propellers' average current and standard deviation.

Ice Thickness	Carriage Speed	TestName-Feature	Avg	STDV
102 mm	0.8 ms ⁻¹	CGDay1-08-29-2013-08-31-18-410 Current_Port	1.05	0.13
	0.8 ms ⁻¹	CGDay1-08-29-2013-08-31-18-410 Current_Starboard	-0.99	0.13
	1.3 ms ⁻¹	CGDay1-08-29-2013-08-41-50-333 Current_Port	1.1	0.14
	1.3 ms ⁻¹	CGDay1-08-29-2013-08-41-50-333 Current_Starboard	-0.95	0.12
	1.8 ms ⁻¹	CGDay1-08-29-2013-09-06-17-112 Current_Port	1.03	0.16
	1.8 ms ⁻¹	CGDay1-08-29-2013-09-06-17-112 Current_Starboard	-0.89	0.14
127 mm	0.8 ms ⁻¹	CGDay1-09-05-2013-09-29-08-662 Current_Port	1.33	0.18
	0.8 ms ⁻¹	CGDay1-09-05-2013-09-29-08-662 Current_Starboard	-1.45	0.14
	1.3 ms ⁻¹	CGDay1-09-05-2013-09-49-52-008 Current_Port	1.42	0.19
	1.3 ms ⁻¹	CGDay1-09-05-2013-09-49-52-008 Current_Starboard	-1.47	0.24
	1.8 ms ⁻¹	CGDay1-09-05-2013-10-15-13-615 Current_Port	1.28	0.35
	1.8 ms ⁻¹	CGDay1-09-05-2013-10-15-13-615 Current_Starboard	-1.3	0.42
152 mm	0.8 ms ⁻¹	CGDay1-09-05-2013-11-02-12-579 Current_Port	1.38	0.18
	0.8 ms ⁻¹	CGDay1-09-05-2013-11-02-12-579 Current_Starboard	-0.91	0.15
	1.3 ms ⁻¹	CGDay1-09-05-2013-11-13-28-655 Current_Port	1.37	0.24
	1.3 ms ⁻¹	CGDay1-09-05-2013-11-13-28-655 Current_Starboard	-1.38	0.25
	1.8 ms ⁻¹	CGDay1-09-05-2013-11-28-16-096 Current_Port	1.47	0.26
	1.8 ms ⁻¹	CGDay1-09-05-2013-11-28-16-096 Current_Starboard	-1.39	0.4
Open Water	0.8 ms ⁻¹	CGDay1-09-06-2013-09-44-03-571 Current_Port	0.97	0.06
	0.8 ms ⁻¹	CGDay1-09-06-2013-09-44-03-571 Current_Starboard	-0.94	0.06
	1.3 ms ⁻¹	CGDay1-09-06-2013-09-47-13-817 Current_Port	0.96	0.05
	1.3 ms ⁻¹	CGDay1-09-06-2013-09-47-13-817 Current_Starboard	-0.9	0.06

Figure 30 plots the average current shown in Table 5. Figure 31 plots the standard deviation.

Figure 30. Plot of average current for open, outboard propellers.

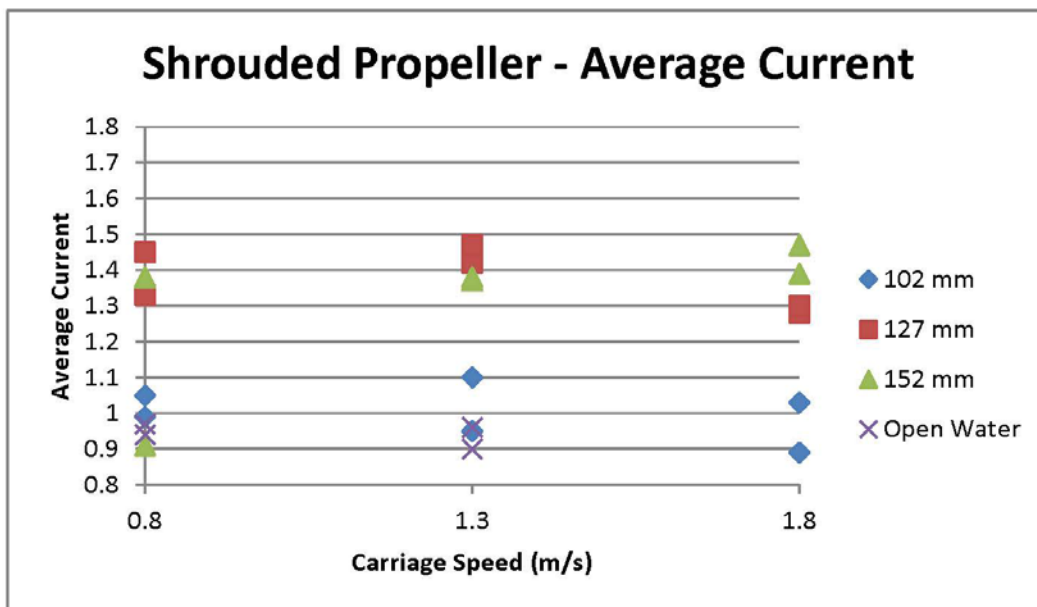
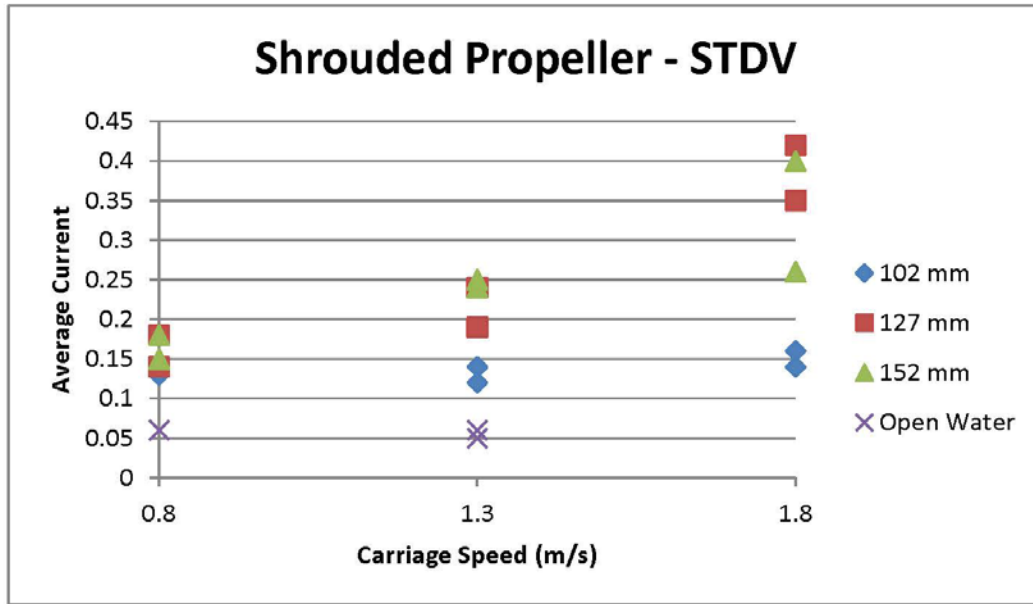


Figure 31. Plot of standard deviation for open, outboard propeller current.



From the Grams software, a plot of the quantity of impacts is shown in Figure 32. The mean area under each peak is plotted in Figure 33.

From the standard deviation plot of the current data, there is an increase in the standard deviation value with increase in boat speed and thickness of brash ice. In other words, this trend is attributed to increase in ice impacts on propellers with increase in boat speed and thickness of brash ice. This is similar to the results presented in the open-propeller plots.

Figure 32. Plot of the number impacts on propellers at various carriage speeds.

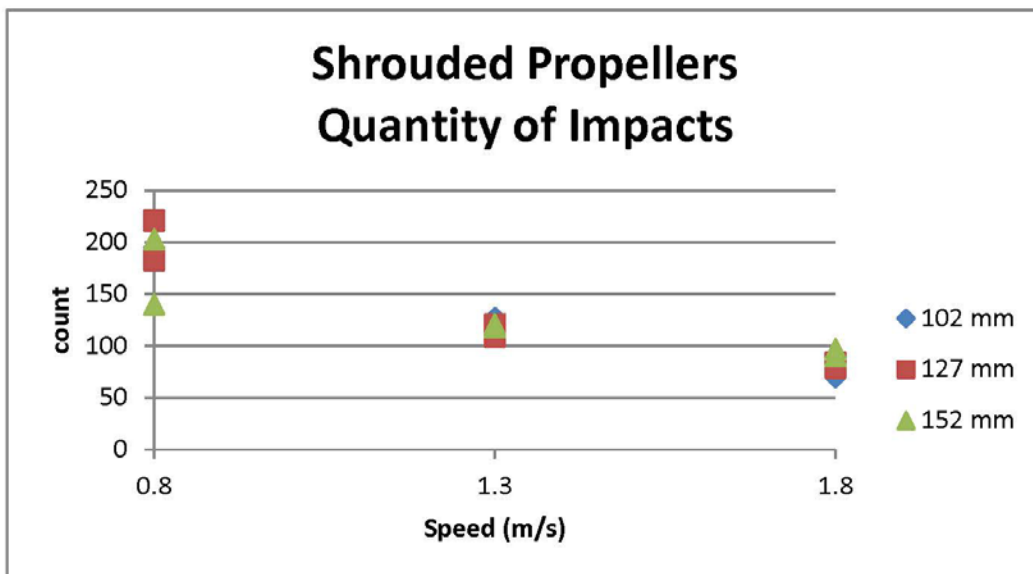
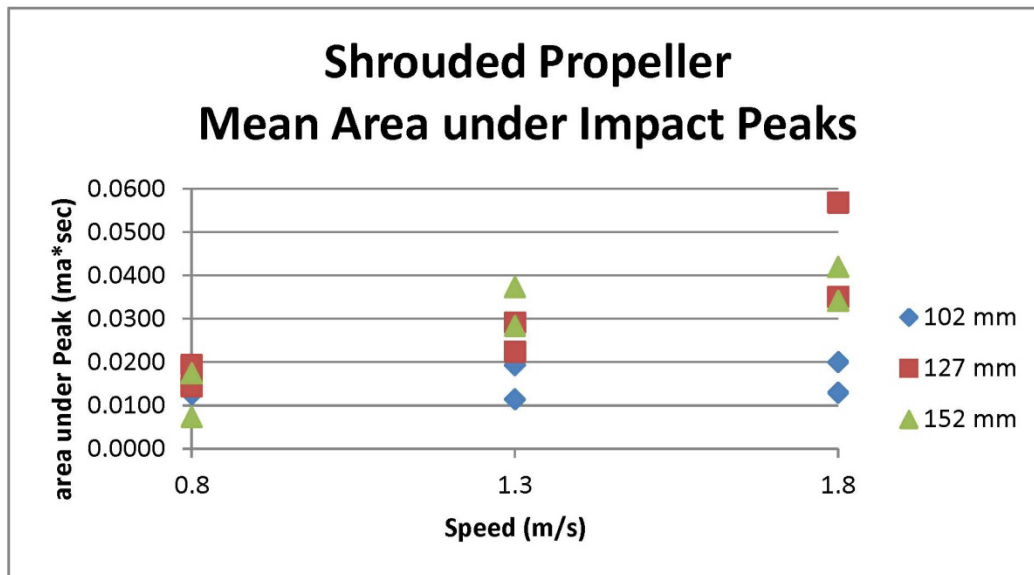


Figure 33. Plot of mean area under a spike at various carriage speeds.



Waterjet Intake System

Table 6 lists the average and the standard deviation of the current data for tests with three ice thicknesses and three carriage speeds. The average and the standard deviation are calculated when carriage position was between 8 m and 18 m at a constant speed.

Figure 34 plots the average current Figure 35 plots the standard deviation shown in Table 6.

From the Grams software, a plot of the quantity of impacts is shown in Figure 36. The mean area under each peak is plotted in Figure 37.

From the standard deviation plot of the current data there is an increase in the standard deviation value with increase in boat speed and thickness of brush ice. Both these phenomena mirror the results of the open- and shrouded-propeller tests.

Table 6. Waterjet intake system average current and standard deviation.

Ice Thickness	Carriage Speed	TestName-Feature	Avg	STDV
102 mm	0.8 ms ⁻¹	CGDay1-09-12-2013-13-37-02-278 Current_Port	0.42	0.09
	0.8 ms ⁻¹	CGDay1-09-12-2013-13-37-02-278 Current_Starboard	0.53	0.09
	1.3 ms ⁻¹	CGDay1-09-12-2013-13-48-09-556 Current_Port	0.47	0.1
	1.3 ms ⁻¹	CGDay1-09-12-2013-13-48-09-556 Current_Starboard	0.53	0.12
	1.8 ms ⁻¹	CGDay1-09-12-2013-13-58-45-632 Current_Port	0.51	0.13
	1.8 ms ⁻¹	CGDay1-09-12-2013-13-58-45-632 Current_Starboard	0.45	0.08
127 mm	0.8 ms ⁻¹	CGDay1-09-12-2013-14-34-53-372 Current_Port	0.46	0.1
	0.8 ms ⁻¹	CGDay1-09-12-2013-14-34-53-372 Current_Starboard	0.56	0.1
	1.3 ms ⁻¹	CGDay1-09-12-2013-14-43-10-291 Current_Port	0.47	0.11
	1.3 ms ⁻¹	CGDay1-09-12-2013-14-43-10-291 Current_Starboard	0.58	0.12
	1.8 ms ⁻¹	CGDay1-09-12-2013-14-53-02-074 Current_Port	0.47	0.15
	1.8 ms ⁻¹	CGDay1-09-12-2013-14-53-02-074 Current_Starboard	0.44	0.07
152 mm	0.8 ms ⁻¹	CGDay1-09-12-2013-15-40-59-196 Current_Port	0.38	0.08
	0.8 ms ⁻¹	CGDay1-09-12-2013-15-40-59-196 Current_Starboard	0.5	0.08
	1.3 ms ⁻¹	CGDay1-09-12-2013-15-51-33-517 Current_Port	0.37	0.07
	1.3 ms ⁻¹	CGDay1-09-12-2013-15-51-33-517 Current_Starboard	0.54	0.08
	1.8 ms ⁻¹	CGDay1-09-12-2013-16-04-19-708 Current_Port	0.3	0.08
	1.8 ms ⁻¹	CGDay1-09-12-2013-16-04-19-708 Current_Starboard	0.43	0.1
Open Water	0.8 ms ⁻¹	CGDay1-09-13-2013-10-13-43-335 Current_Port	0.29	0.05
	0.8 ms ⁻¹	CGDay1-09-13-2013-10-13-43-335 Current_Starboard	0.32	0.06
	1.3 ms ⁻¹	CGDay1-09-13-2013-10-18-10-492 Current_Port	0.27	0.05
	1.3 ms ⁻¹	CGDay1-09-13-2013-10-18-10-492 Current_Starboard	0.32	0.06
	1.8 ms ⁻¹	CGDay1-09-13-2013-10-23-15-738 Current_Port	0.27	0.05
	1.8 ms ⁻¹	CGDay1-09-13-2013-10-23-15-738 Current_Starboard	0.37	0.06

Figure 34. Plot of average current for waterjet intake system.

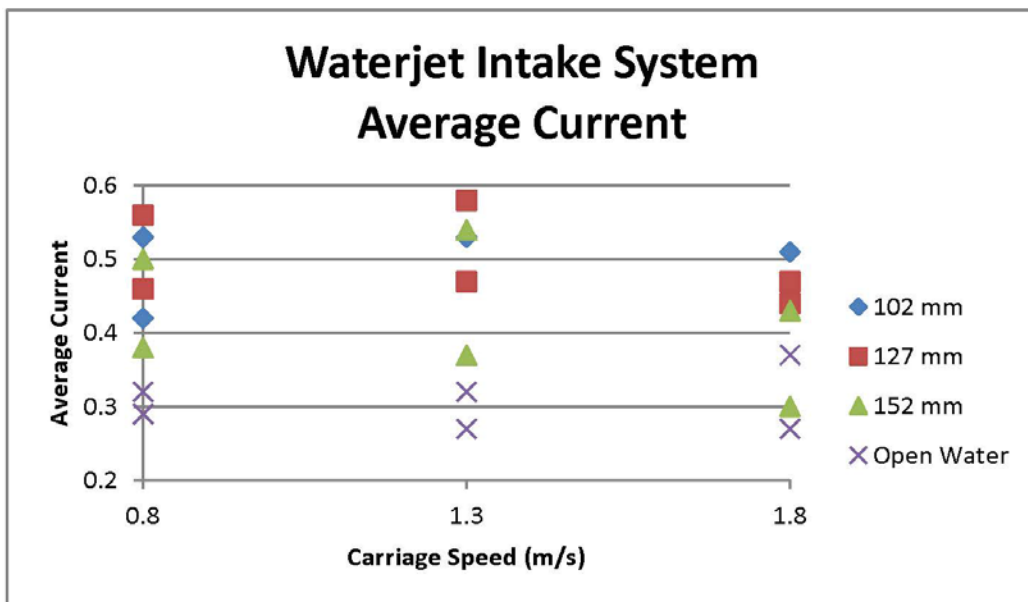


Figure 35. Plot of standard deviation for waterjet intake system current.

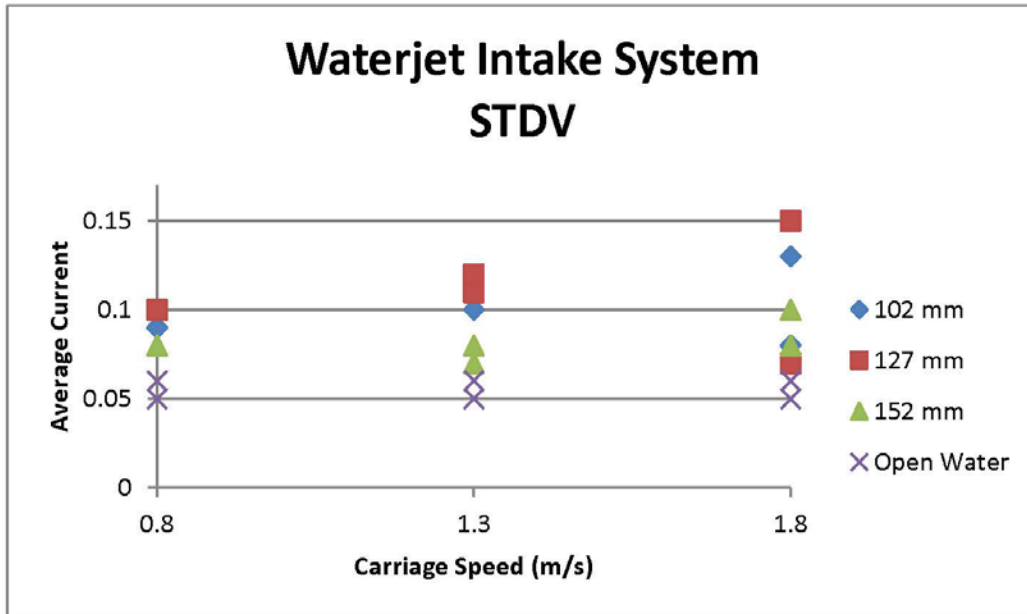


Figure 36. Plot of the number impacts on propellers at various carriage speeds.

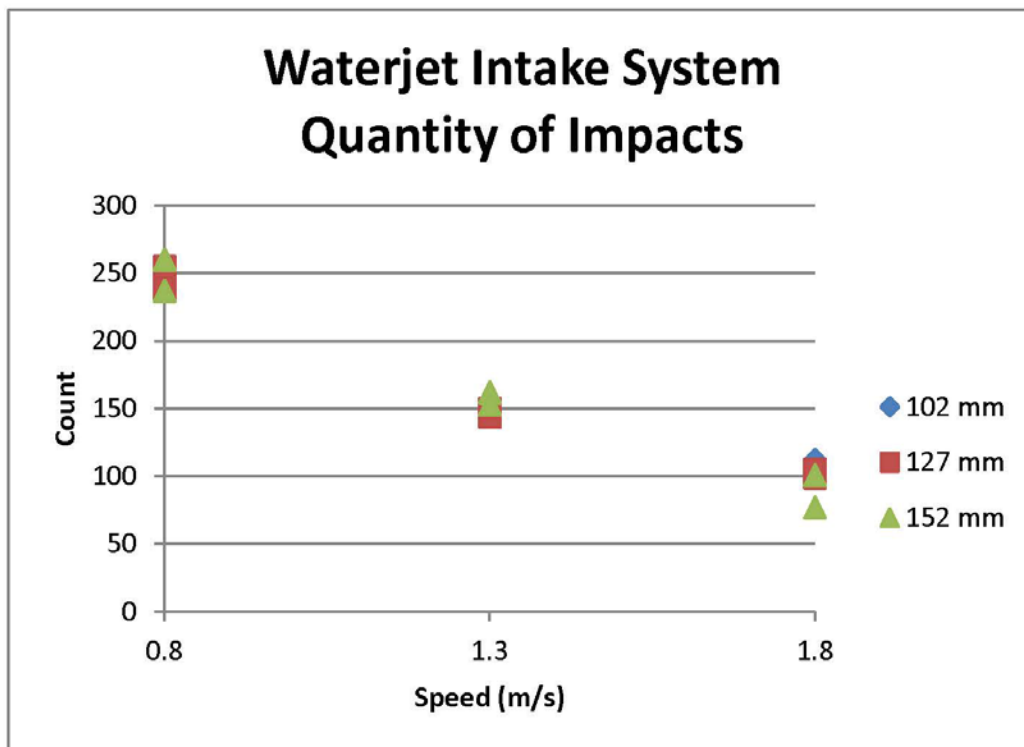
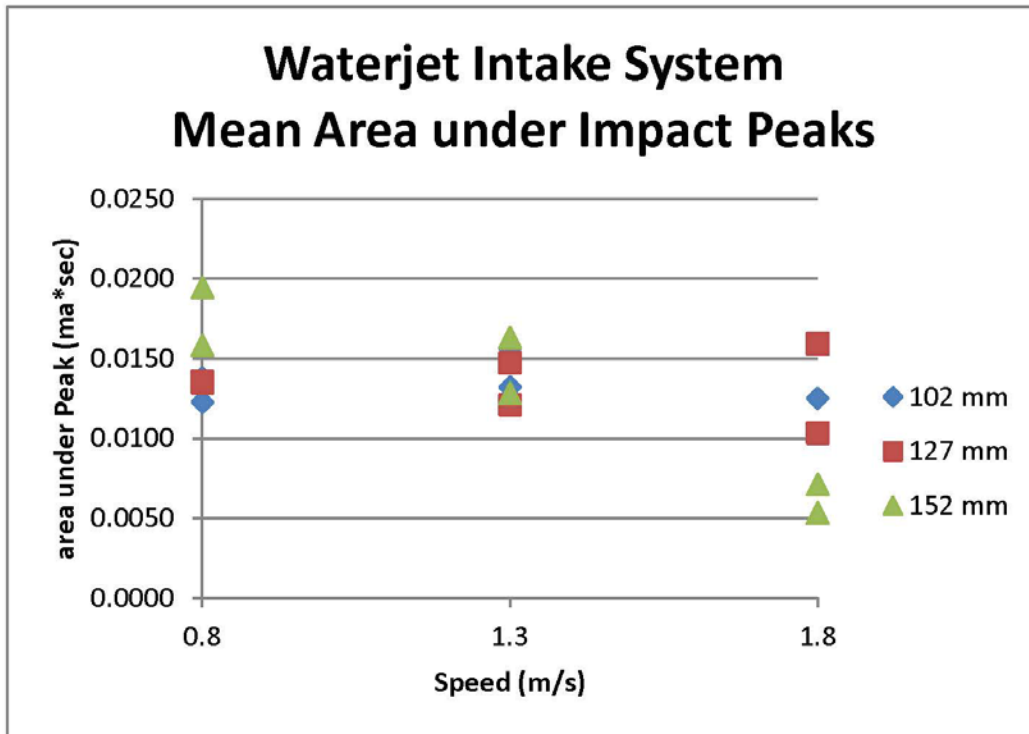


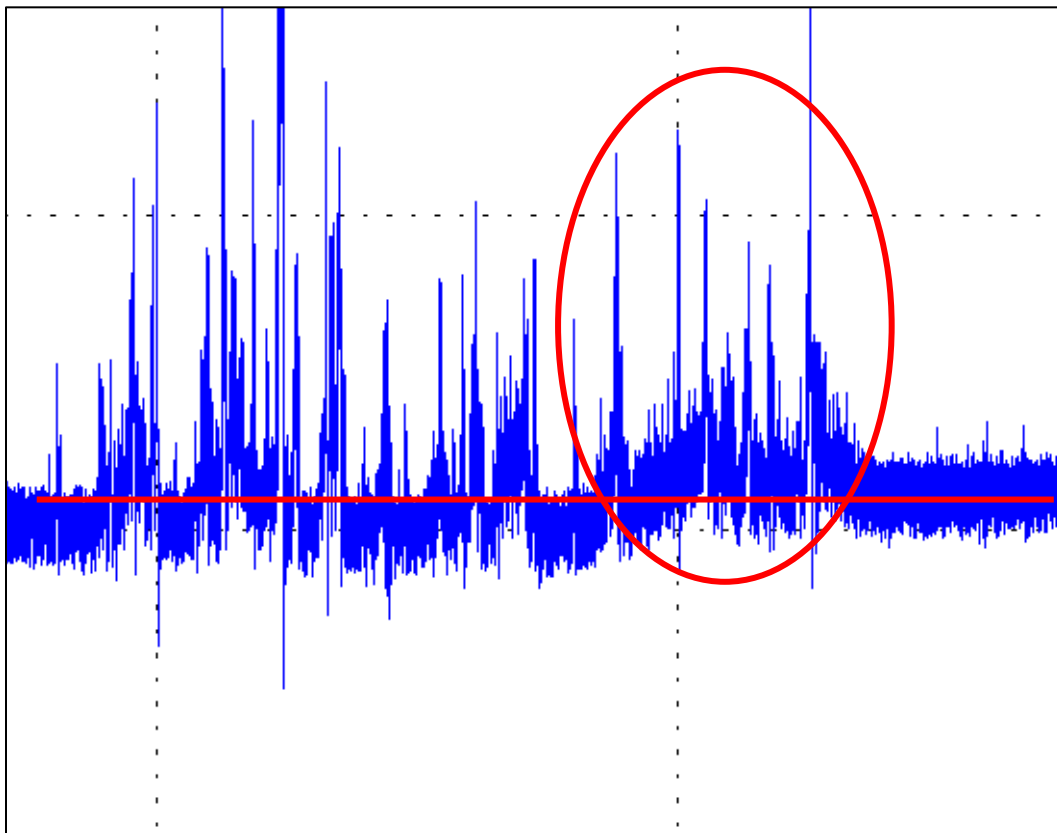
Figure 37. Plot of mean area under a spike at various carriage speeds.



5 Conclusions and Recommendations

As the boat travels at faster speeds through the brash ice field, the number of interactions between the ice and the propellers are reduced, yet the average load to the motors during these impacts increases. It appears that at lower speeds, the brash ice has time to come into contact with the propellers but is quickly pushed away by the propellers once impact is made. As the speed of the boat increases, the brash ice pieces don't have time to accumulate in the propeller area. However, when the pieces do accumulate, they get trapped in the propeller area, either causing the propeller's blades to *mill* at the ice chunks, or they restrict water flow, which also increases the load to the motor. This phenomenon is shown in Figure 38.

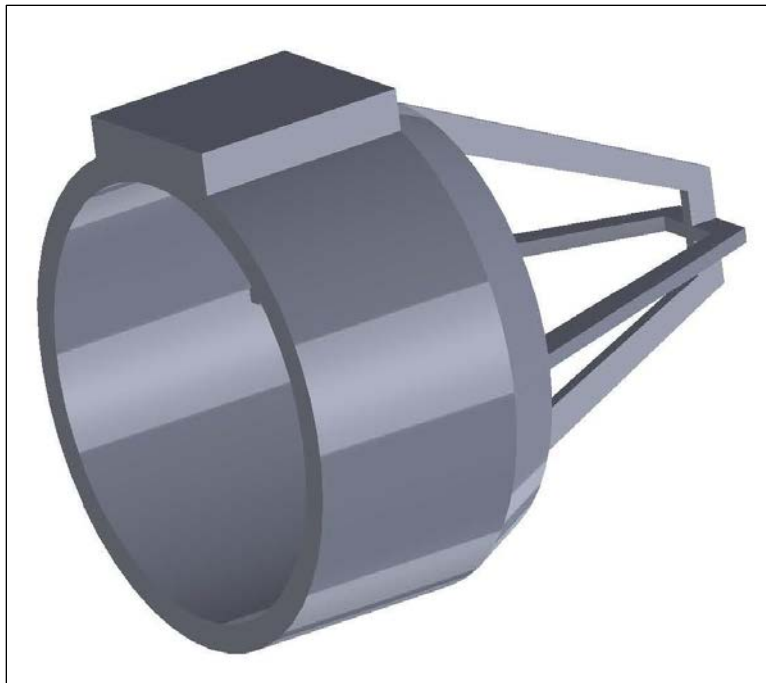
Figure 38. Ramping up of motor current that may be caused either by a trapped piece of brash ice or the propellers milling an ice piece.



The data show that with the shrouds installed, the standard deviation of the current increases compared to the open propellers. It was thought that the shrouds would protect the propellers from ice impacts, which they may have

done, but a secondary effect is that the brash ice, once in the propeller area, could not be forced away by the propellers as could be done in the open-propeller tests. This could mean that shrouds may still offer protection to the propellers but a different configuration is more appropriate. One thought is to use a wire-cage shroud where the propellers are still protected from large pieces of brash ice, but the flow dynamics near the propellers can flush these pieces away. An example of a possible shroud is shown in Figure 39.

Figure 39. Possible revised shroud.



Evidence showed that the model waterjet intake system did not become clogged with ice fragments and that no large pieces of brash ice entered the intake tunnel during testing. It would be difficult to say that this would be the case at full scale. Even if grates were installed over the intake hull opening on the full-scale (the model's intake was open), the hydrodynamics may *pull* the ice into the intake opening whereas the model's propulsion system did not do this. The grates on the full-scale intake may also retain brash ice pieces which in turn would restrict flow to the propulsion impellers. Nevertheless, it appears that the ice flow along the hull bottom prevents large ingestion of brash ice, which would give greater protection for the impellers of the full-scale waterjet system.

A recommendation is presented that all boats operating in brash ice fields should operate at slow speeds, less than 9 kilometers per hour (km/h) (5 knots) to prevent increased strain on the outboard motors and possible damage to the propulsion system. If propulsion speeds faster than 9 km/h are maintained, it can be expected that the propellers will need to be replaced more often and the life expectancy of the engines will be reduced as compared to a boat operated solely in open water.

6 Future Research

The effects of shroud design for outboard propellers should be further investigated. There may be an optimized design where the brash ice cannot contact the propellers and not restrict the water flow if brash ice starts to accumulate around the shroud. Several commercial off-the-shelf shrouds could be selected along with possible new designs for similar testing as was conducted in this evaluation.

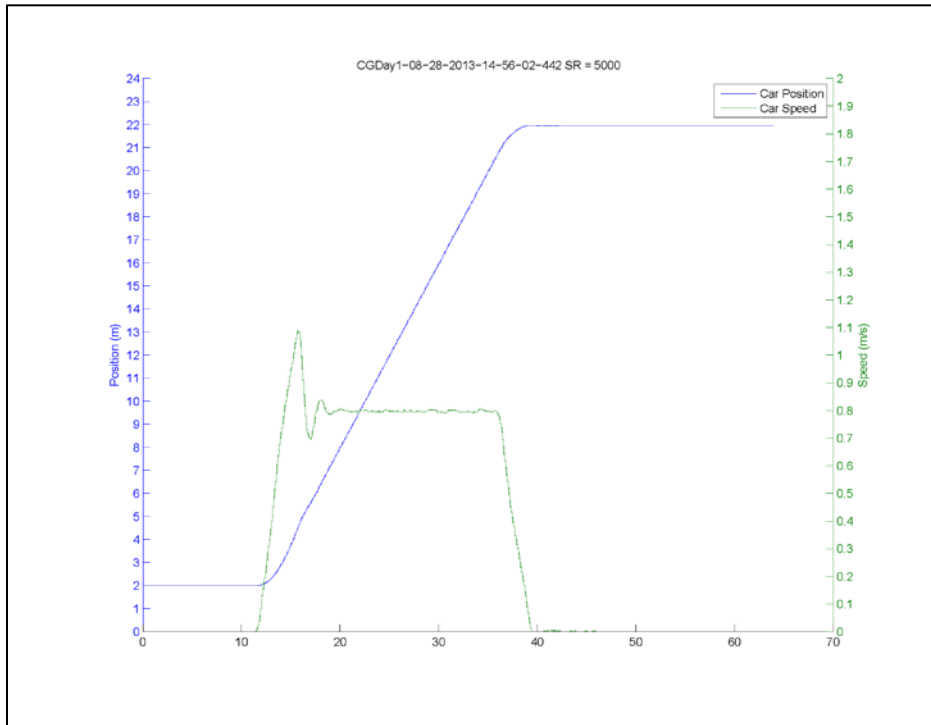
To generate accurate understanding of a waterjet intake system and its interaction in a brash ice field, a full-scale testing program should be completed. The full-scale system would provide both the hull and the impeller draw of water and ice into the intake.

References

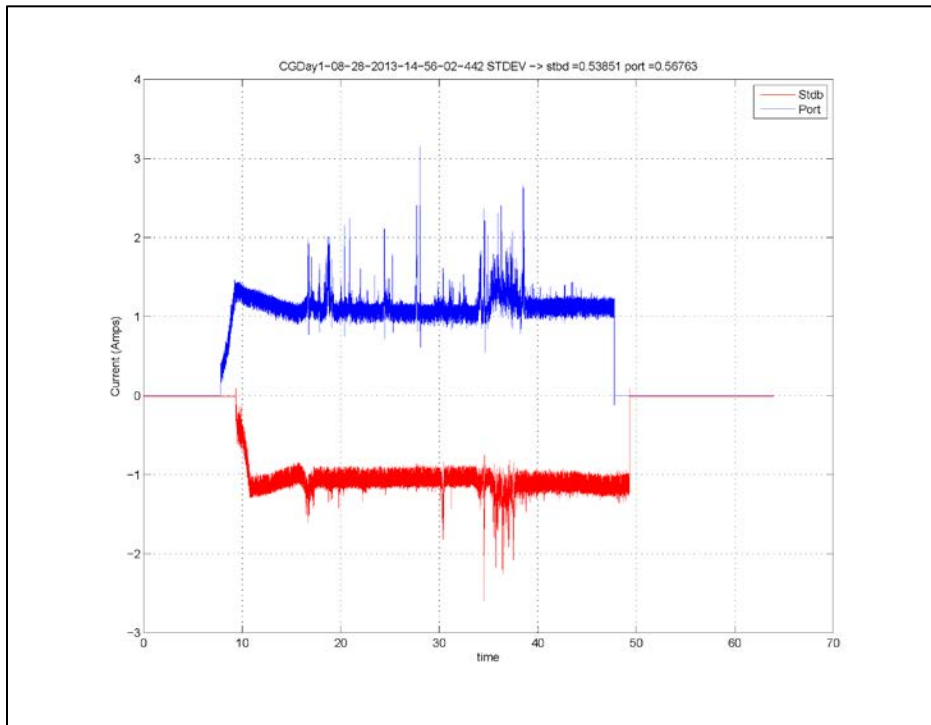
- Hirayama, K. 1983. *Properties of urea-doped ice in the CRREL test basin*. CRREL Research Report 83-08. Hanover, NH: US Army Engineer Research and Development Center.
- Laskow, V. 1988. *Ice flow and blockage investigation of shrouded propellers*. Transport Development Centre Report TP-9640E. Montreal, QC: Transport Canada, Transportation Development Centre.
- Metcalf, B., L. Faul, E. Bumiller, and J. Slutsky. 2005. *Resistance tests of a systematic series of U.S. Coast Guard planing hulls*. NSWCCD-50-TR2005/063. West Bethesda, MD: Carderock Division, Naval Surface Warfare Center.
- Re, S., and B. Veitch. 2007. Lifeboat operational performance in cold environments. In *Design and construction of vessels operating in low temperature environments*. Ottawa, ON: The Royal Institution of Naval Architects, NRC-CNRC.
- Riska, K. 2011. Design of ice breaking ships. In *Cold regions science and marine technology*. United Nations Educational, Scientific and Cultural Organization (UNESCO) and Encyclopedia of Life Support Systems (EOLSS). <http://www.arctisearch.com/Design+of+Ice+Breaking+Ships>
- Sampson, R., M. Atlar, and N. Sasaki. 2009. Propeller ice interaction—effect of proximity. *First International Symposium on Marine Propellers (SMP'09)*. Trondheim, Norway.
- Walker, D., N. Bose, H. Yamaguchi, and S. Jones. 1997. Hydrodynamic loads on ice-class propellers during propeller-ice interaction. *J. Marine Sci. Tech.* 2:12–20.
- Wang, J., A., Akinturk, N. Bose, and S. Jones. 2007. An overview of model tests and numerical predictions for propeller-ice interaction. In *Proceedings, 8th Canadian Marine Hydromechanics and Structures Conference (CMHSC)*, 16–17 October 2007. St. John's, NL.

Appendix A: Open-Propellers Plots

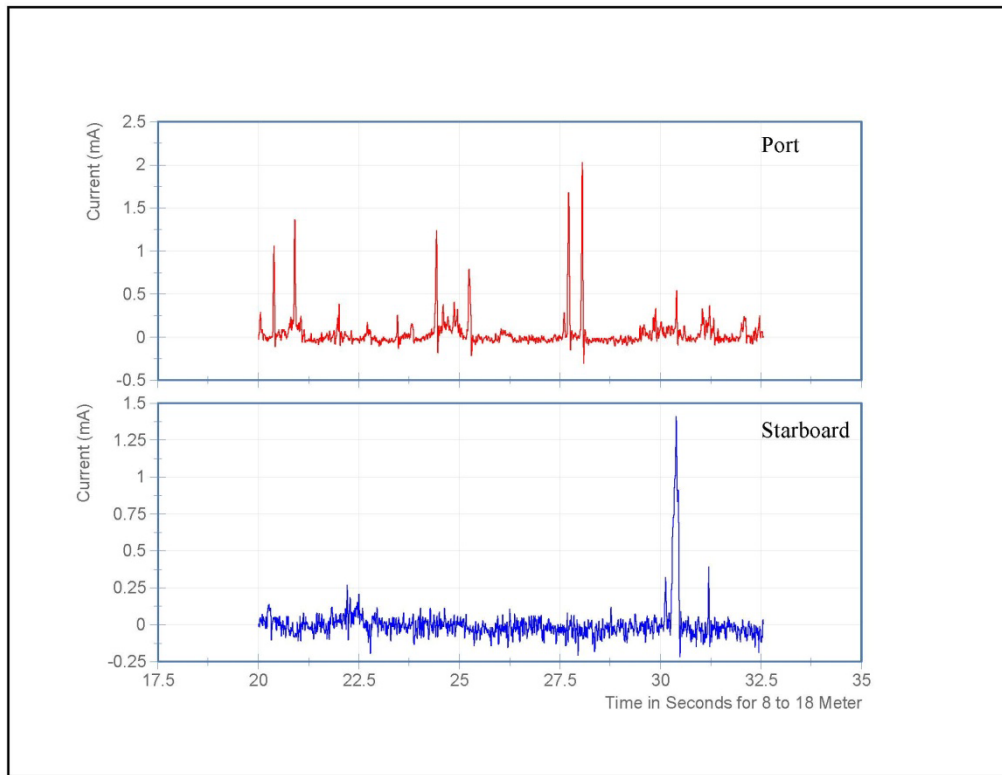
102 mm-thick ice field, carriage speed of 0.8 ms⁻¹
Speed and position plot vs. time



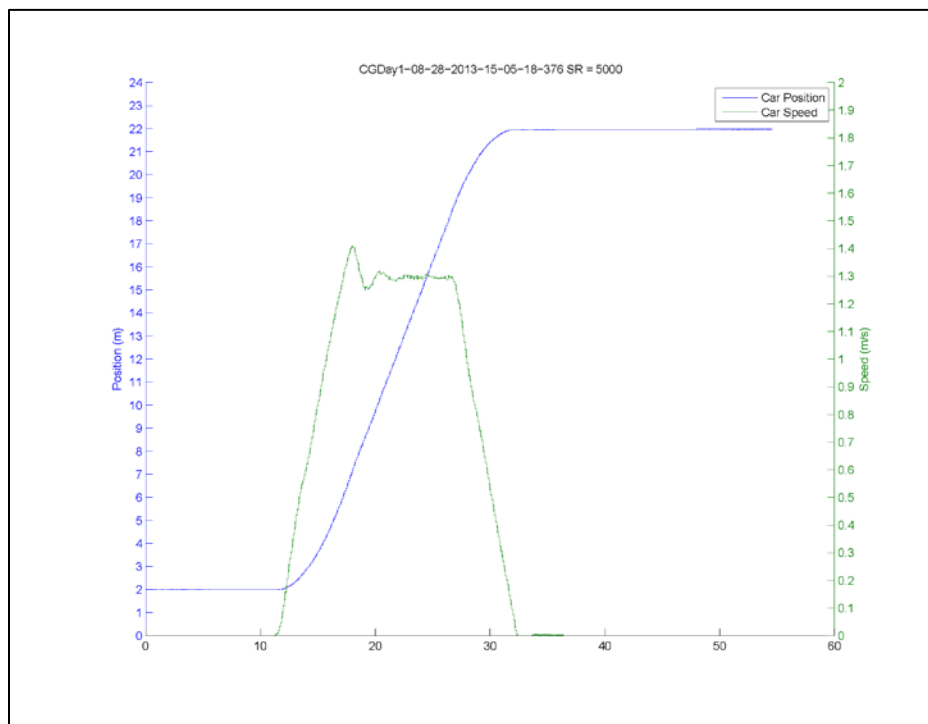
102 mm-thick ice field, carriage speed of 0.8 ms⁻¹
Current vs. time



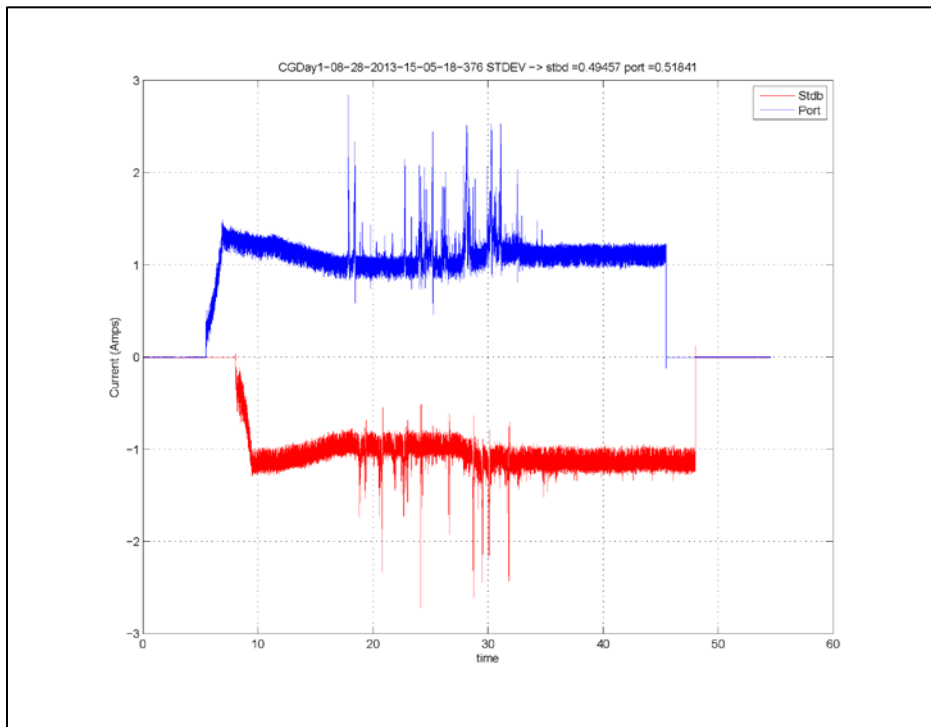
102 mm-thick ice field, carriage speed of 0.8 ms⁻¹
 Current (Grams smoothing) vs. time (from 8 m to 18 m during constant carriage velocity)



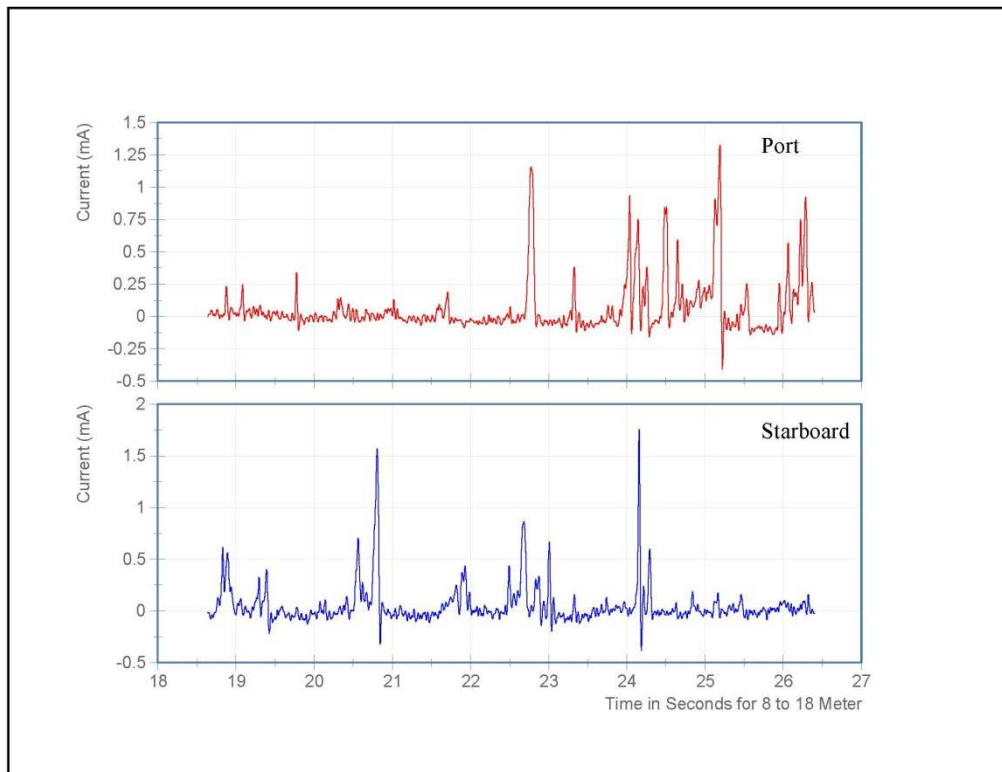
102 mm-thick ice field, carriage speed of 1.3 ms⁻¹
 Speed and position plot vs. time



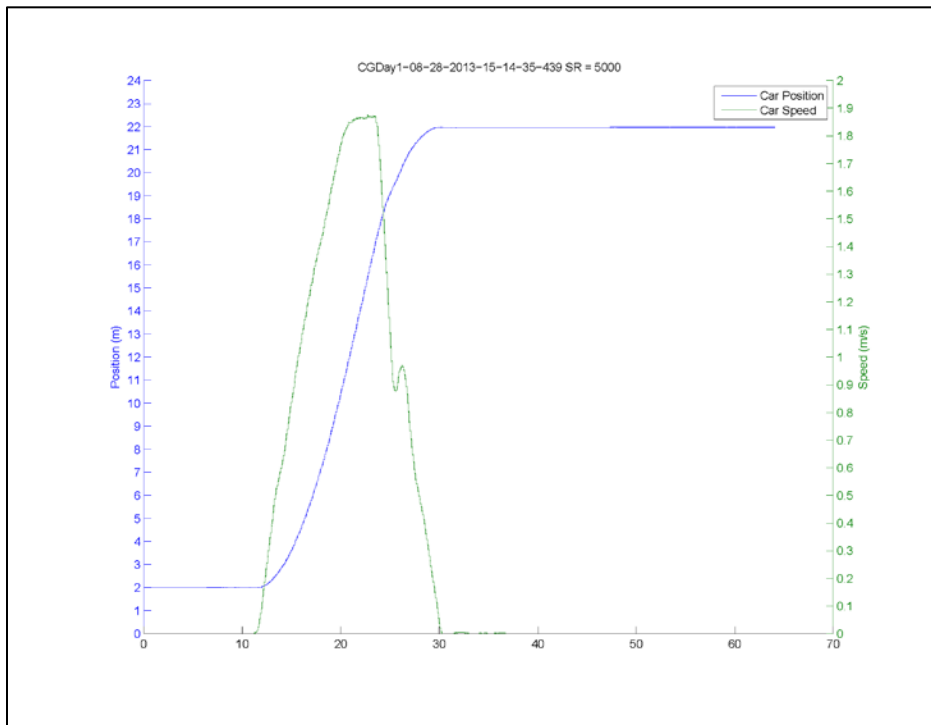
102 mm-thick ice field, carriage speed of 1.3 ms⁻¹
Current vs. time



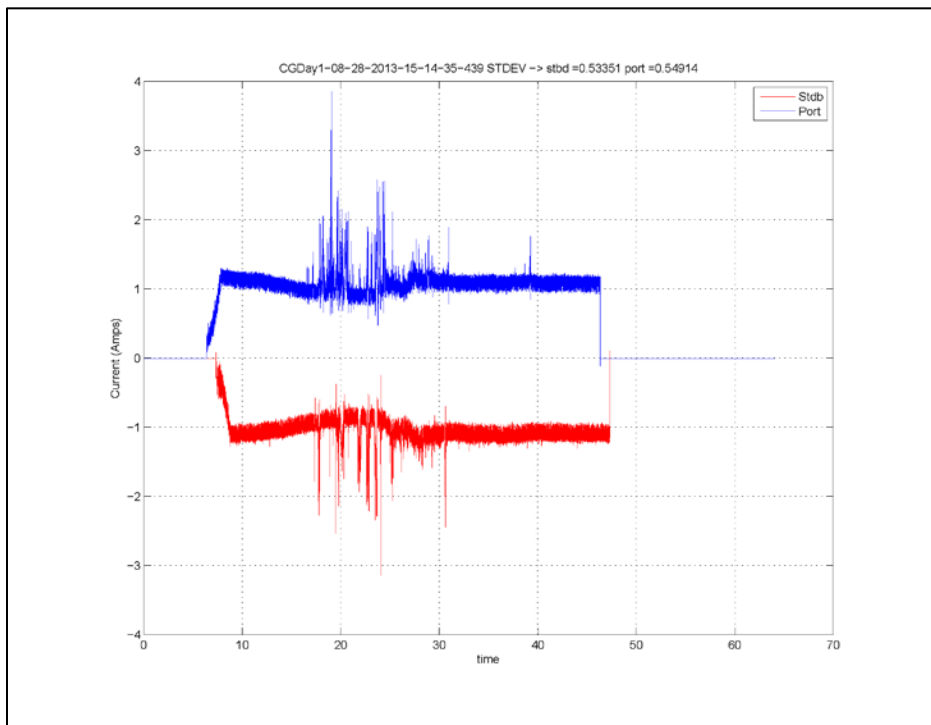
102 mm-thick ice field, carriage speed of 1.3 ms⁻¹
Current (Grams smoothing) vs. time (from 8 m to 18 m during constant carriage velocity)



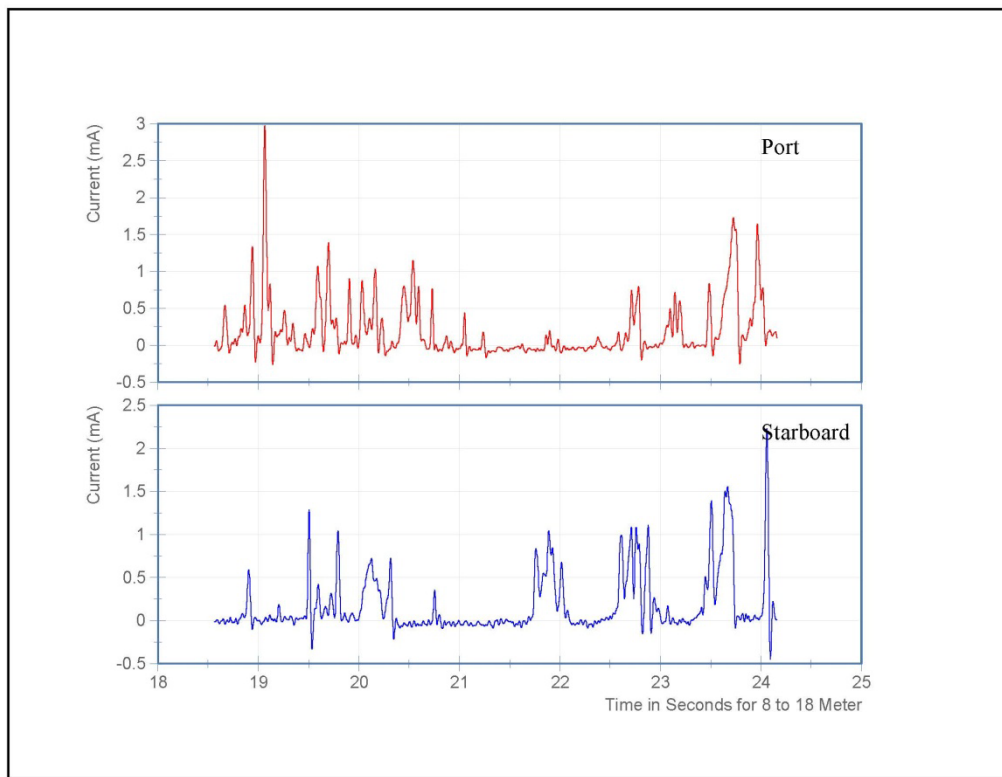
102 mm-thick ice field, carriage speed of 1.8 ms⁻¹
Speed and position plot vs. time



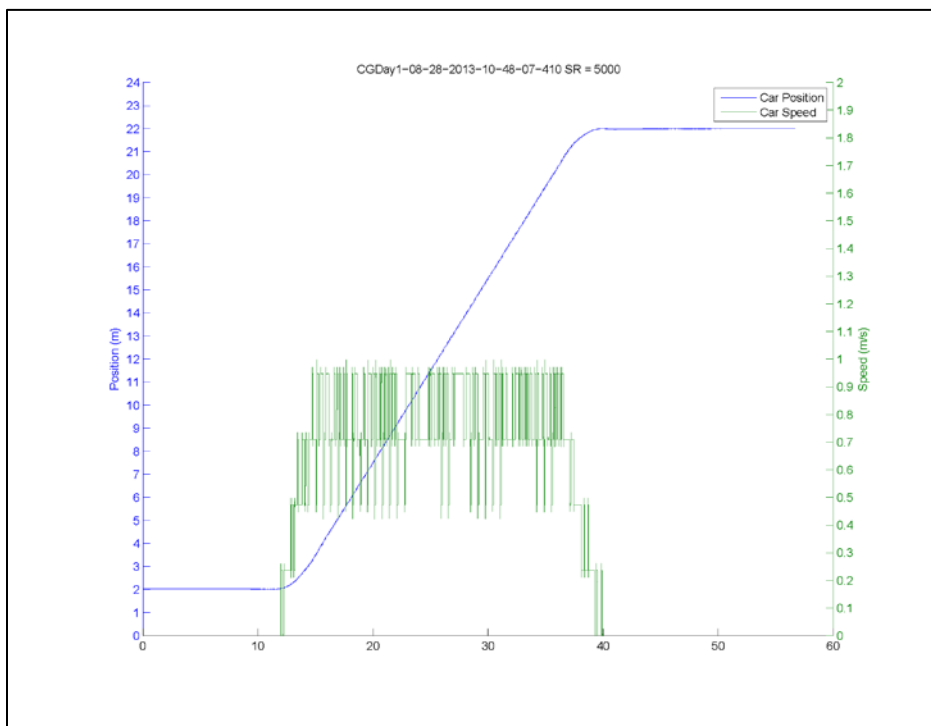
102 mm-thick ice field, carriage speed of 1.8 ms⁻¹
Current vs. time



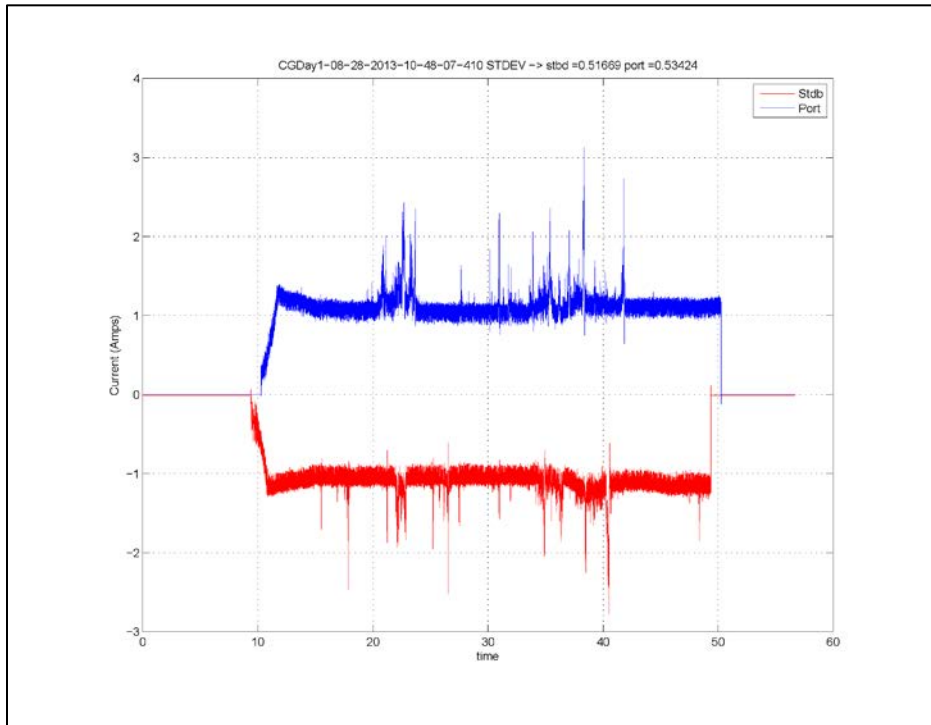
102 mm-thick ice field, carriage speed of 1.8 ms⁻¹
Current (Grams smoothing) vs. time (from 8 m to 18 m during constant carriage velocity)



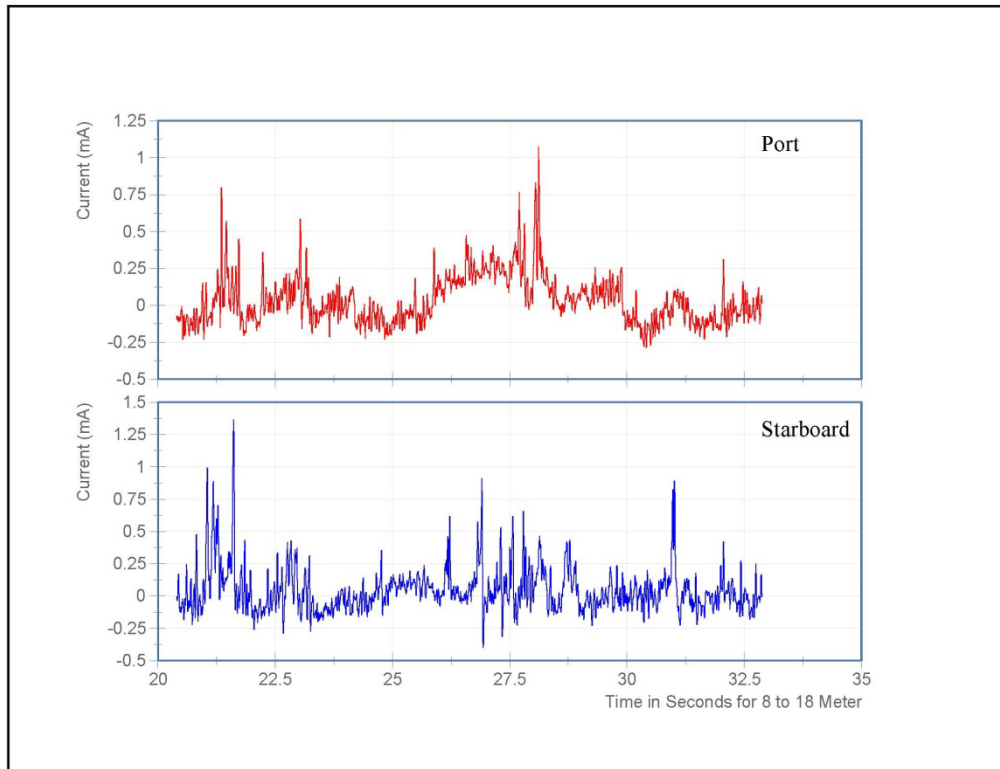
127 mm-thick ice field, carriage speed of 0.8 ms⁻¹
Speed and position plot vs. time



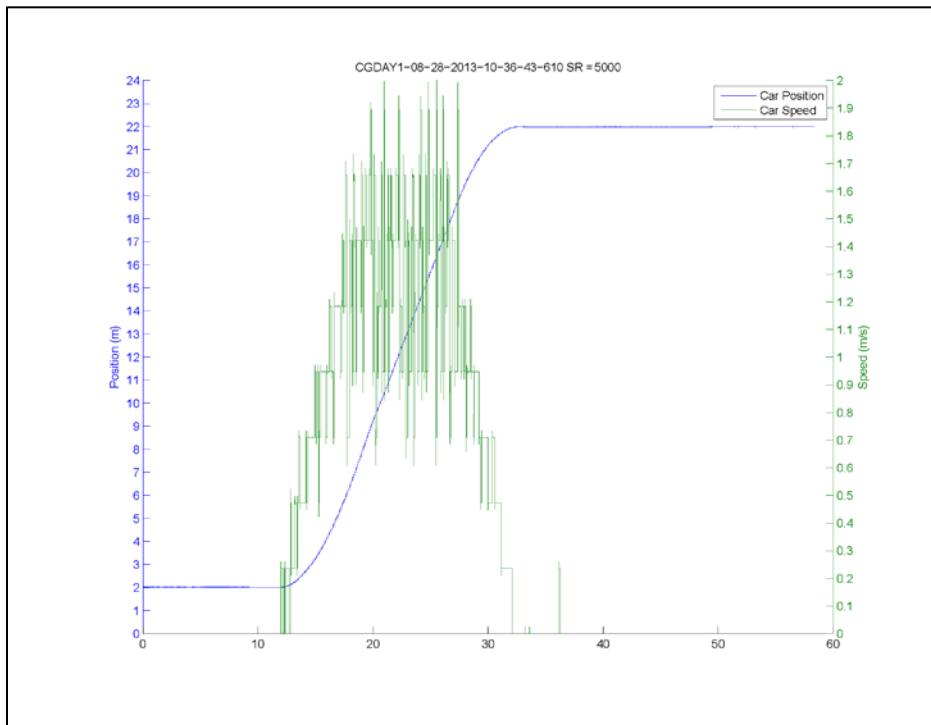
127 mm-thick ice field, carriage speed of 0.8 ms⁻¹
Current vs. time



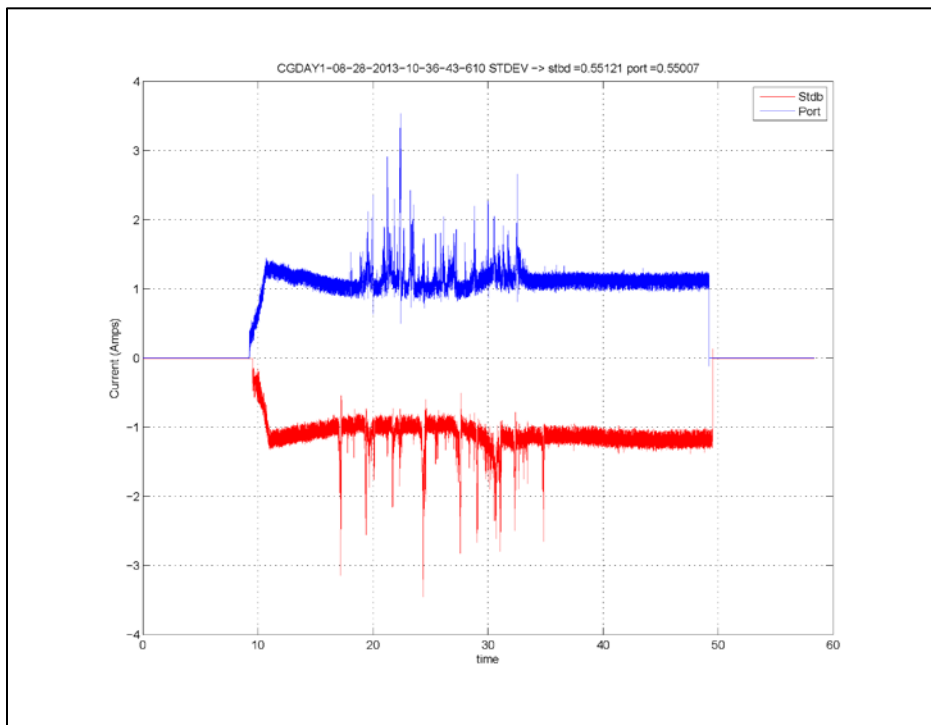
127 mm-thick ice field, carriage speed of 0.8 ms⁻¹
Current (Grams smoothing) vs. time (from 8 m to 18 m during constant carriage velocity)



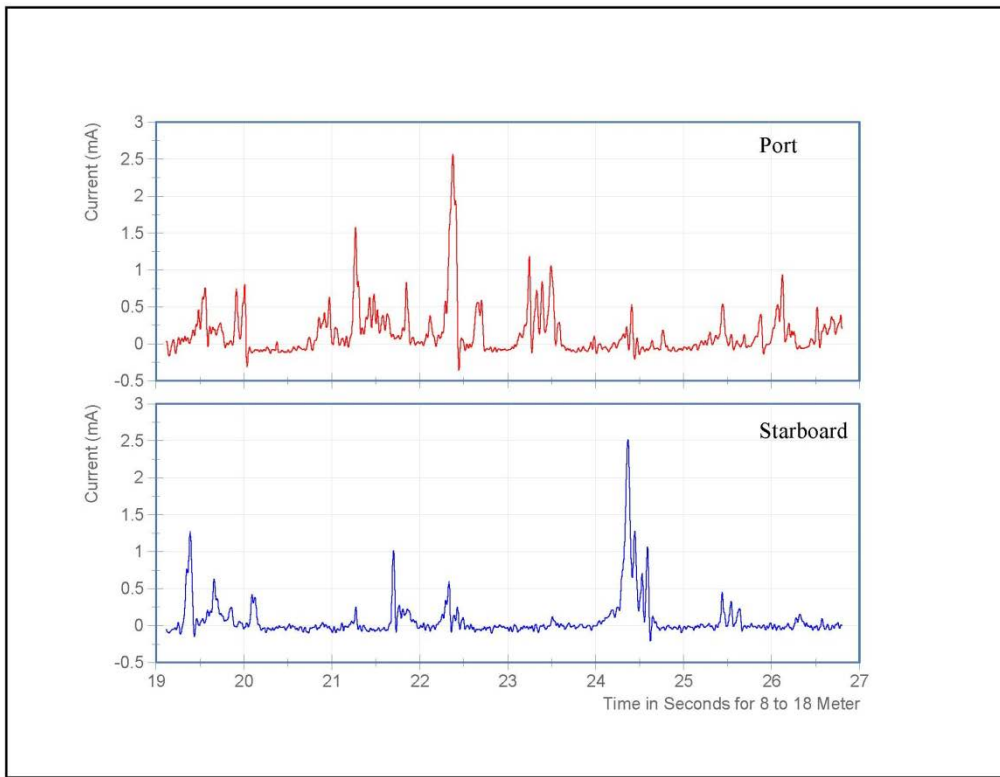
127 mm-thick ice field, carriage speed of 1.3 ms⁻¹
Speed and position plot vs. time



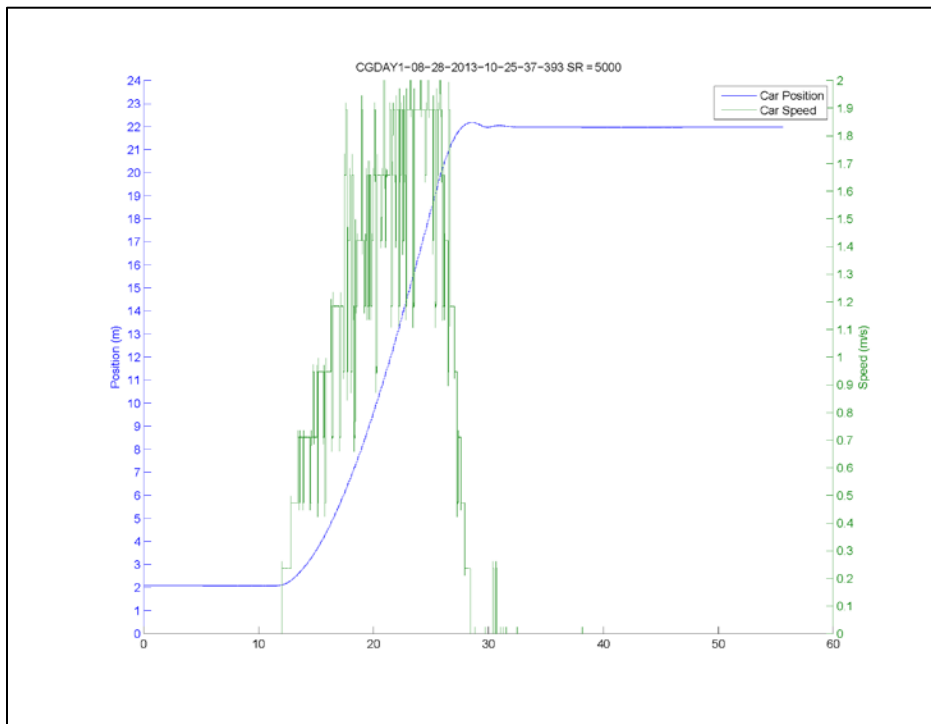
127 mm-thick ice field, carriage speed of 1.3 ms⁻¹
Current vs. time



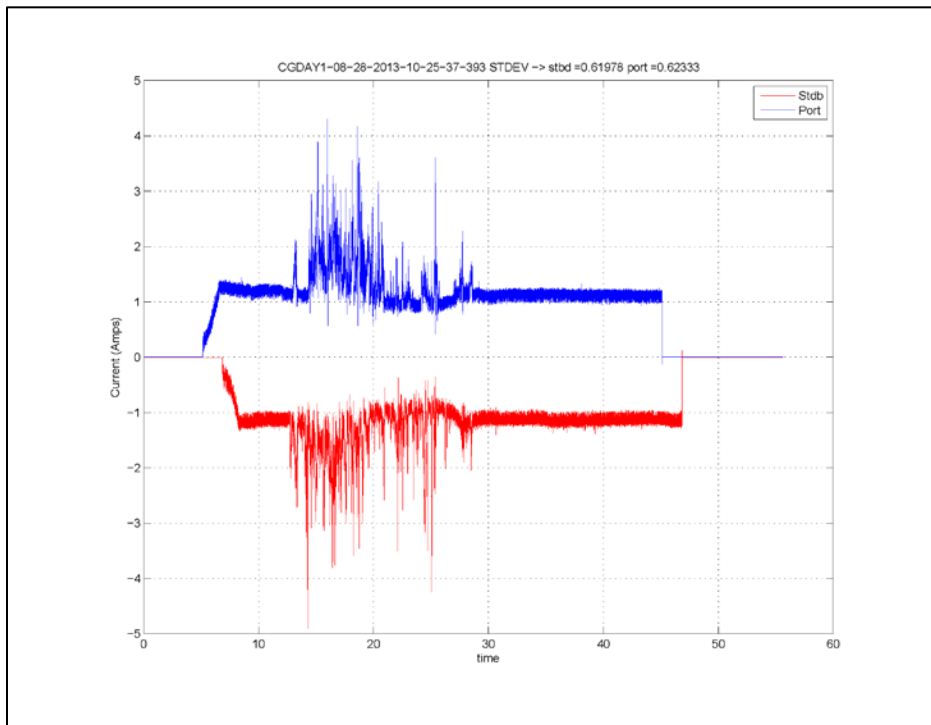
127 mm-thick ice field, carriage speed of 1.3 ms⁻¹
Current (Grams smoothing) vs. time (from 8 m to 18 m during constant carriage velocity)



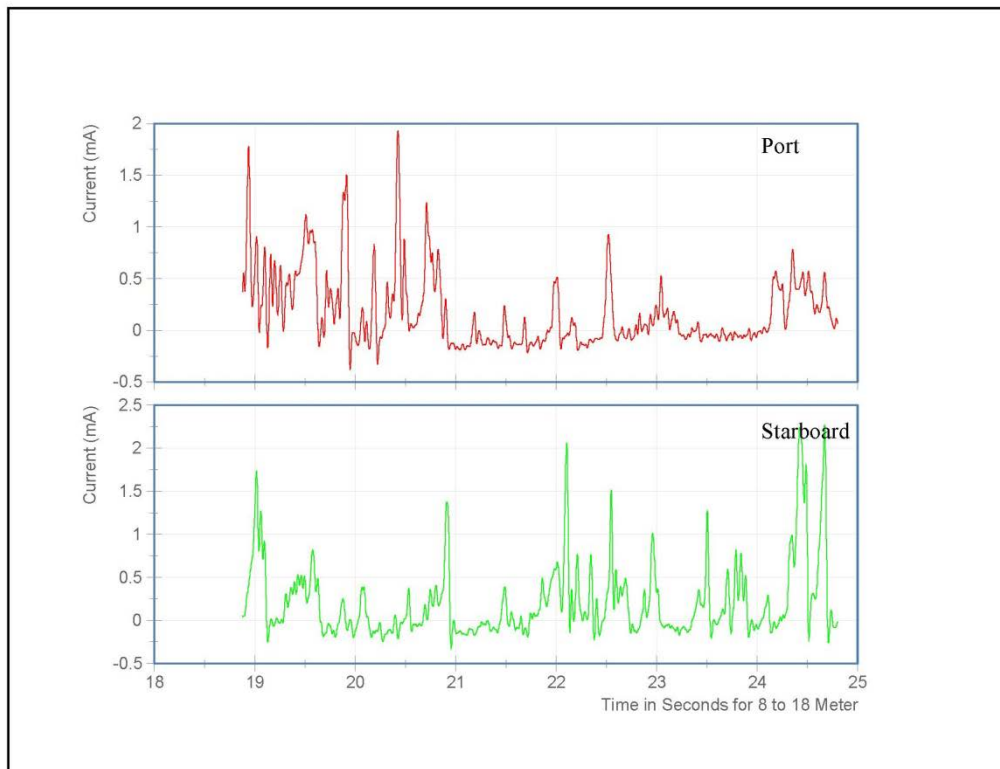
127 mm-thick ice field, carriage speed of 1.8 ms⁻¹
Speed and position plot vs. time



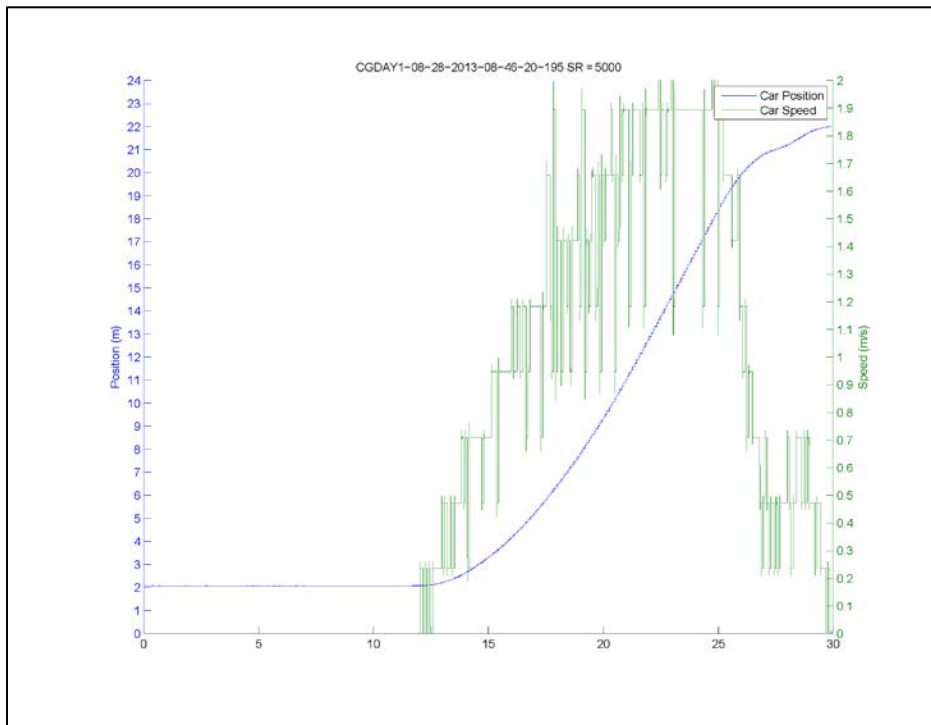
127 mm-thick ice field, carriage speed of 1.8 ms⁻¹
Current vs. time



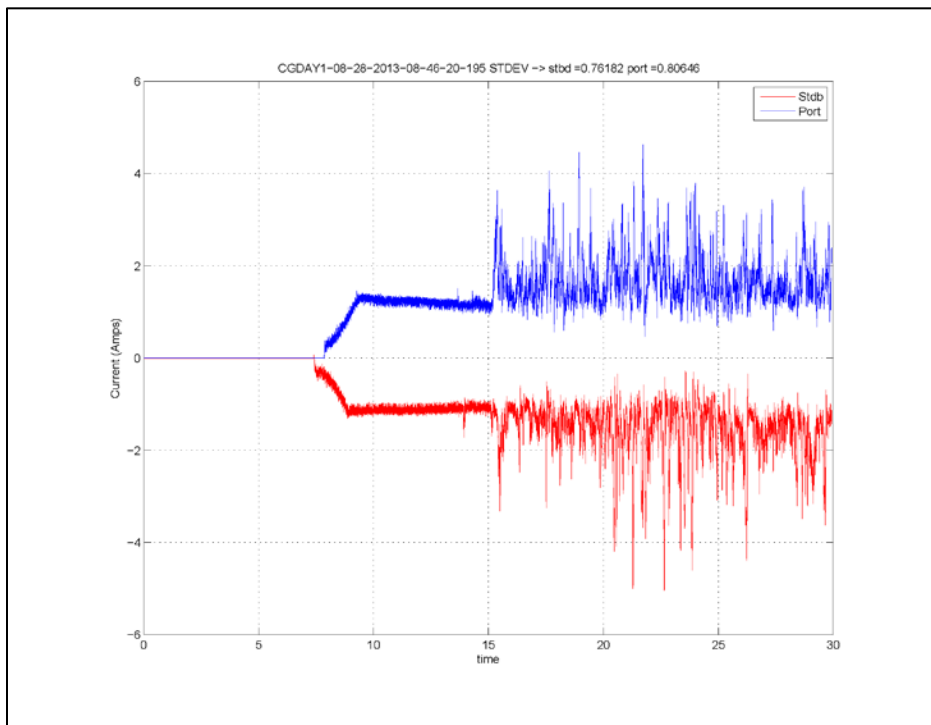
127 mm-thick ice field, carriage speed of 1.8 ms⁻¹
Current (Grams smoothing) vs. time (from 8 m to 18 m during constant carriage velocity)



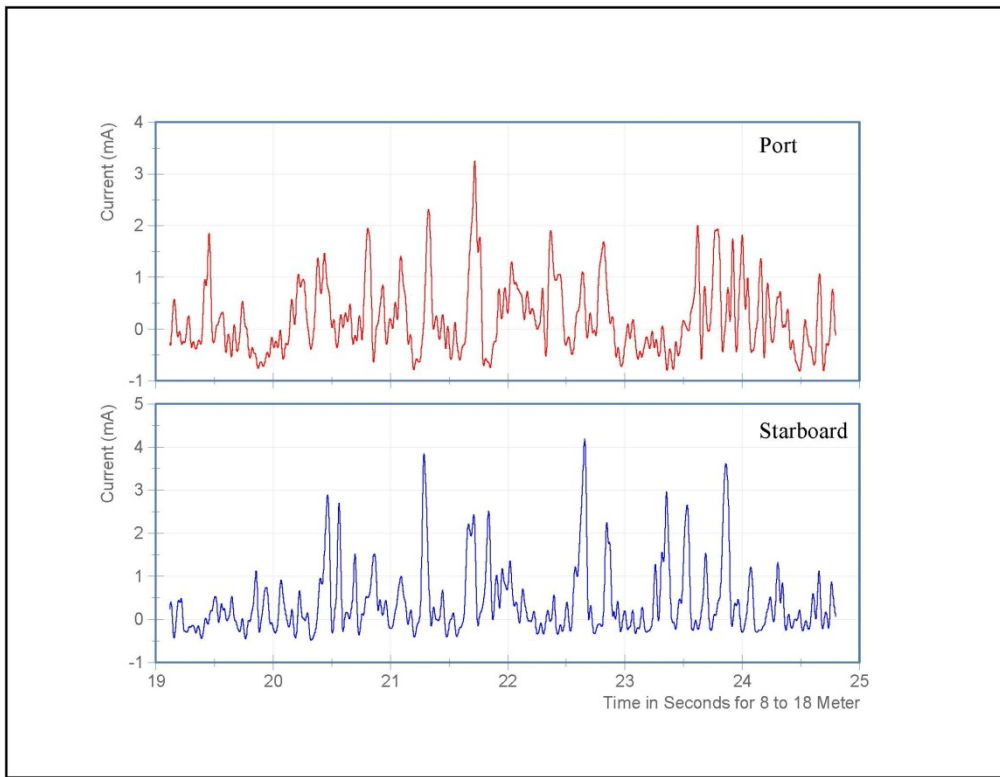
152 mm-thick ice field, carriage speed of 1.8 ms⁻¹
Speed and position plot vs. time



152 mm-thick ice field, carriage speed of 1.8 ms⁻¹
Current vs. time

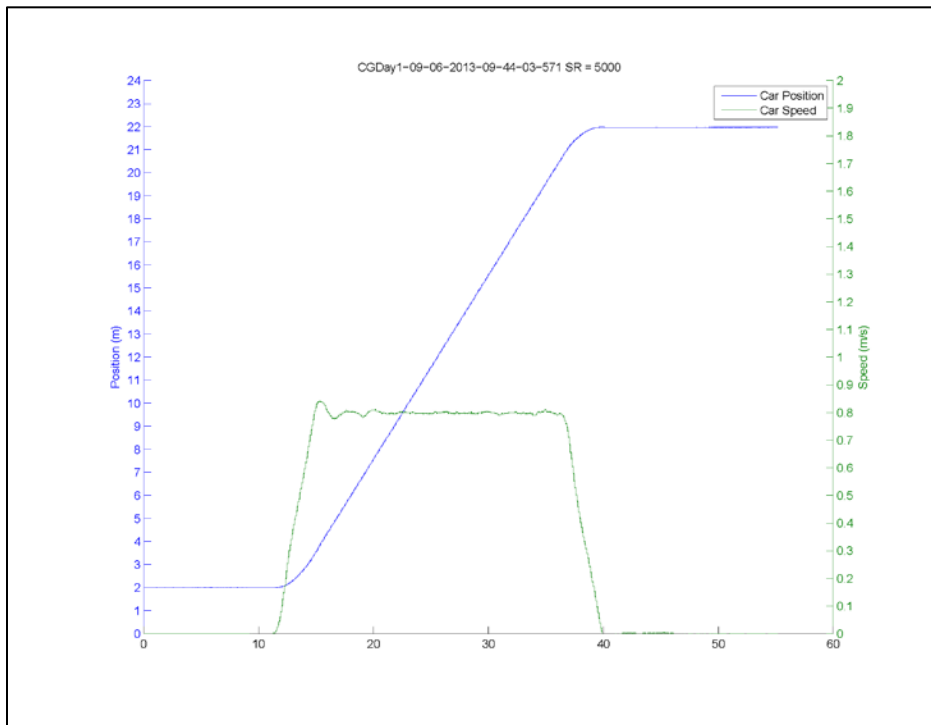


152 mm-thick ice field, carriage speed of 1.8 ms⁻¹
Current (Grams smoothing) vs. time (from 8 m to 18 m during constant carriage velocity)

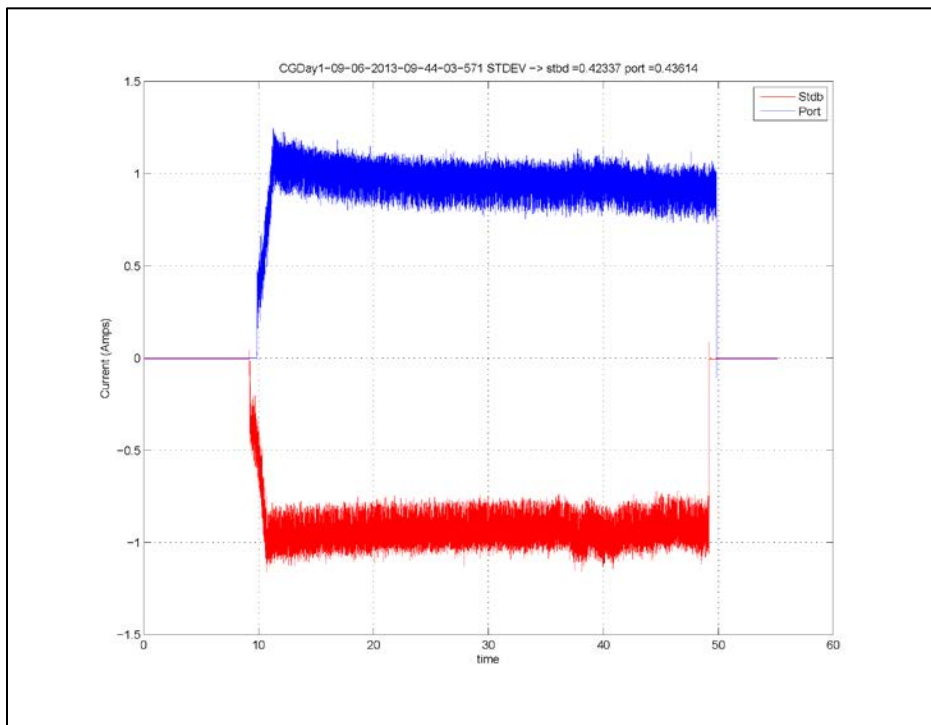


Appendix B: Shrouded-Propellers Plots

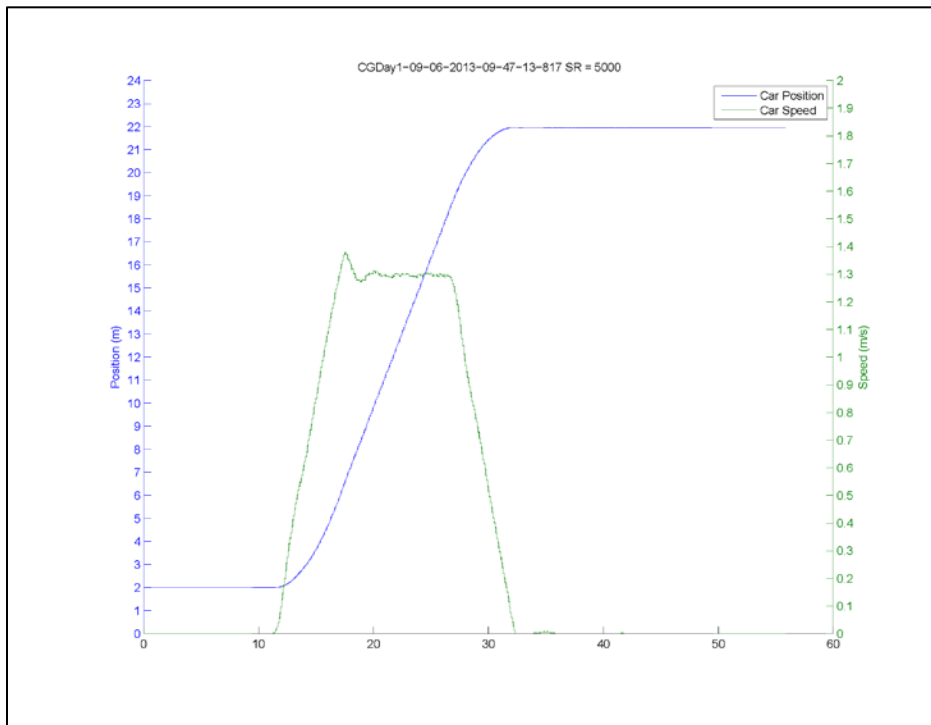
Open-water carriage speed of 0.8 ms⁻¹
Speed and position plot vs. time



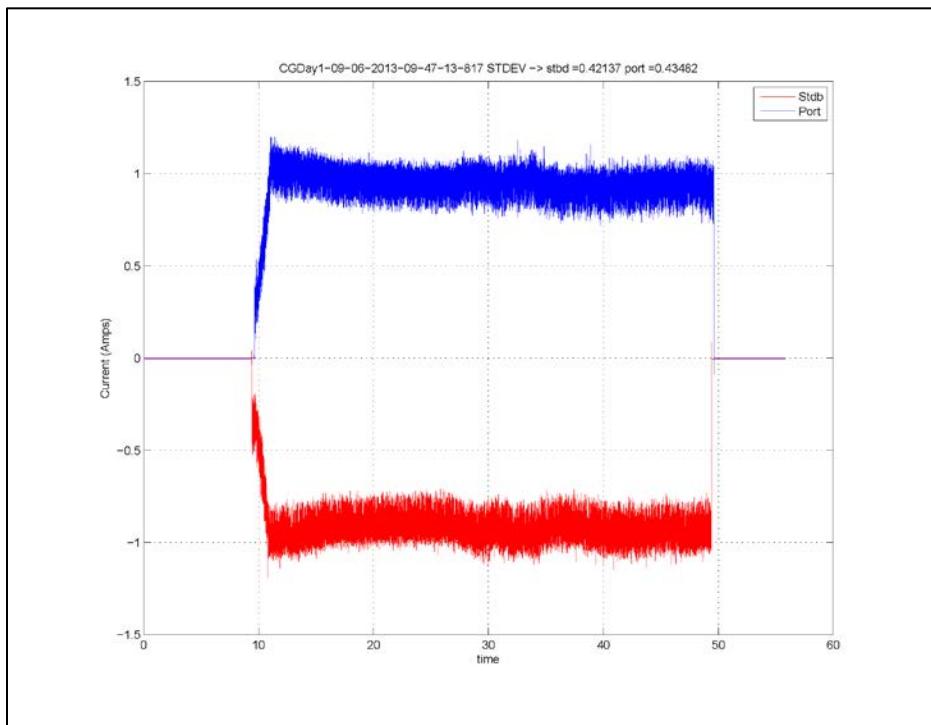
Open-water carriage speed of 0.8 ms⁻¹
Current vs. time



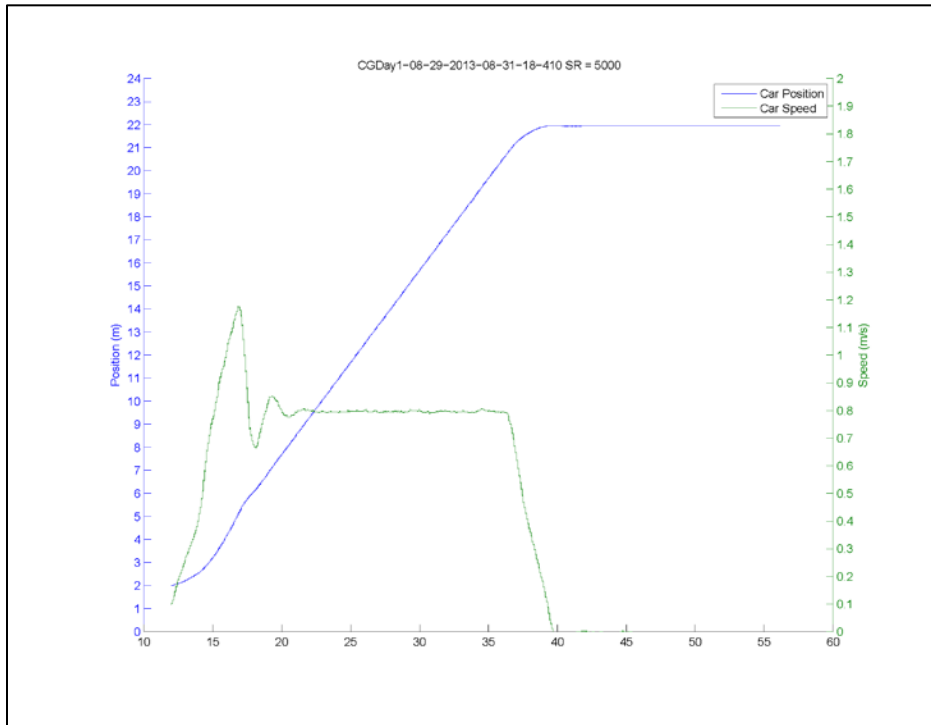
Open-water carriage speed of 1.3 ms⁻¹
Speed and position plot vs. time



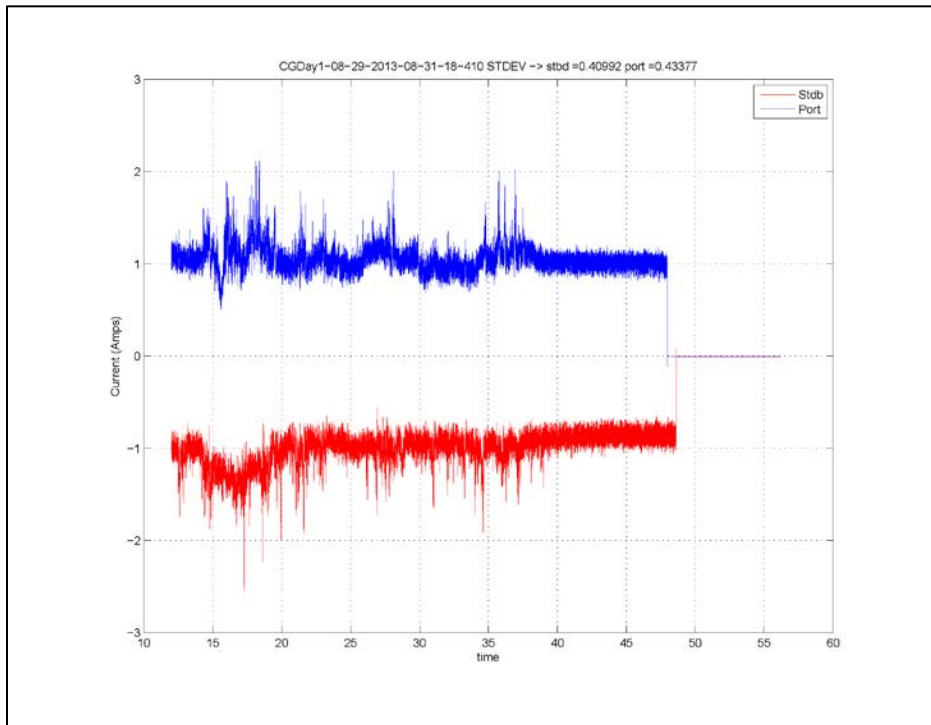
Open-water carriage speed of 1.3 ms⁻¹
Current vs. time



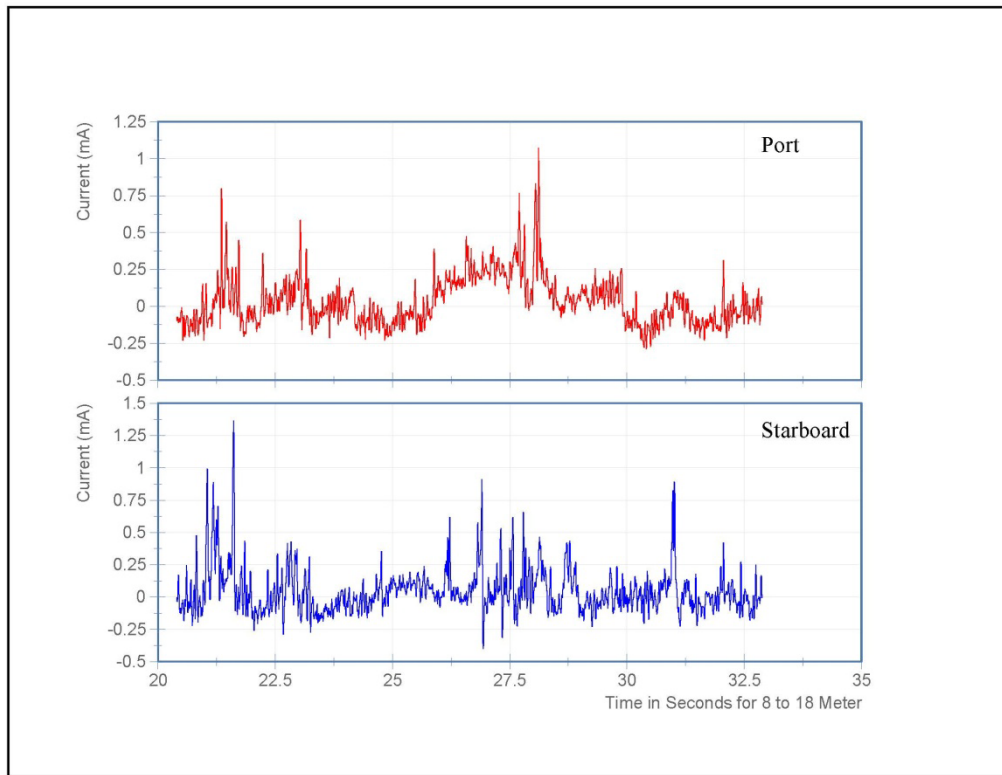
102 mm-thick ice field, carriage speed of 0.8 ms⁻¹
Speed and position plot vs. time



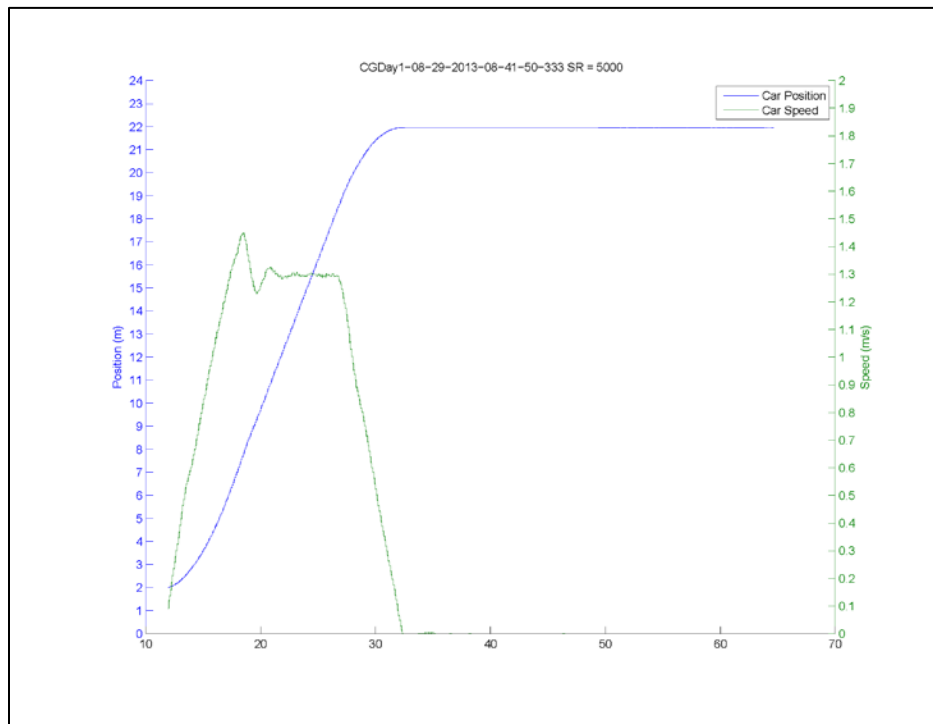
102 mm-thick ice field, carriage speed of 0.8 ms⁻¹
Current vs. time



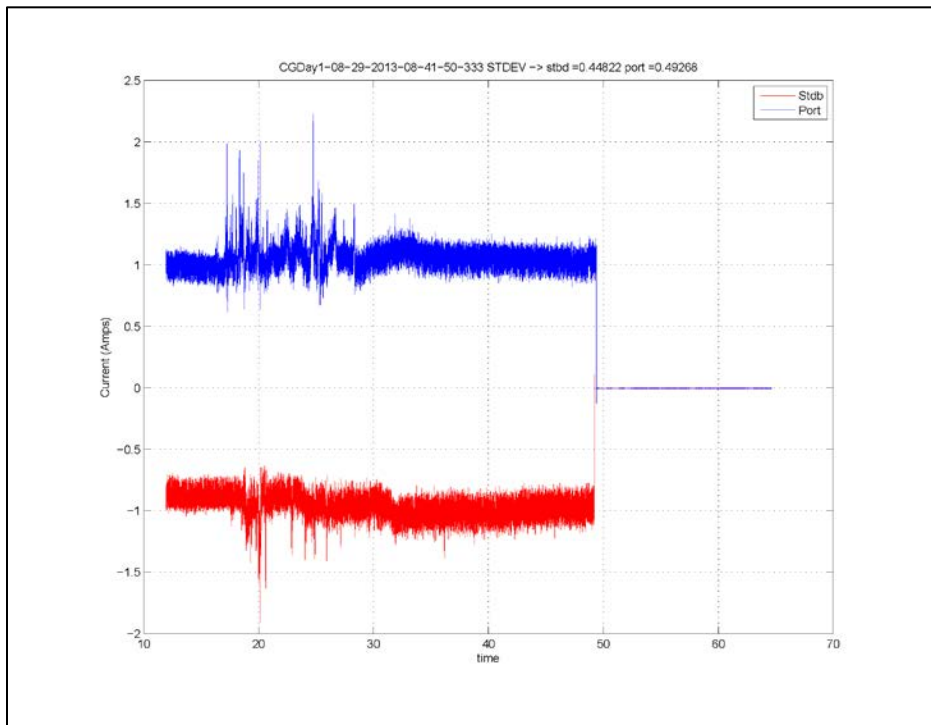
102 mm-thick ice field, carriage speed of 0.8 ms⁻¹
Current (Grams smoothing) vs. time (from 8 m to 18 m during constant carriage velocity)



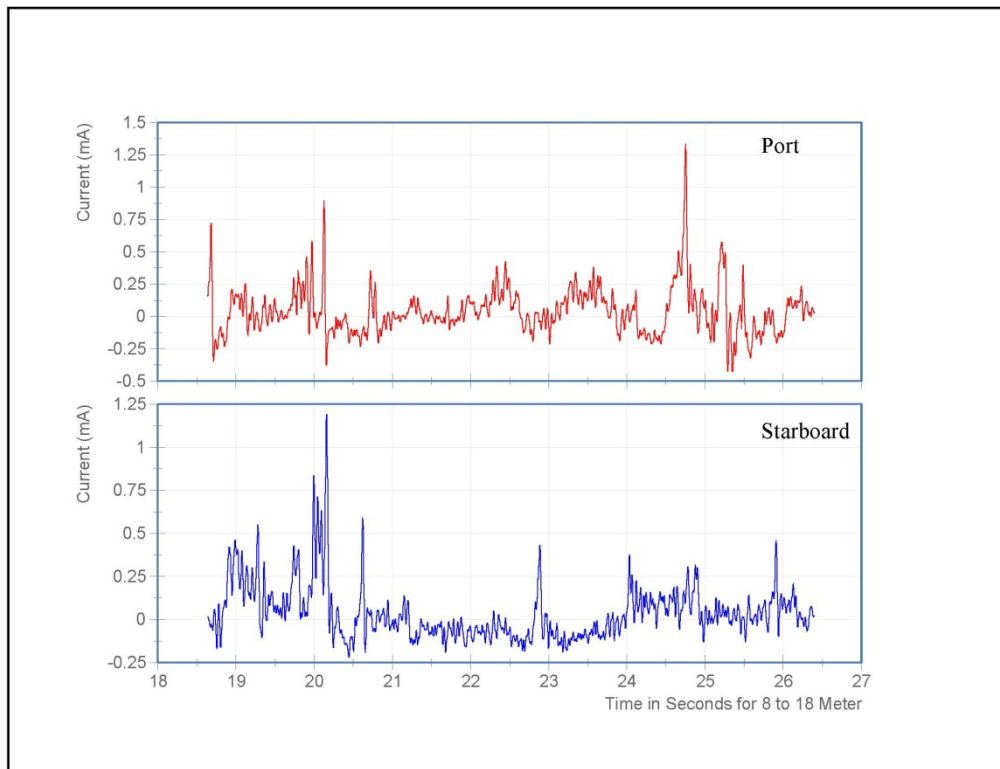
102 mm-thick ice field, carriage speed of 1.3 ms⁻¹
Speed and position plot vs. time



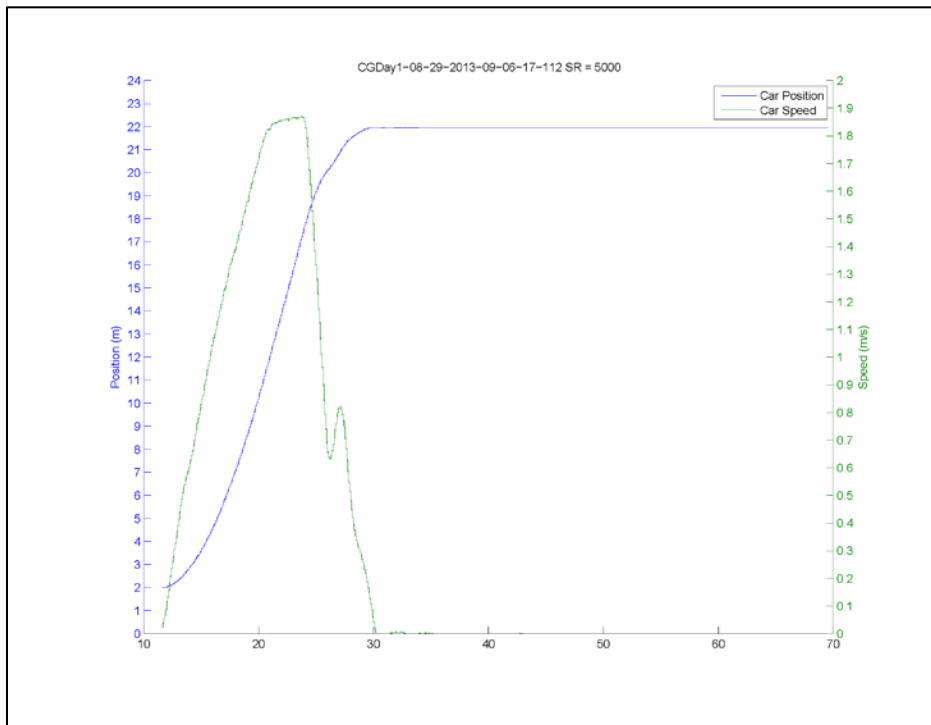
102 mm-thick ice field, carriage speed of 1.3 ms⁻¹
Current vs. time



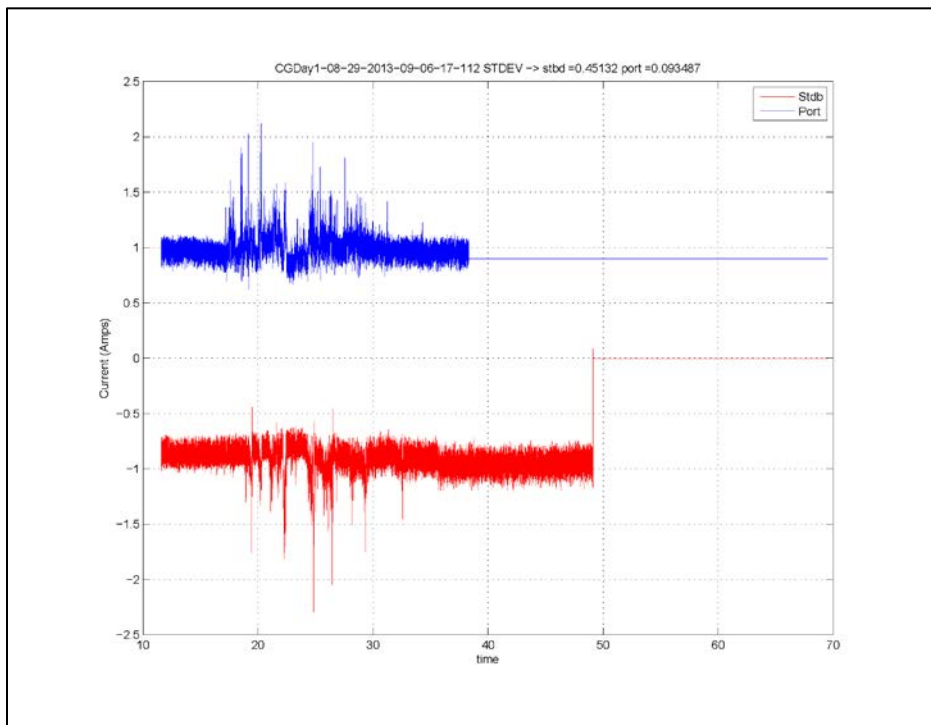
102 mm-thick ice field, carriage speed of 1.3 ms⁻¹
Current (Grams smoothing) vs. time (from 8 m to 18 m during constant carriage velocity)



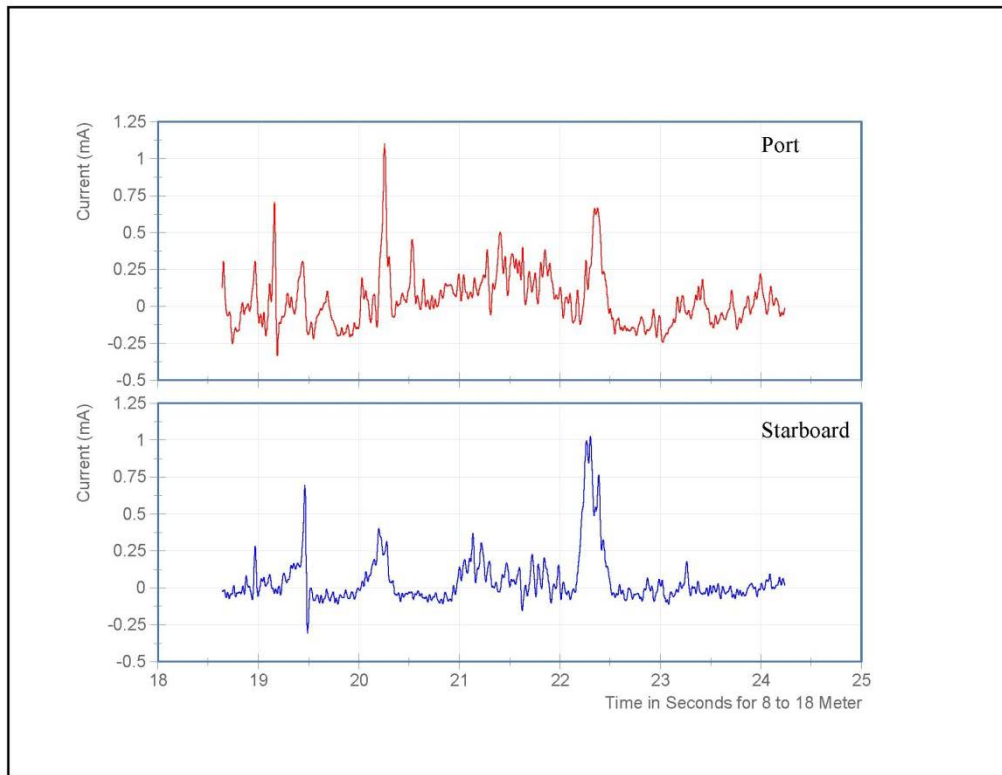
102 mm-thick ice field, carriage speed of 1.8 ms⁻¹
Speed and position plot vs. time



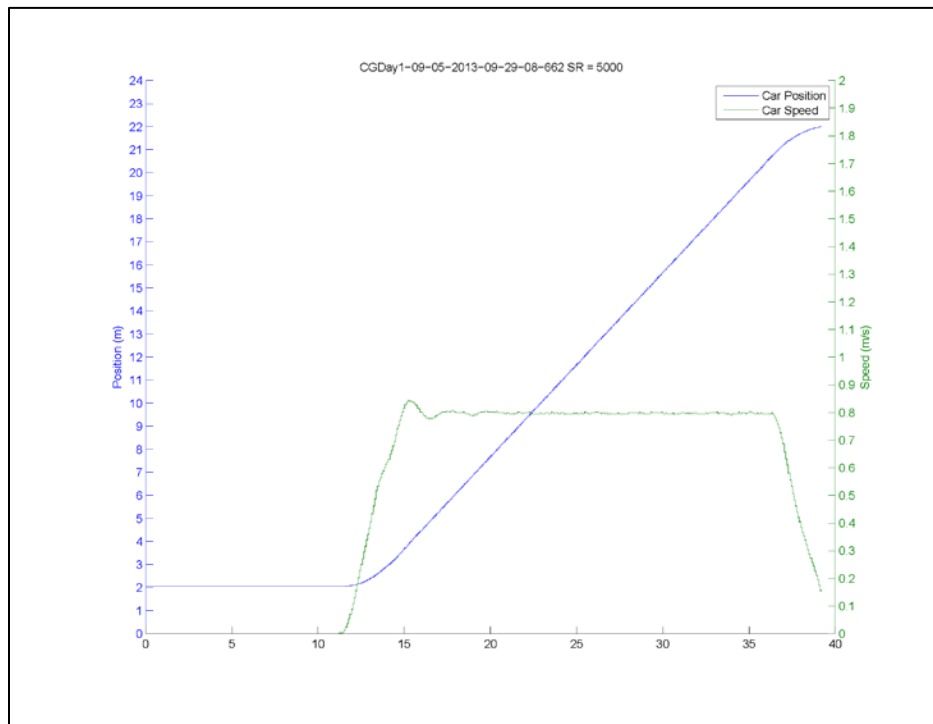
102 mm-thick ice field, carriage speed of 1.8 ms⁻¹
Current vs. time



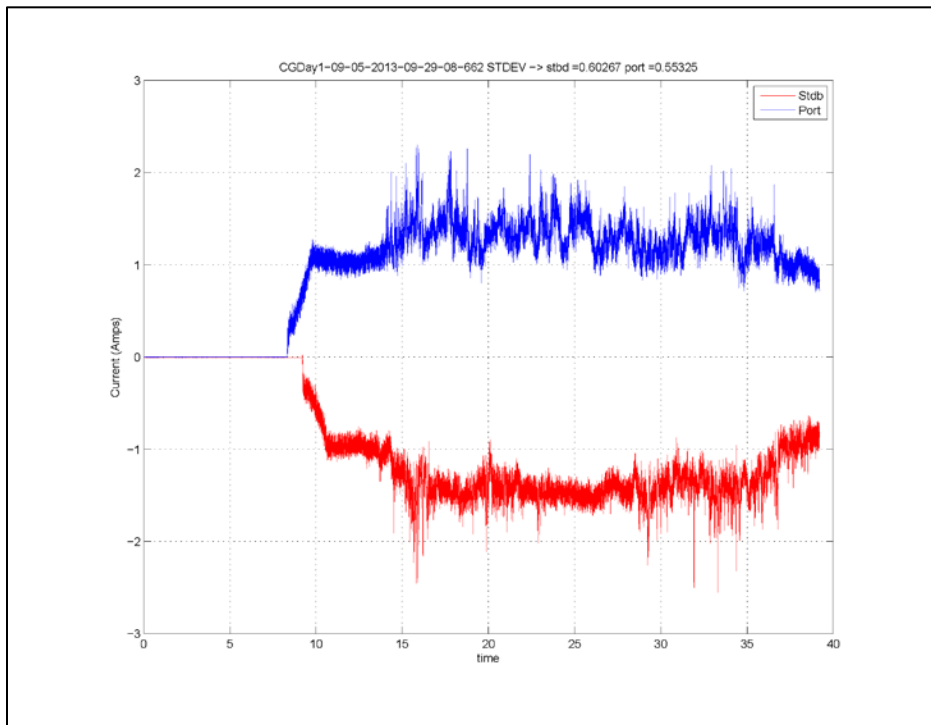
102 mm-thick ice field, carriage speed of 1.8 ms⁻¹
Current (Grams smoothing) vs. time (from 8 m to 18 m during constant carriage velocity)



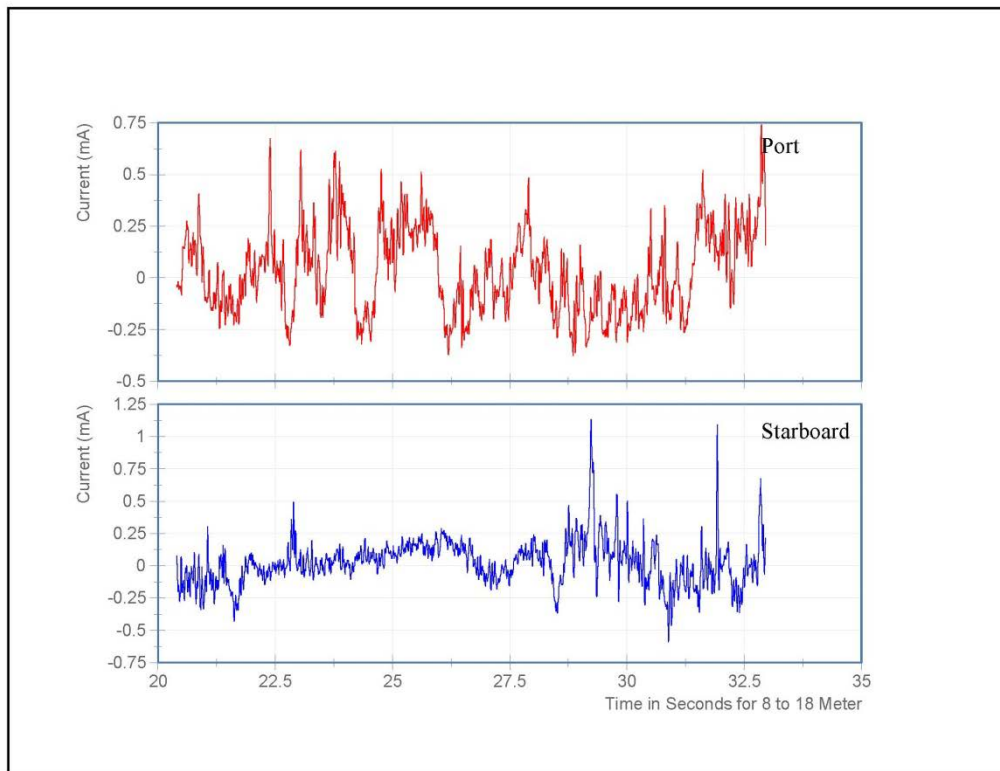
127 mm-thick ice field, carriage speed of 0.8 ms⁻¹
Speed and position plot vs. time



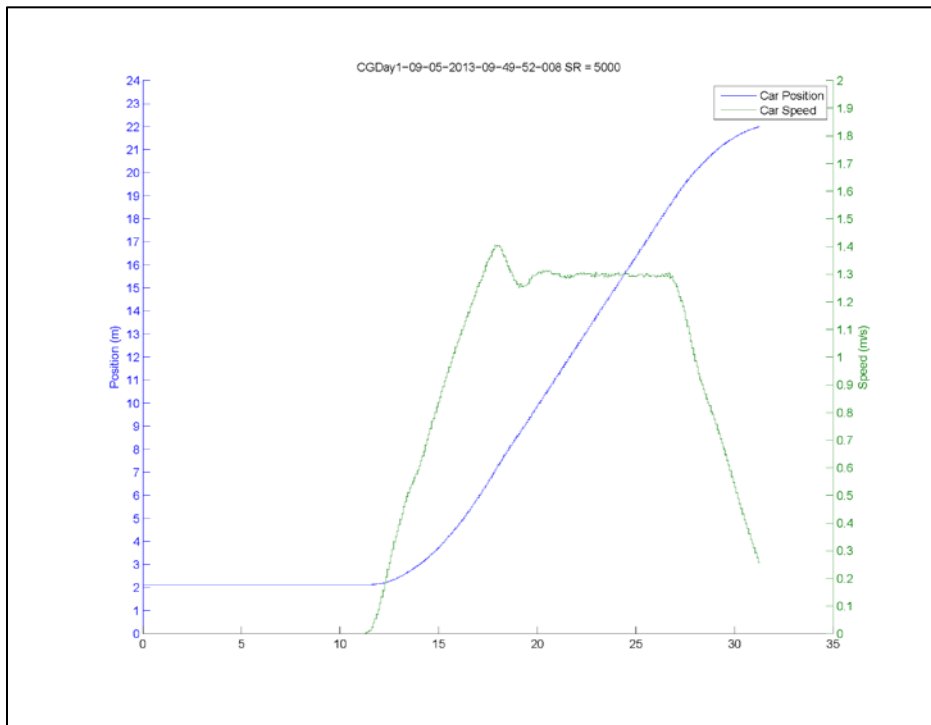
127 mm-thick ice field, carriage speed of 0.8 ms⁻¹
Current vs. time



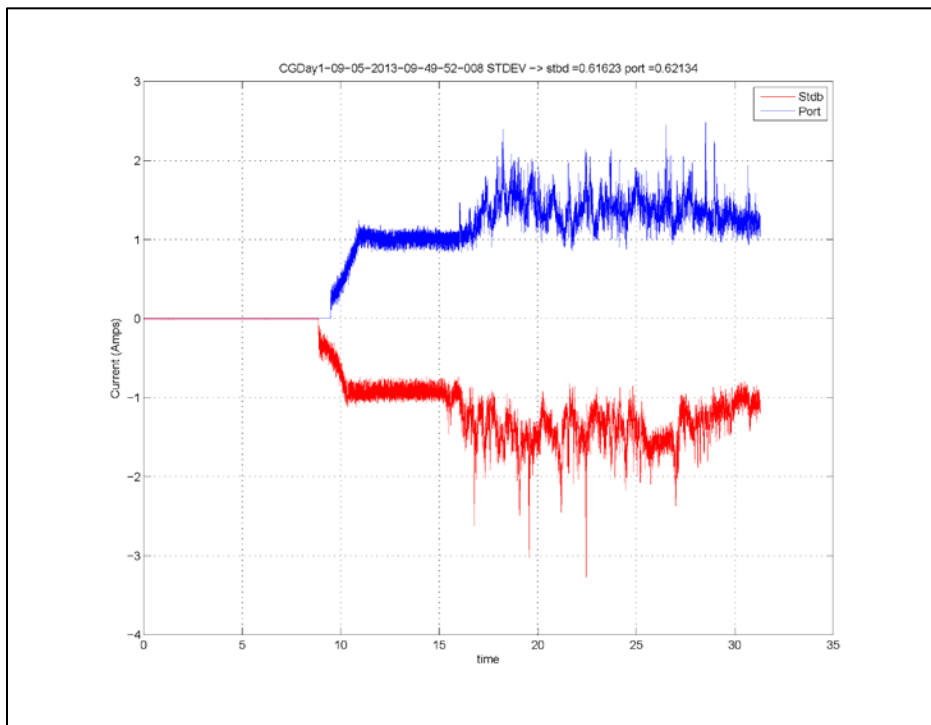
127 mm-thick ice field, carriage speed of 0.8 ms⁻¹
Current (Grams smoothing) vs. time (from 8 m to 18 m during constant carriage velocity)



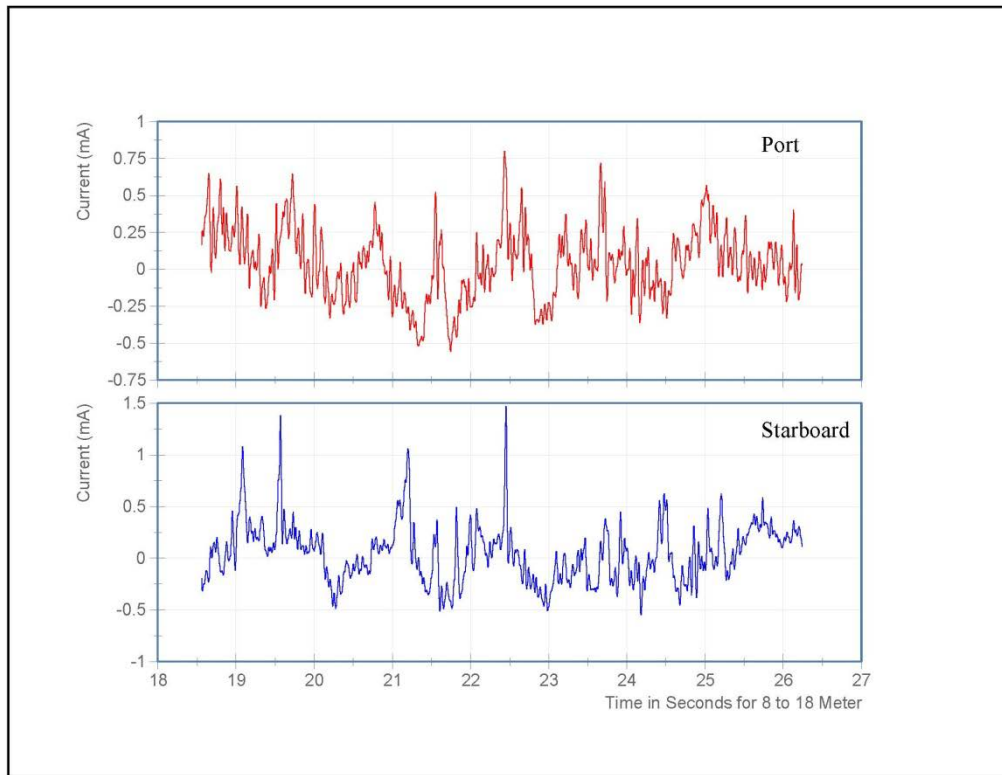
127 mm-thick ice field, carriage speed of 1.3 ms⁻¹
Speed and position plot vs. time



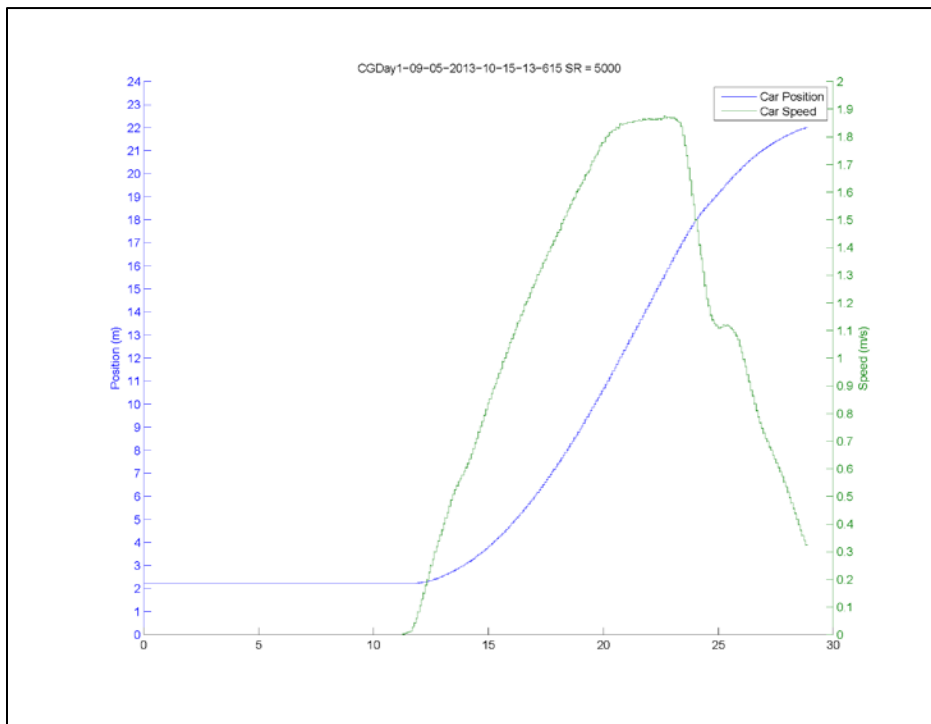
127 mm-thick ice field, carriage speed of 1.3 ms⁻¹
Current vs. time



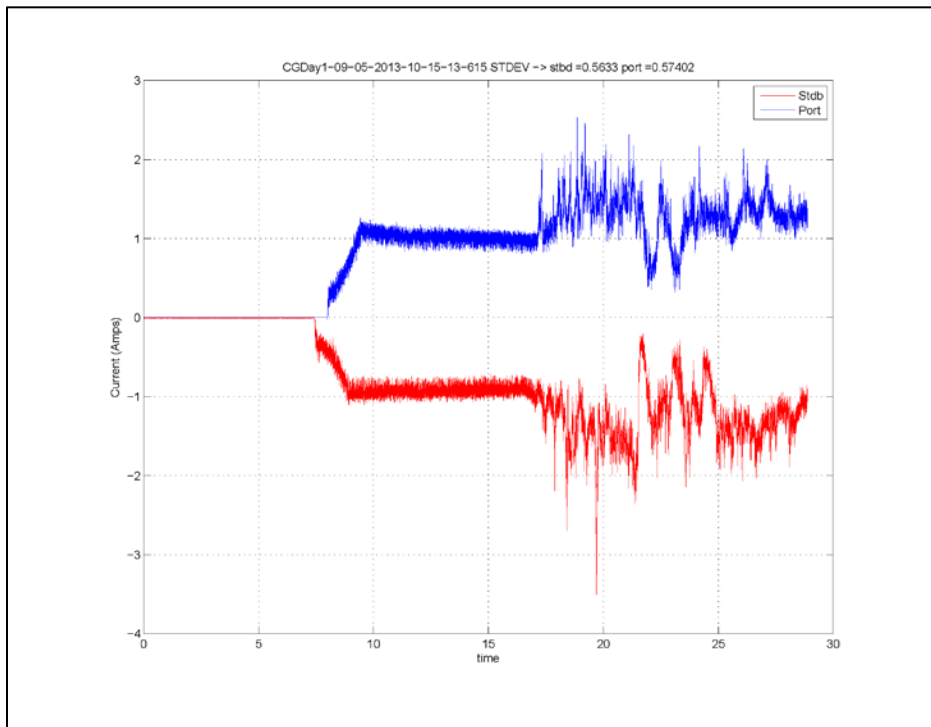
127 mm-thick ice field, carriage speed of 1.3 ms⁻¹
Current (Grams smoothing) vs. time (from 8 m to 18 m during constant carriage velocity)



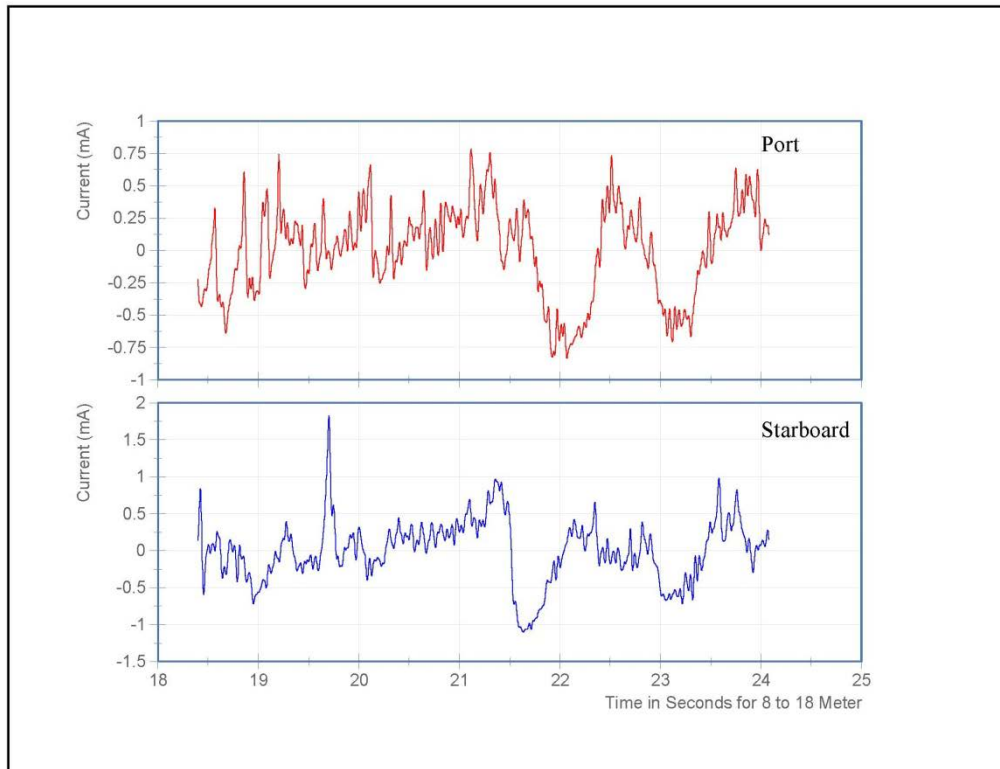
127 mm-thick ice field, carriage speed of 1.8 ms⁻¹
Speed and position plot vs. time



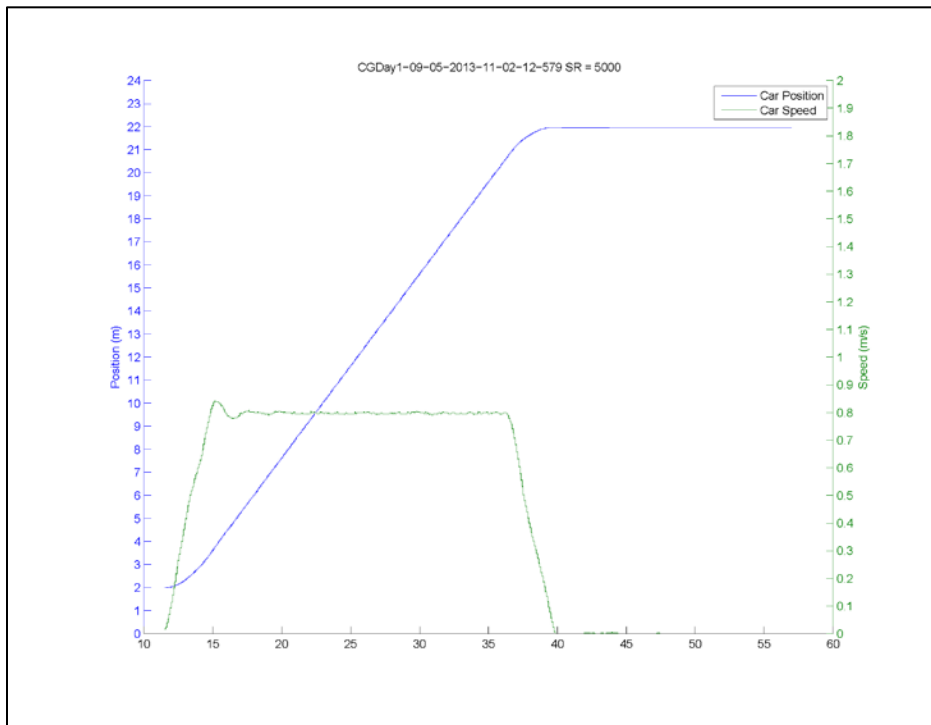
127 mm-thick ice field, carriage speed of 1.8 ms⁻¹
Current vs. time



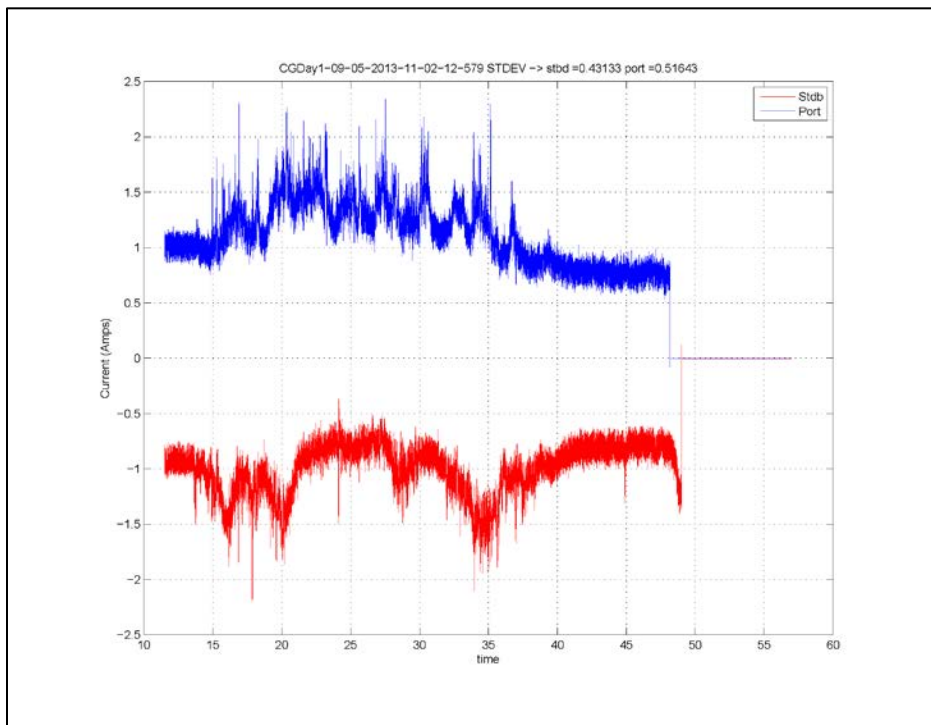
127 mm-thick ice field, carriage speed of 1.8 ms⁻¹
Current (Grams smoothing) vs. time (from 8 m to 18 m during constant carriage velocity)



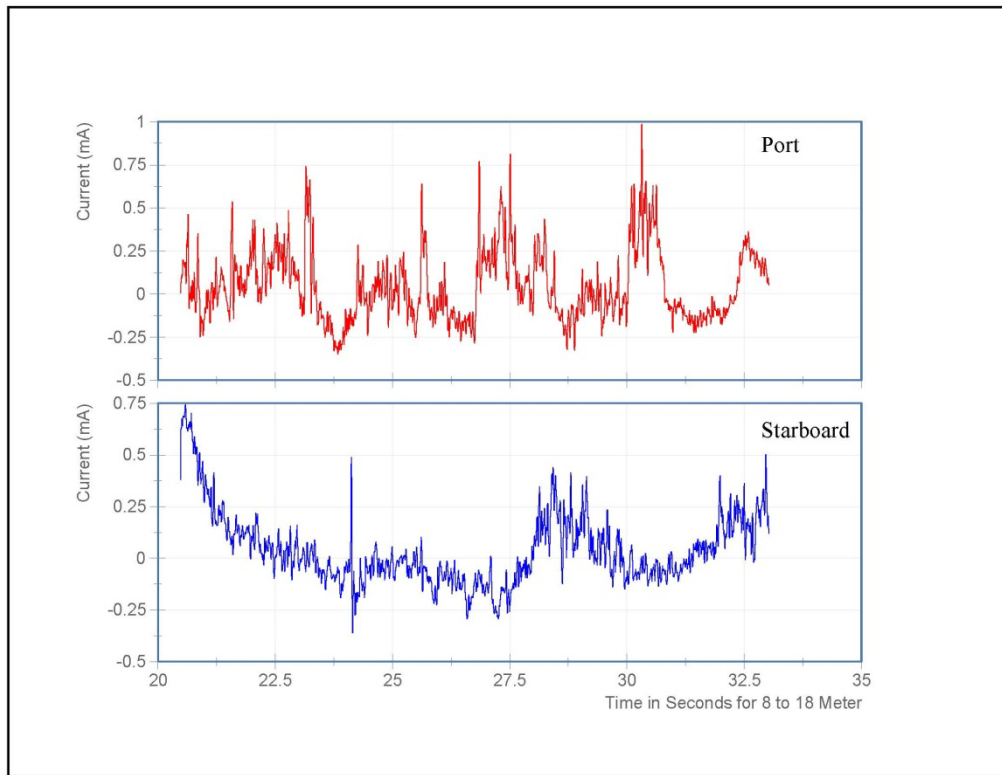
152 mm-thick ice field, carriage speed of 0.8 ms⁻¹
Speed and position plot vs. time



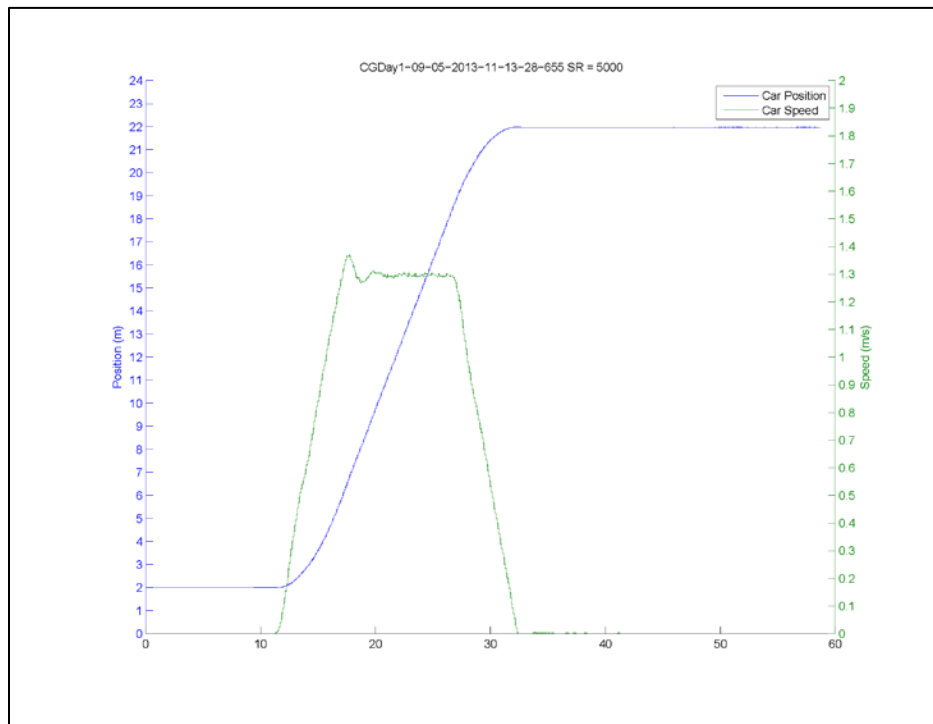
152 mm-thick ice field, carriage speed of 0.8 ms⁻¹
Current vs. time



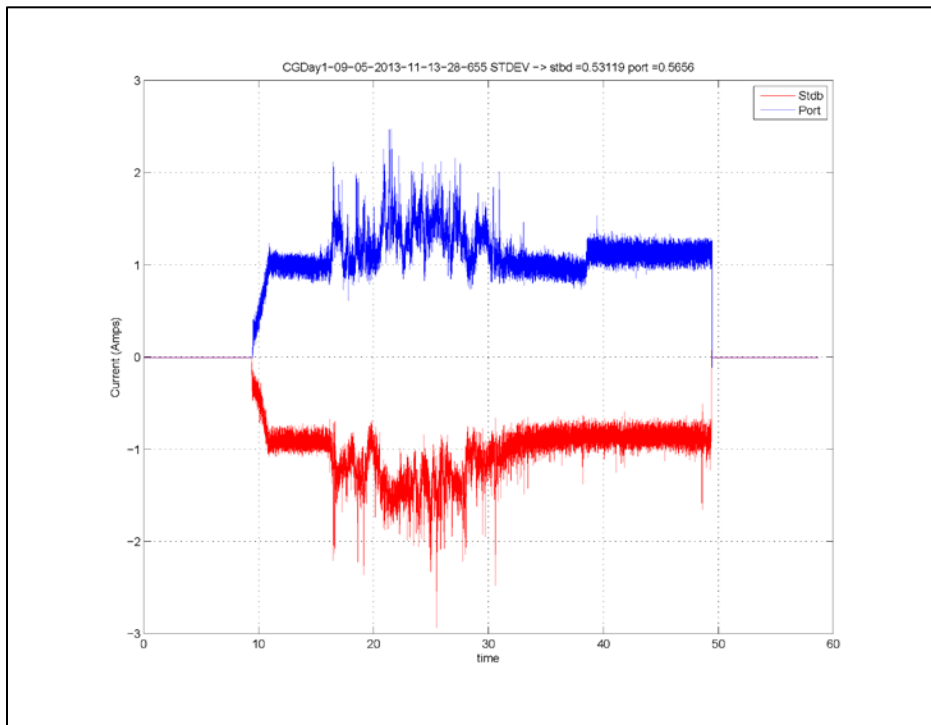
152 mm-thick ice field, carriage speed of 0.8 ms⁻¹
Current (Grams smoothing) vs. time (from 8 m to 18 m during constant carriage velocity)



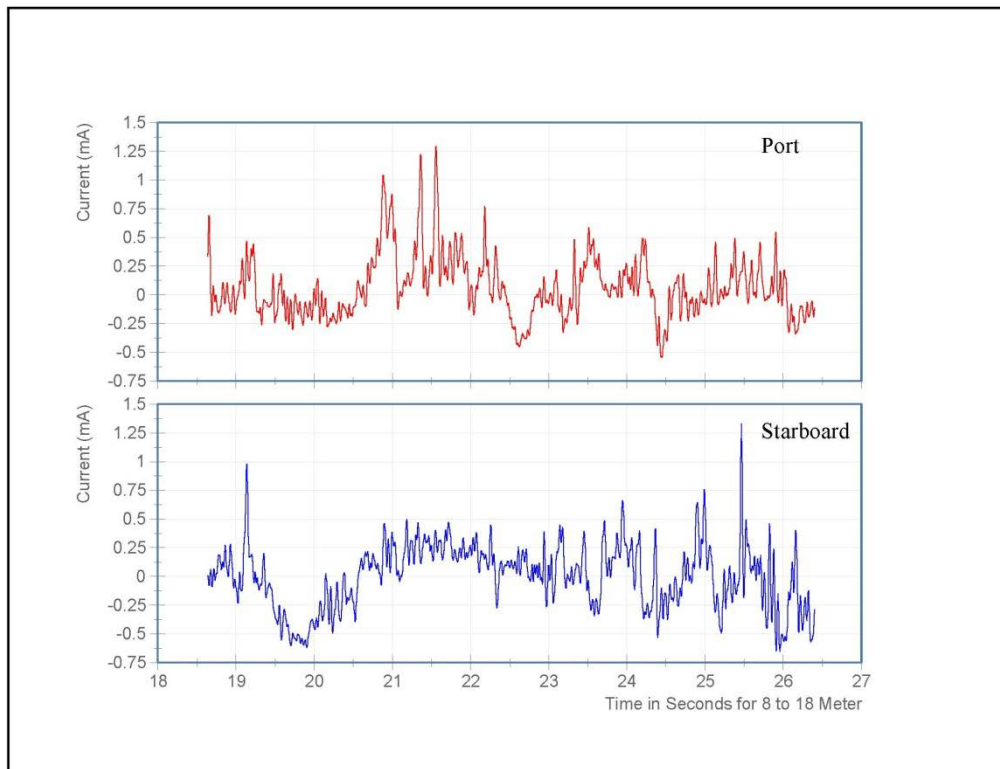
152 mm-thick ice field, carriage speed of 1.3 ms⁻¹
Speed and position plot vs. time



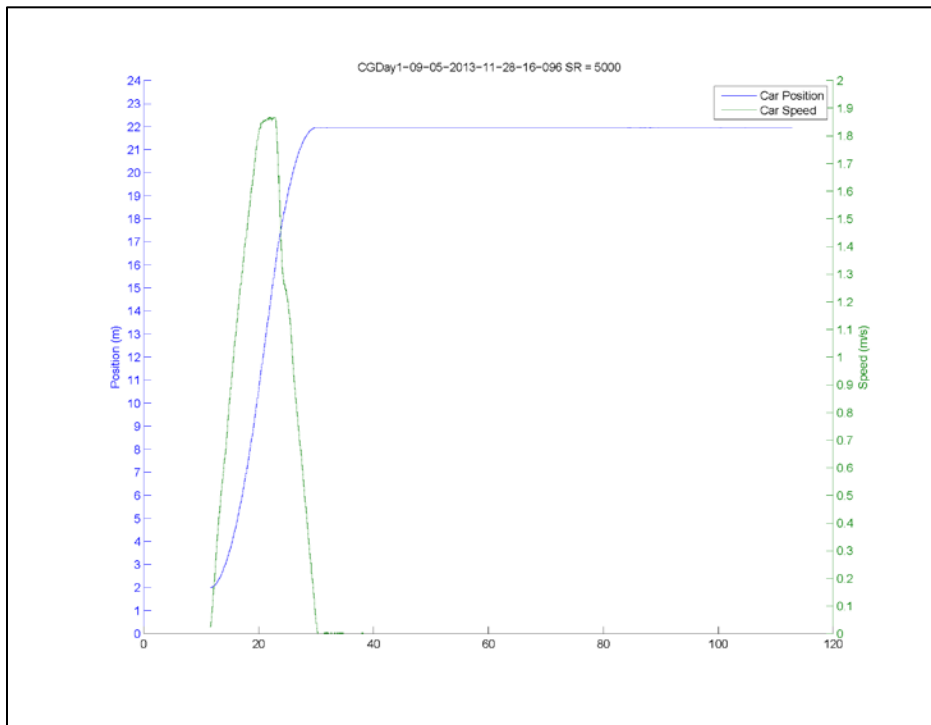
152 mm-thick ice field, carriage speed of 1.3 ms⁻¹
Current vs. time



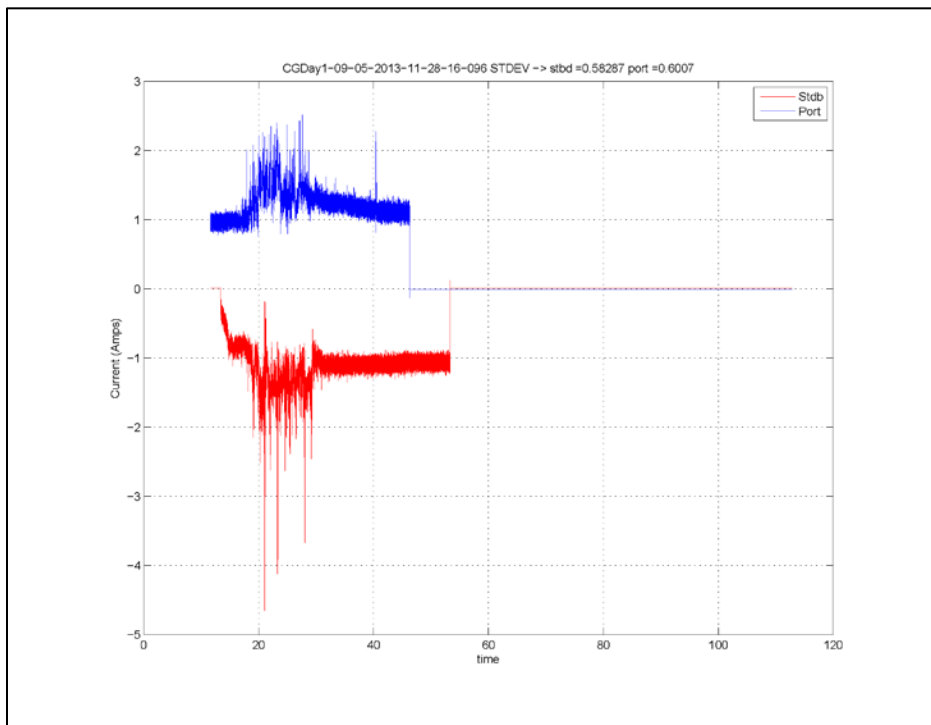
152 mm-thick ice field, carriage speed of 1.3 ms⁻¹
Current (Grams smoothing) vs. time (from 8 m to 18 m during constant carriage velocity)



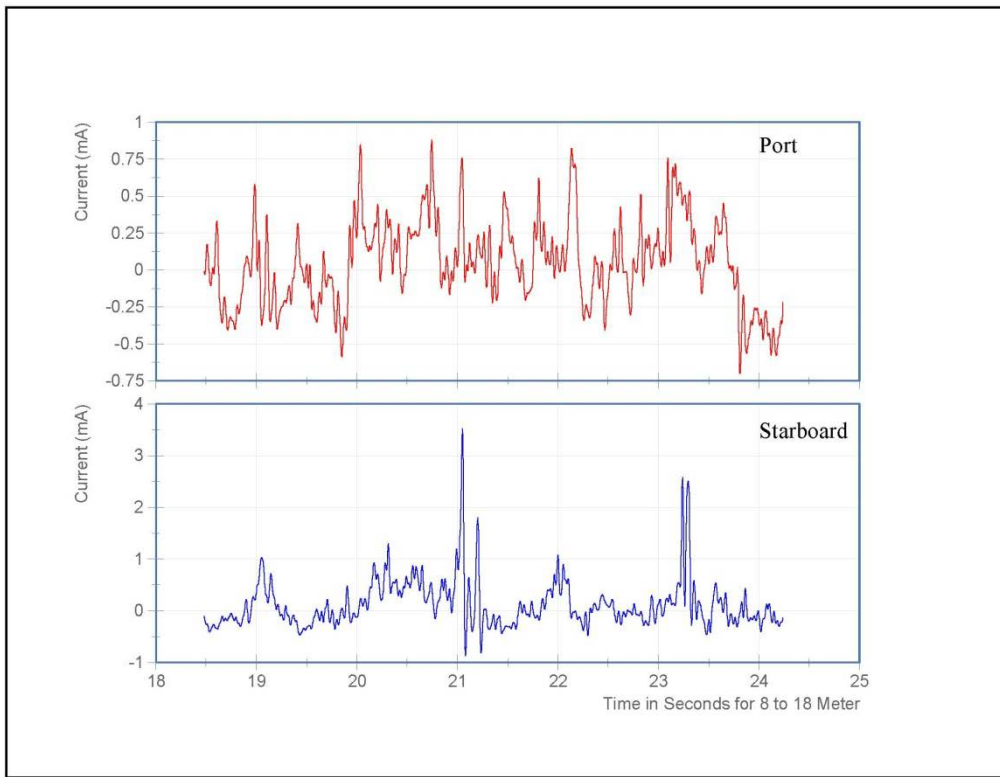
152 mm-thick ice field, carriage speed of 1.8 ms⁻¹
Speed and position plot vs. time



152 mm-thick ice field, carriage speed of 1.8 ms⁻¹
Current vs. time

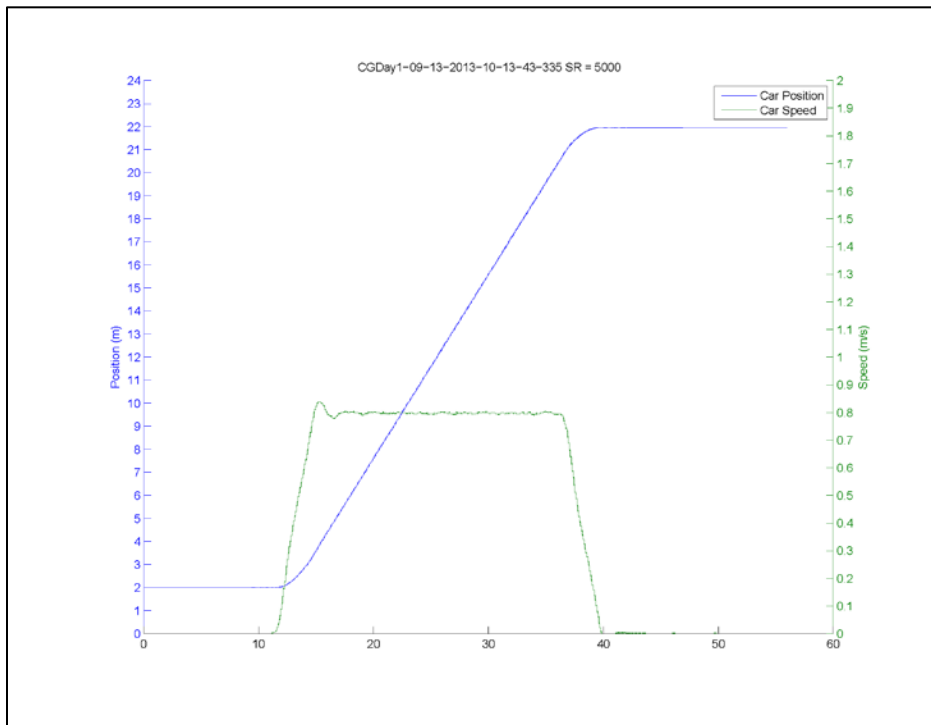


152 mm-thick ice field, carriage speed of 1.8 ms⁻¹
Current (Grams smoothing) vs. time (from 8 m to 18 m during constant carriage velocity)

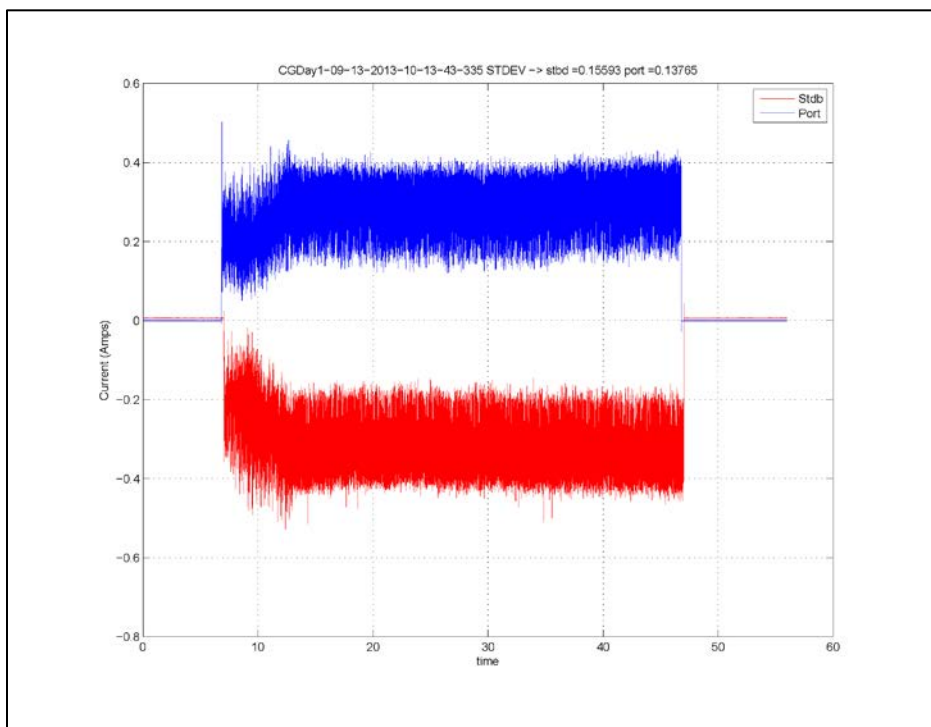


Appendix C: Waterjet Intake System Plots

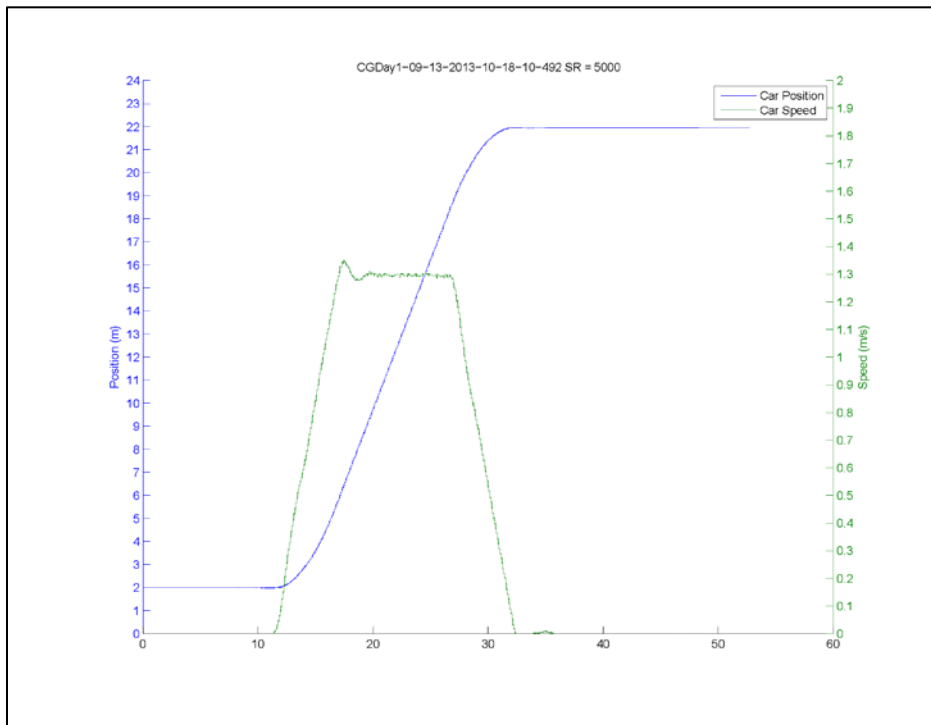
Open-water carriage speed of 0.8 ms⁻¹
Speed and position plot vs. time



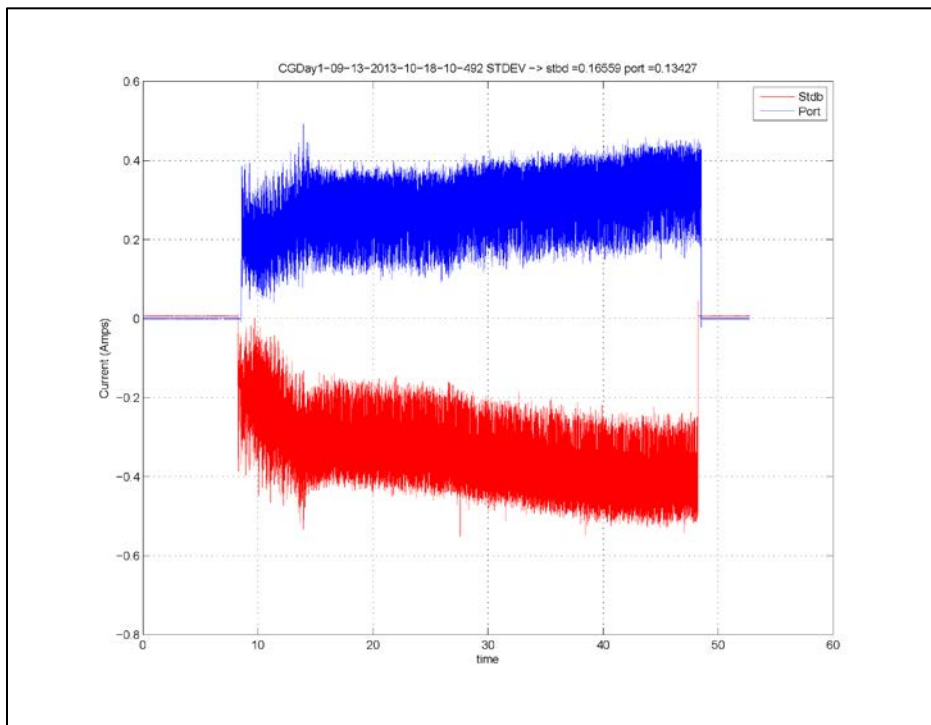
Open-water carriage speed of 0.8 ms⁻¹
Current vs. time



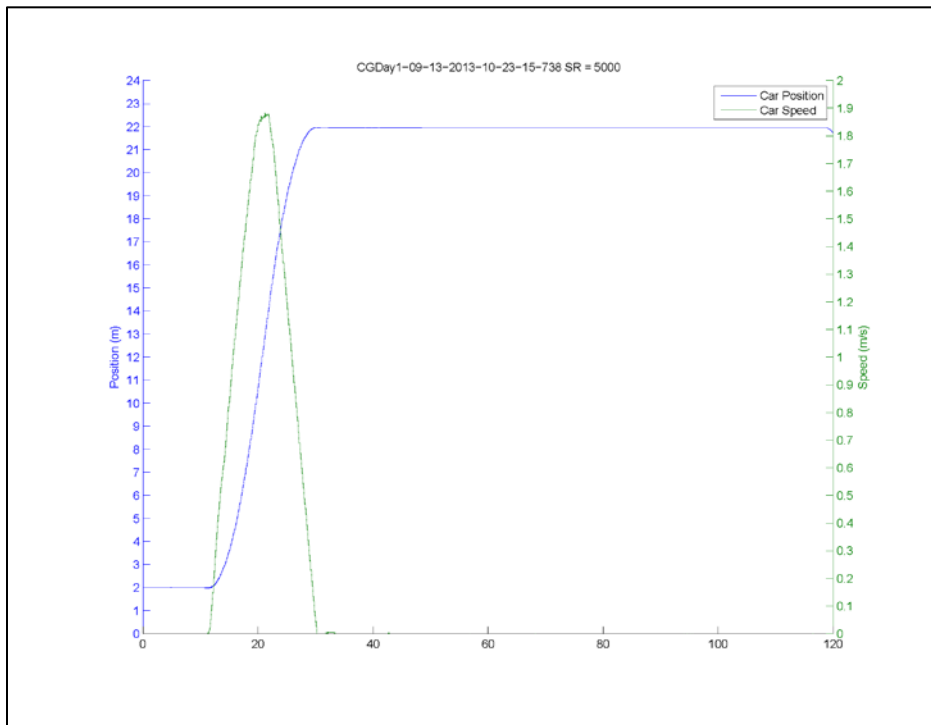
Open-water carriage speed of 1.3 ms⁻¹
Speed and position plot vs. time



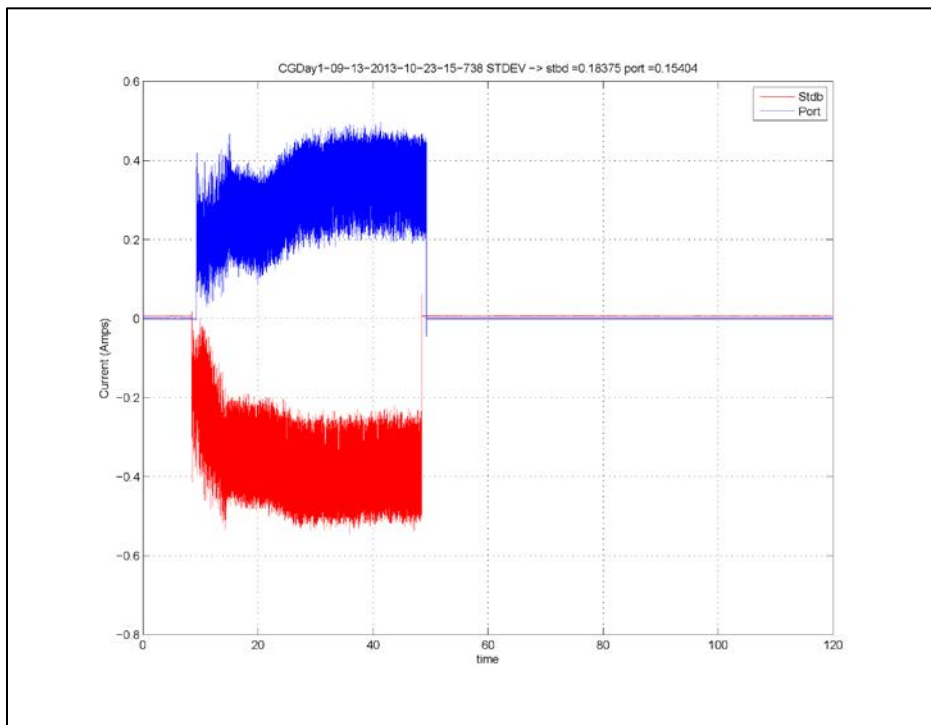
Open-water carriage speed of 1.3 ms⁻¹
Current vs. time



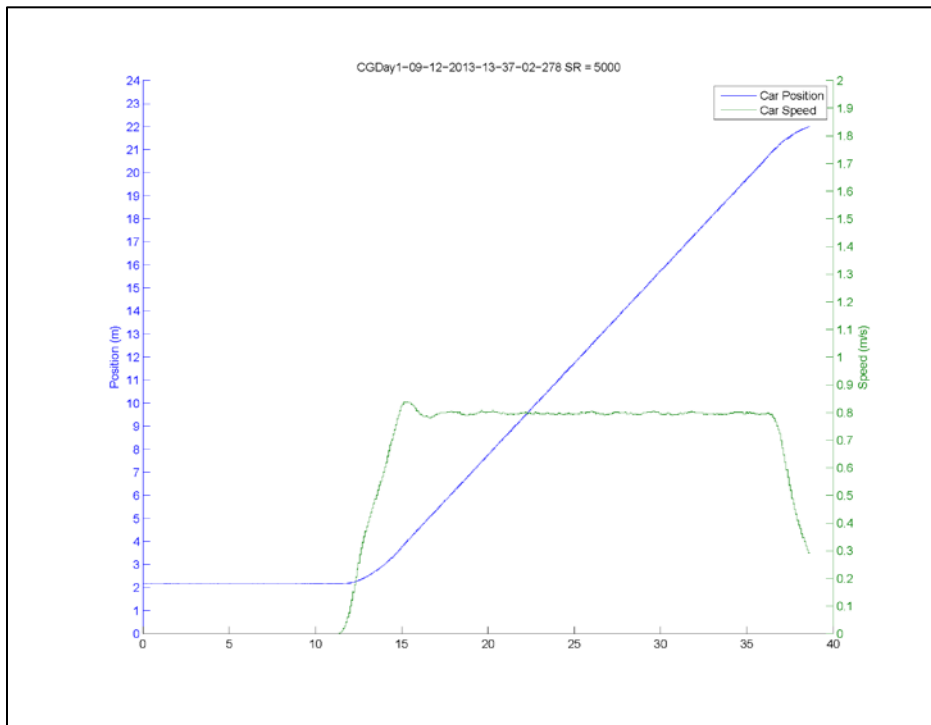
Open-water carriage speed of 1.8 ms⁻¹
Speed and position plot vs. time



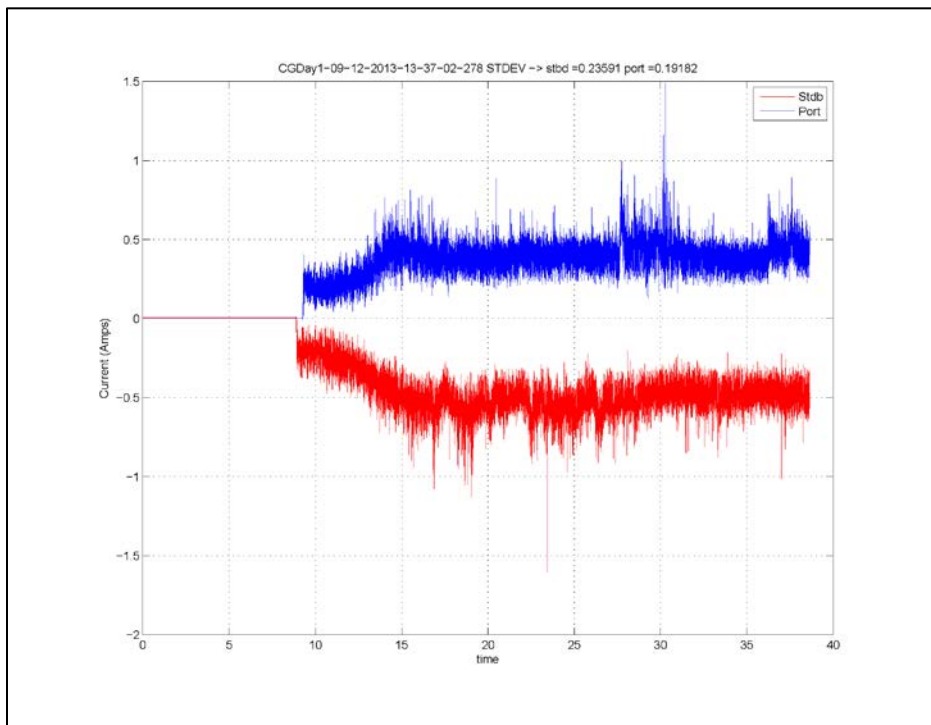
Open-water carriage speed of 1.8 ms⁻¹
Current vs. time



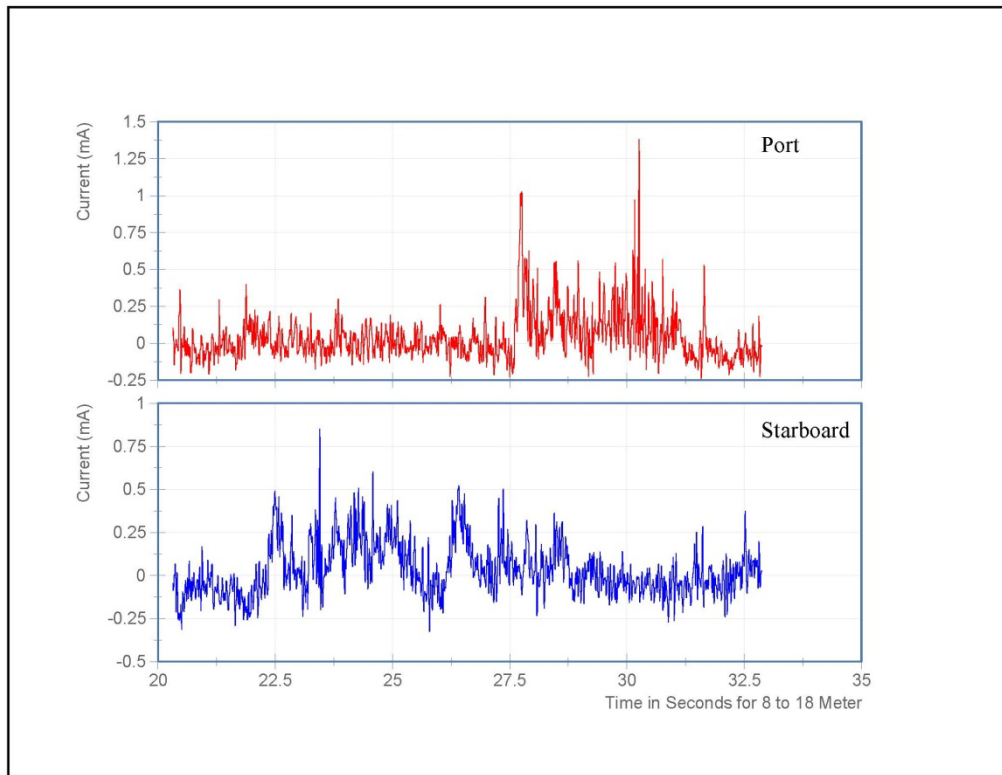
102 mm-thick ice field, carriage speed of 0.8 ms⁻¹
Speed and position plot vs. time



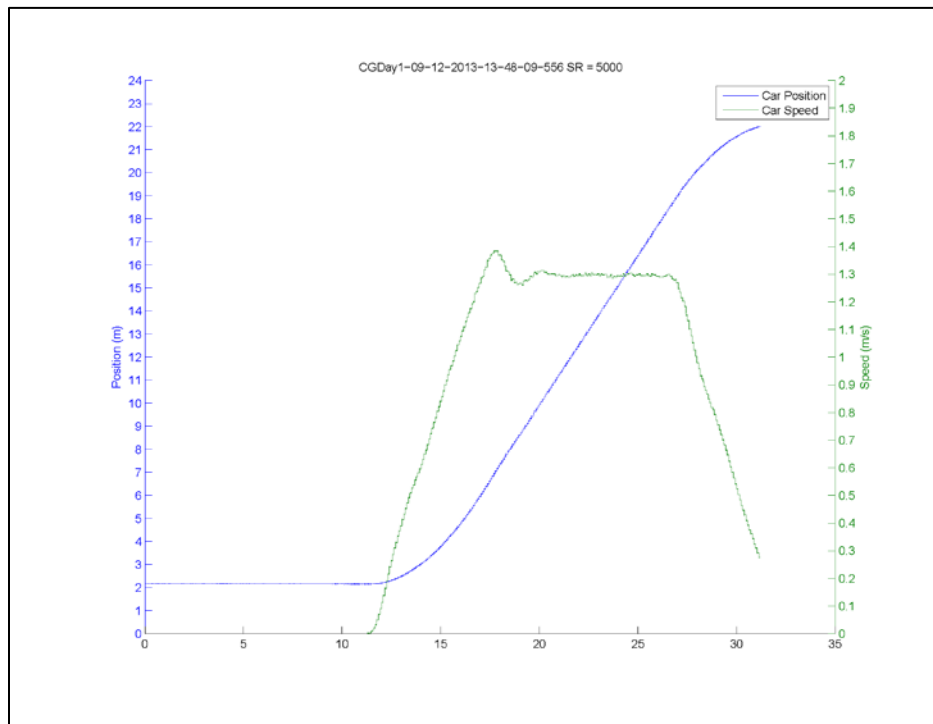
102 mm-thick ice field, carriage speed of 0.8 ms⁻¹
Current vs. time



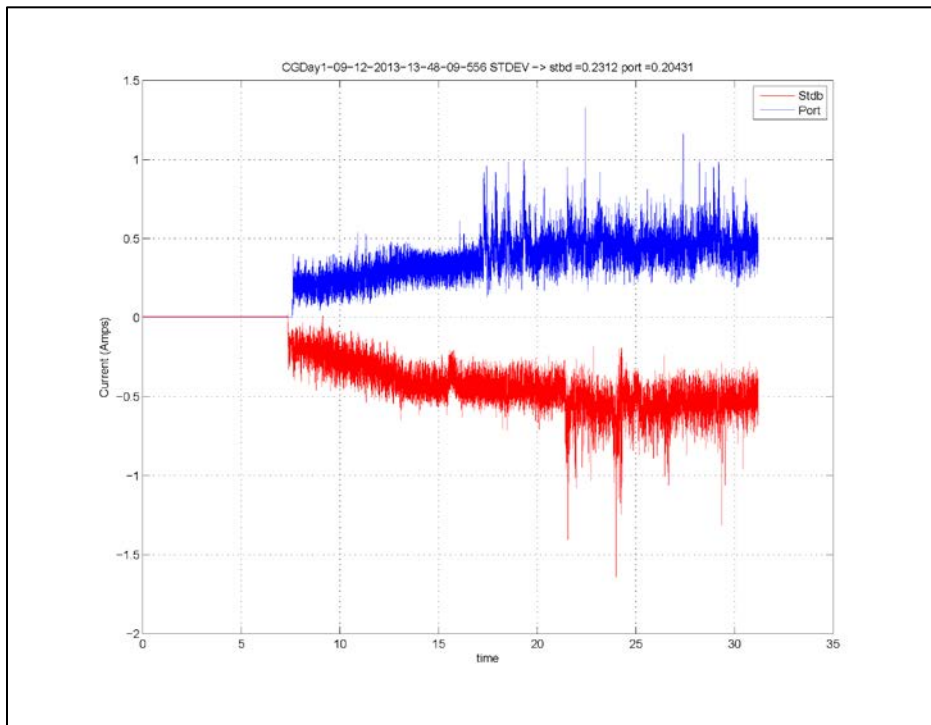
102 mm-thick ice field, carriage speed of 0.8 ms⁻¹
Current (Grams smoothing) vs. time (from 8 m to 18 m during constant carriage velocity)



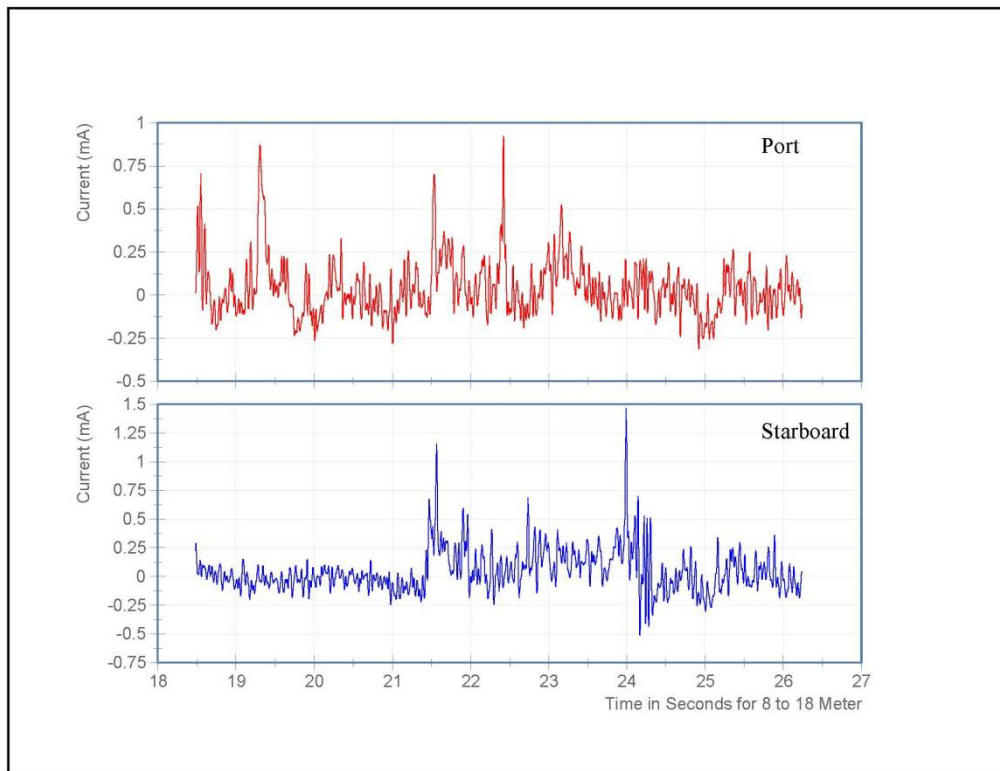
102 mm-thick ice field, carriage speed of 1.3 ms⁻¹
Speed and position plot vs. time



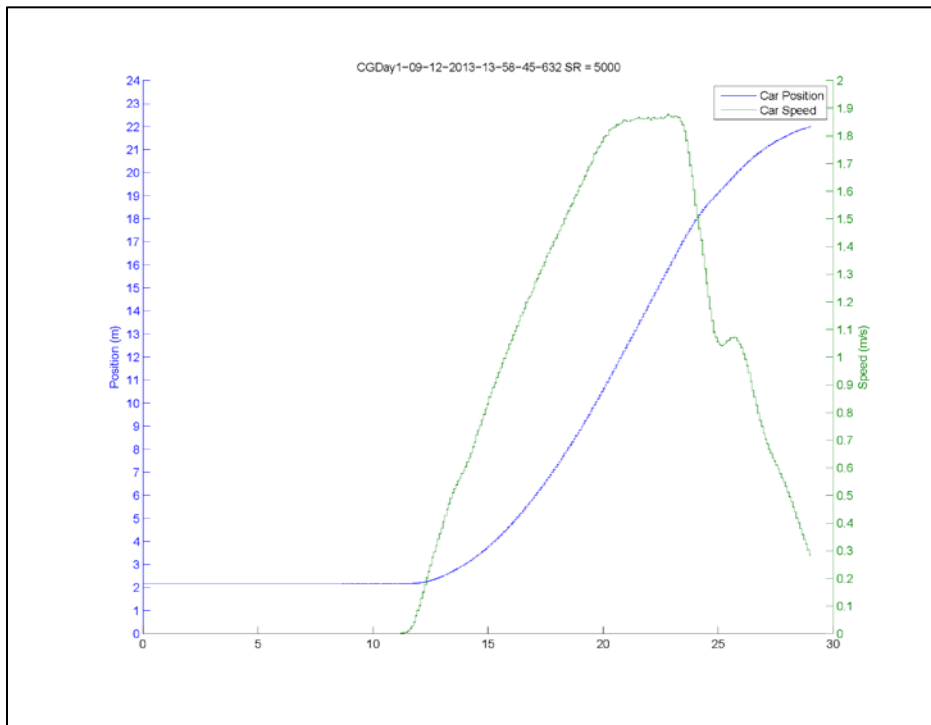
102 mm-thick ice field, carriage speed of 1.3 ms⁻¹
Current vs. time



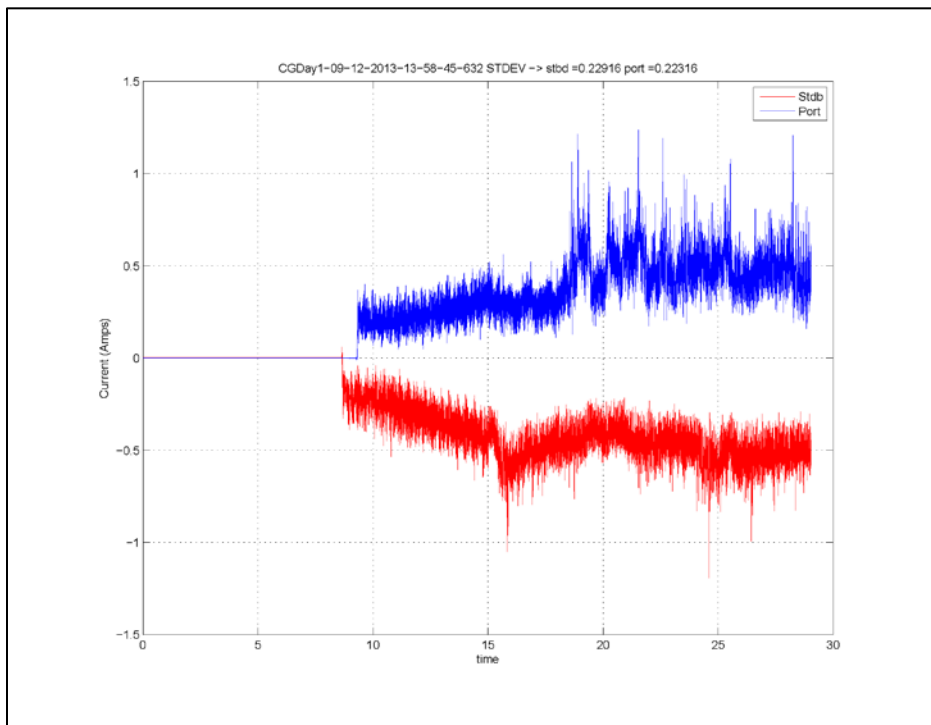
102 mm-thick ice field, carriage speed of 1.3 ms⁻¹
Current (Grams smoothing) vs. time (from 8 m to 18 m during constant carriage velocity)



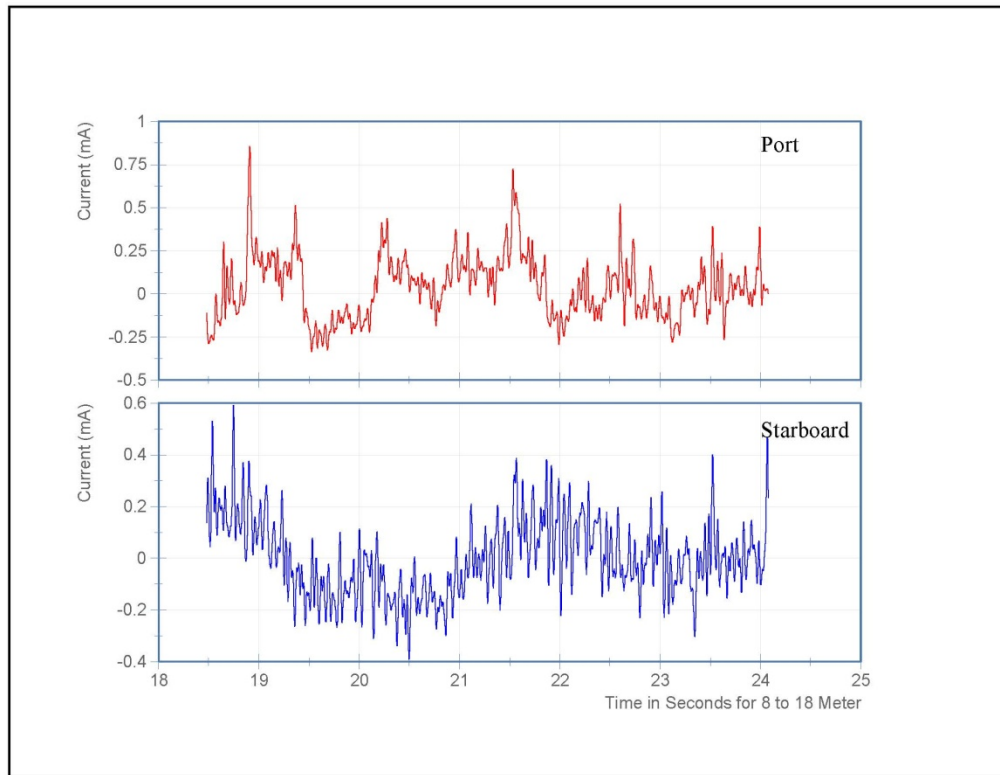
102 mm-thick ice field, carriage speed of 1.8 ms⁻¹
Speed and position plot vs. time



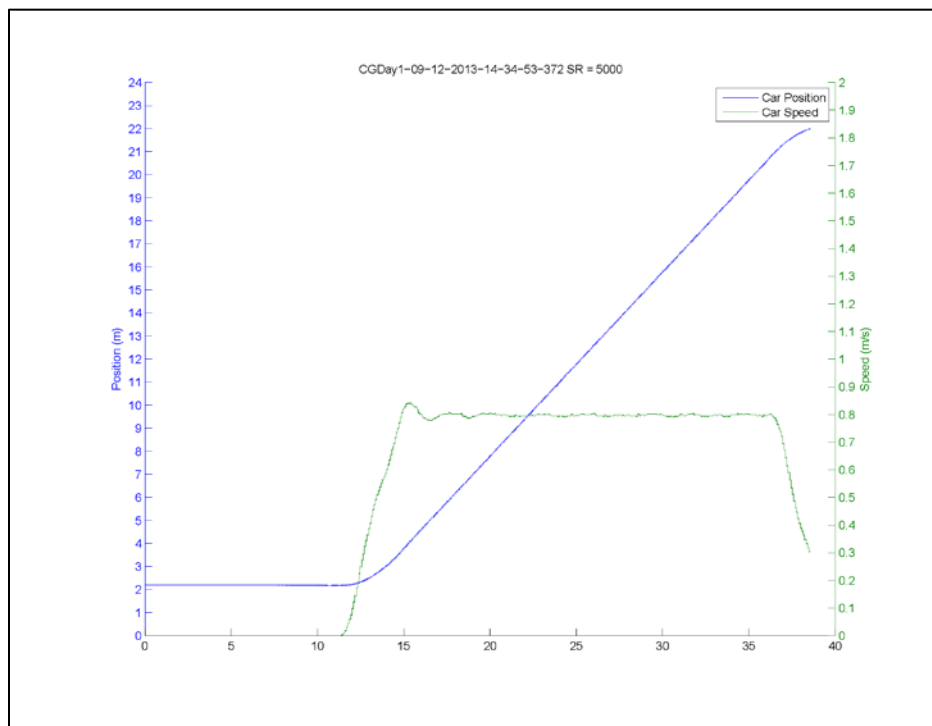
102 mm-thick ice field, carriage speed of 1.8 ms⁻¹
Current vs. time



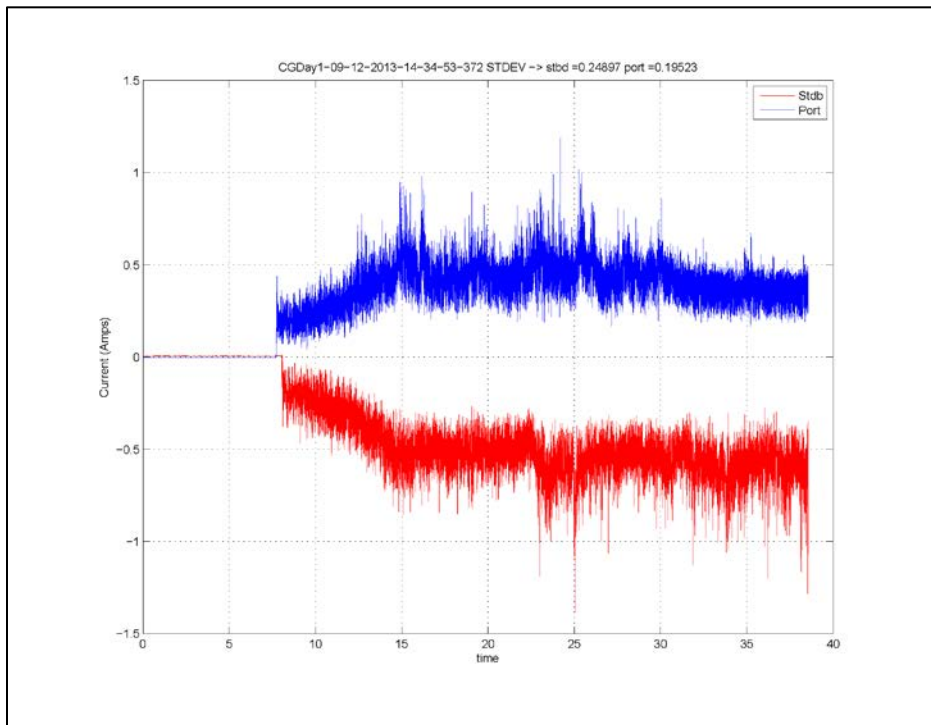
102 mm-thick ice field, carriage speed of 1.8 ms⁻¹
Current (Grams smoothing) vs. time (from 8 m to 18 m during constant carriage velocity)



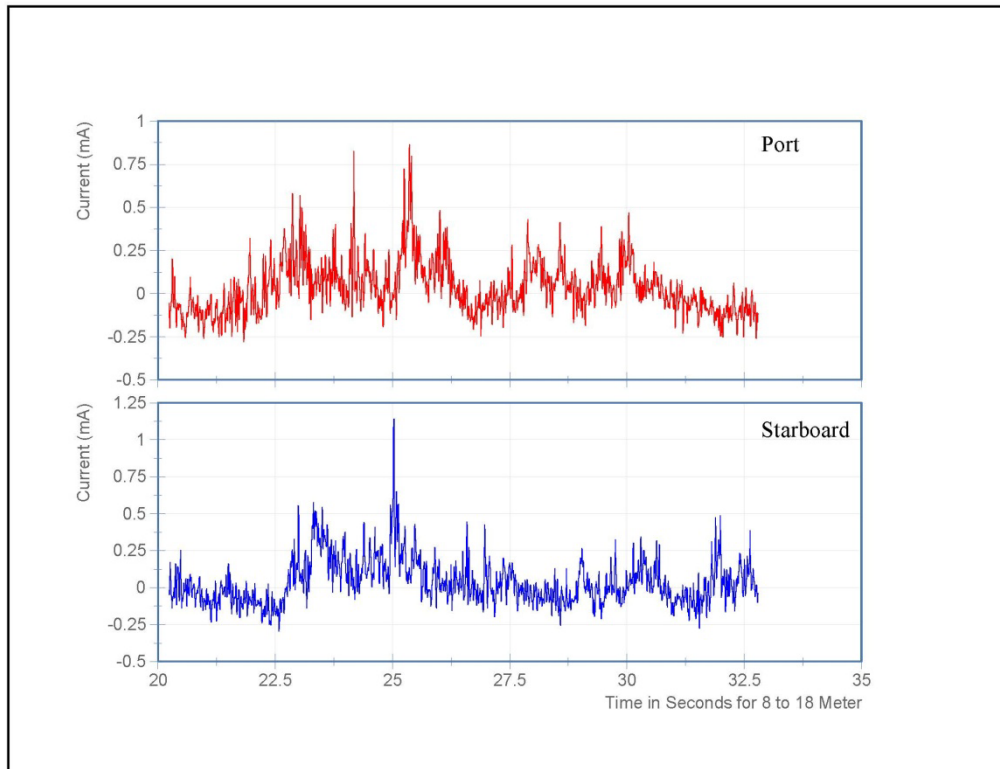
127 mm-thick ice field, carriage speed of 0.8 ms⁻¹
Speed and position plot vs. time



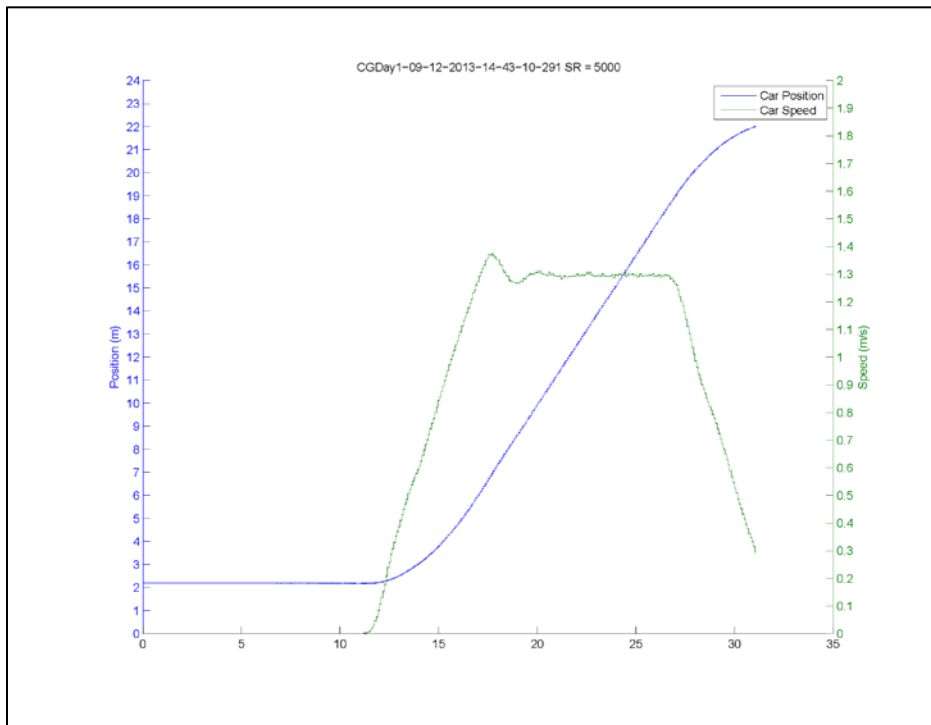
127 mm-thick ice field, carriage speed of 0.8 ms⁻¹
Current vs. time



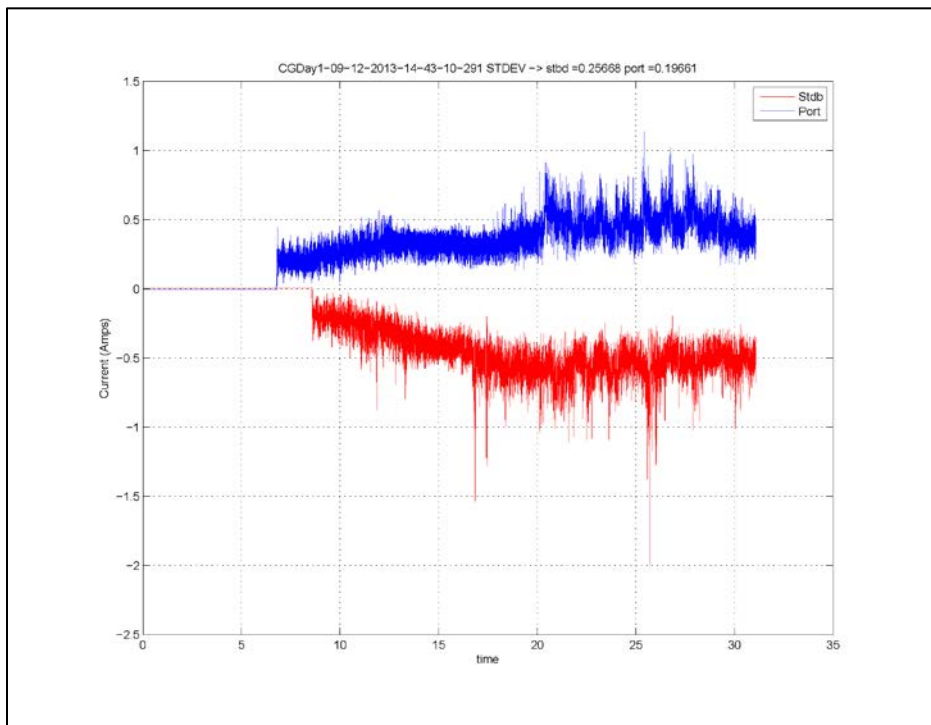
127 mm-thick ice field, carriage speed of 0.8 ms⁻¹
Current (Grams smoothing) vs. time (from 8 m to 18 m during constant carriage velocity)



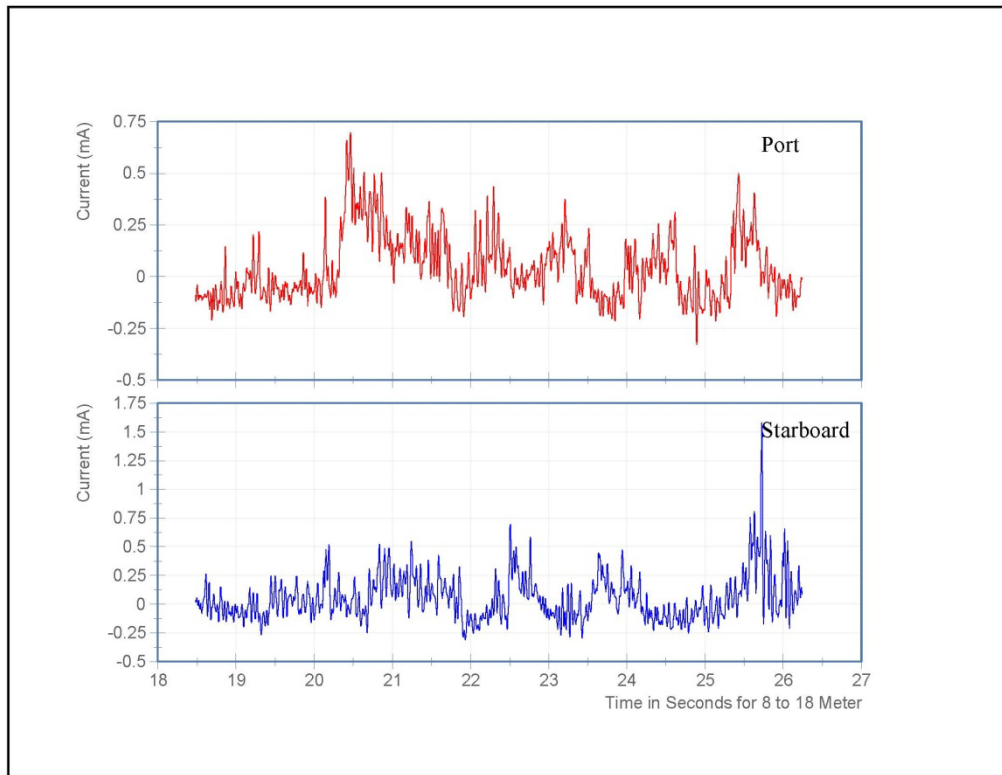
127 mm-thick ice field, carriage speed of 1.3 ms⁻¹
Speed and position plot vs. time



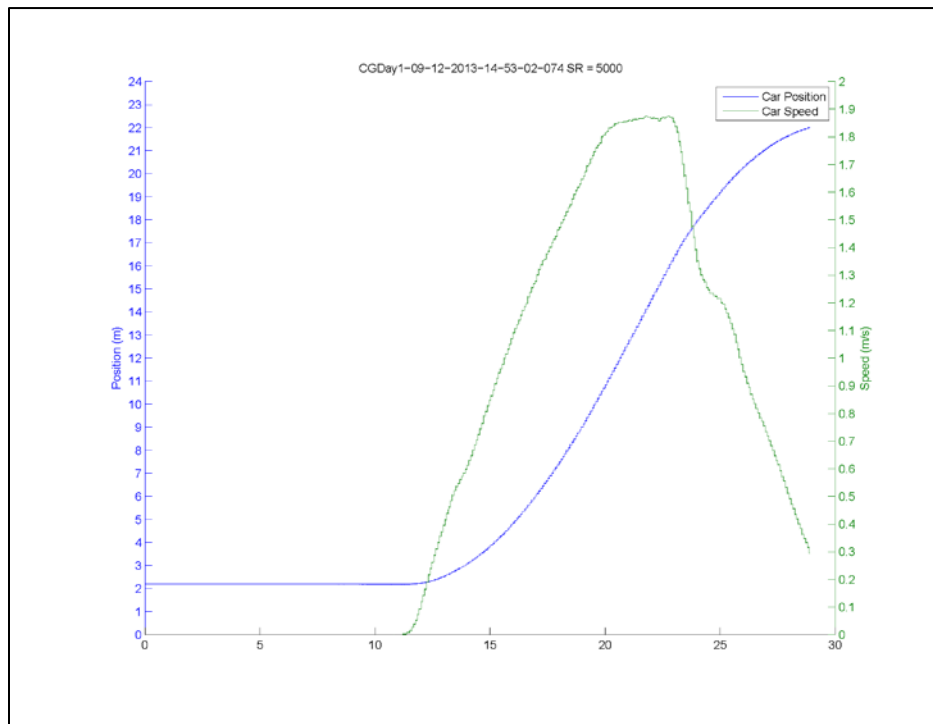
127 mm-thick ice field, carriage speed of 1.3 ms⁻¹
Current vs. time



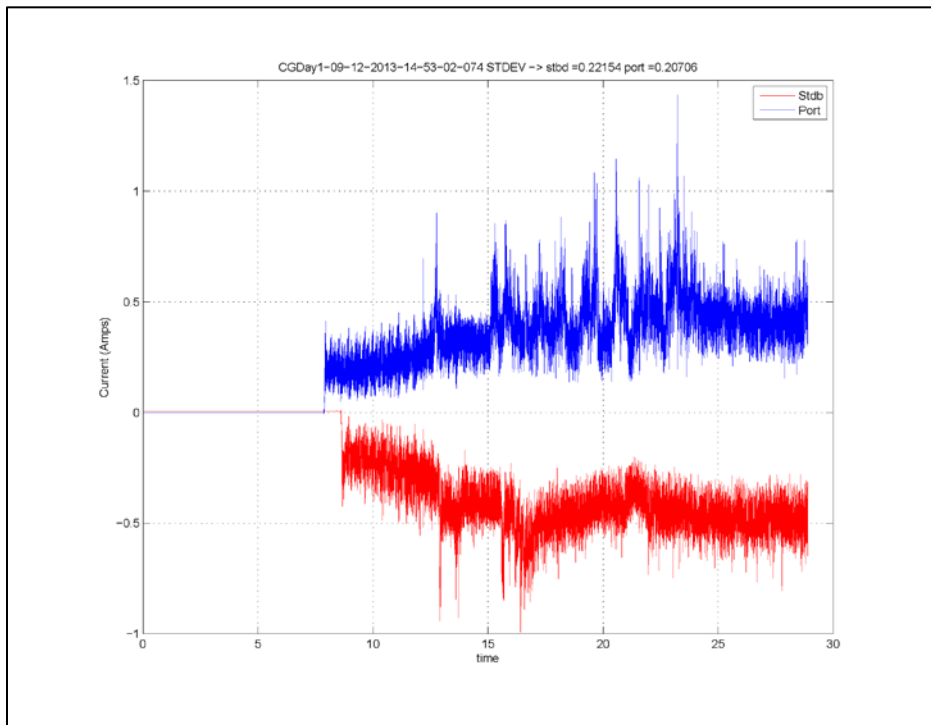
127 mm-thick ice field, carriage speed of 1.3 ms⁻¹
Current (Grams smoothing) vs. time (from 8 m to 18 m during constant carriage velocity)



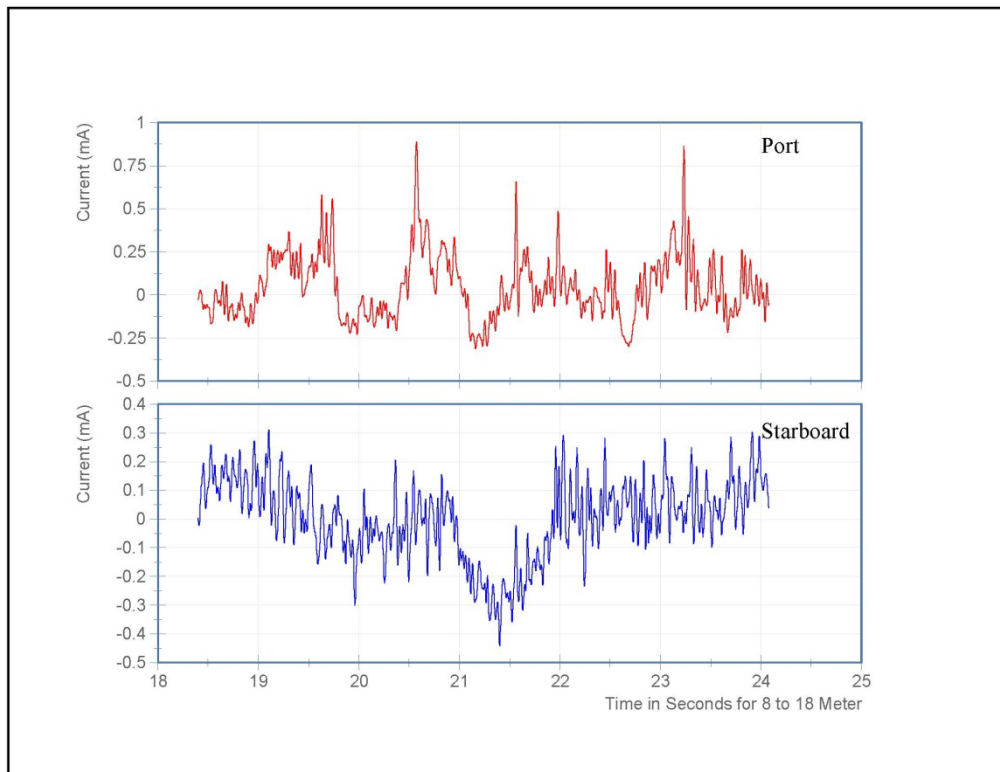
127 mm-thick ice field, carriage speed of 1.8 ms⁻¹
Speed and position plot vs. time



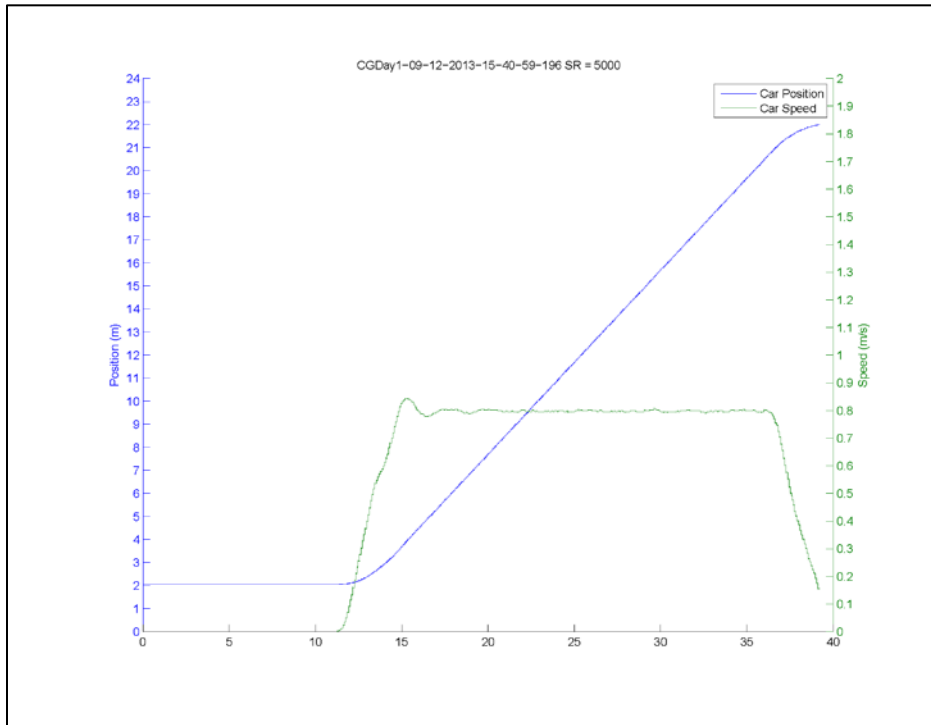
127 mm-thick ice field, carriage speed of 1.8 ms⁻¹
Current vs. time



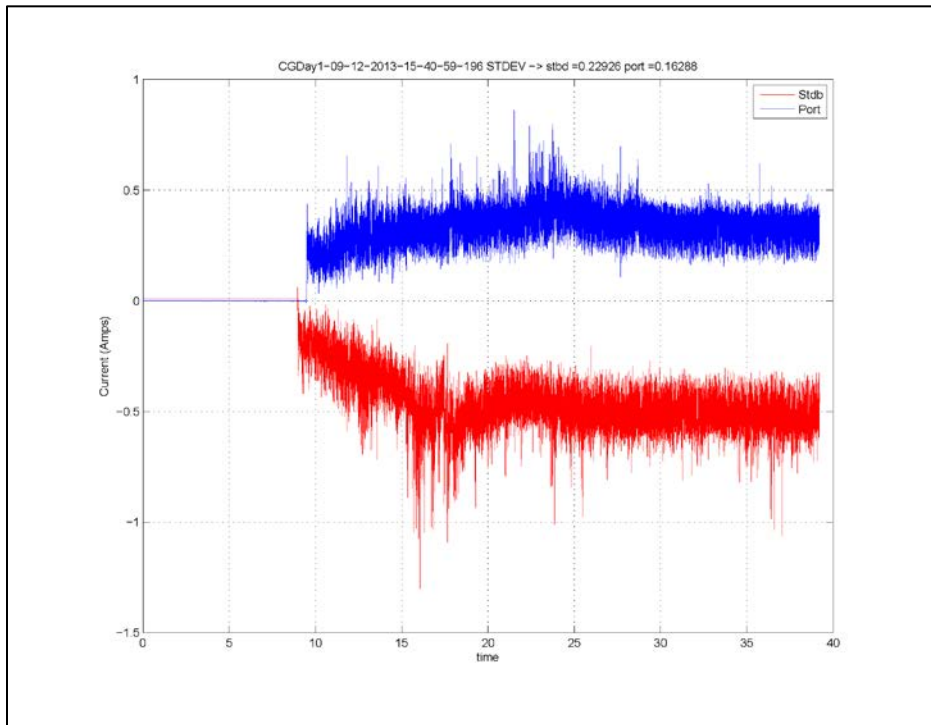
127 mm-thick ice field, carriage speed of 1.8 ms⁻¹
Current (Grams smoothing) vs. time (from 8 m to 18 m during constant carriage velocity)



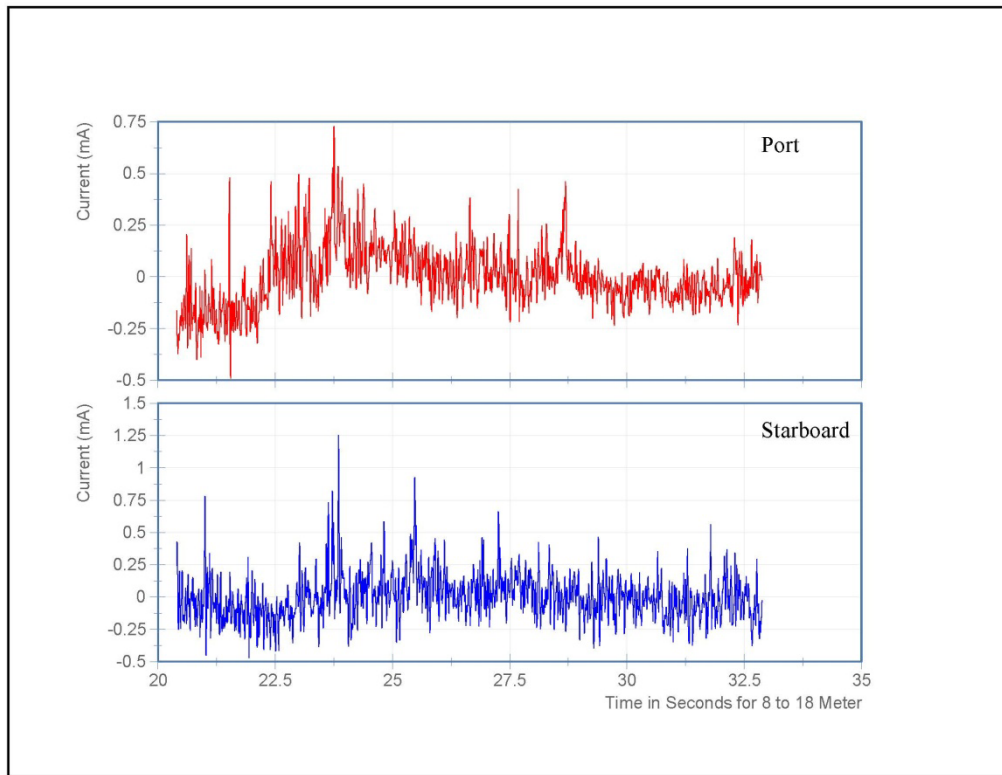
152 mm-thick ice field, carriage speed of 0.8 ms⁻¹
Speed and position plot vs. time



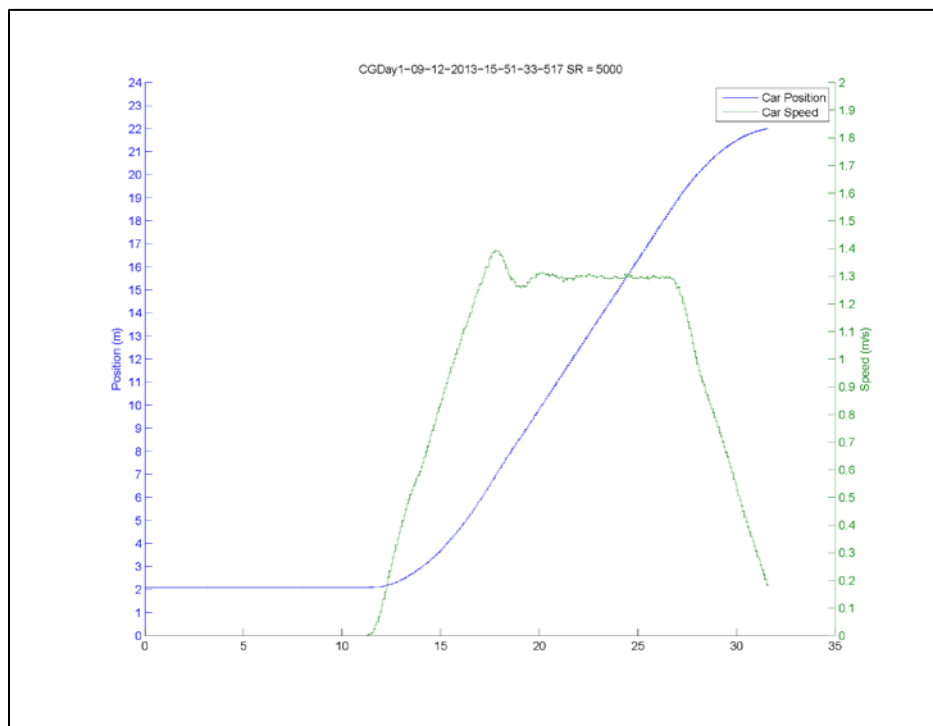
152 mm-thick ice field, carriage speed of 0.8 ms⁻¹
Current vs. time



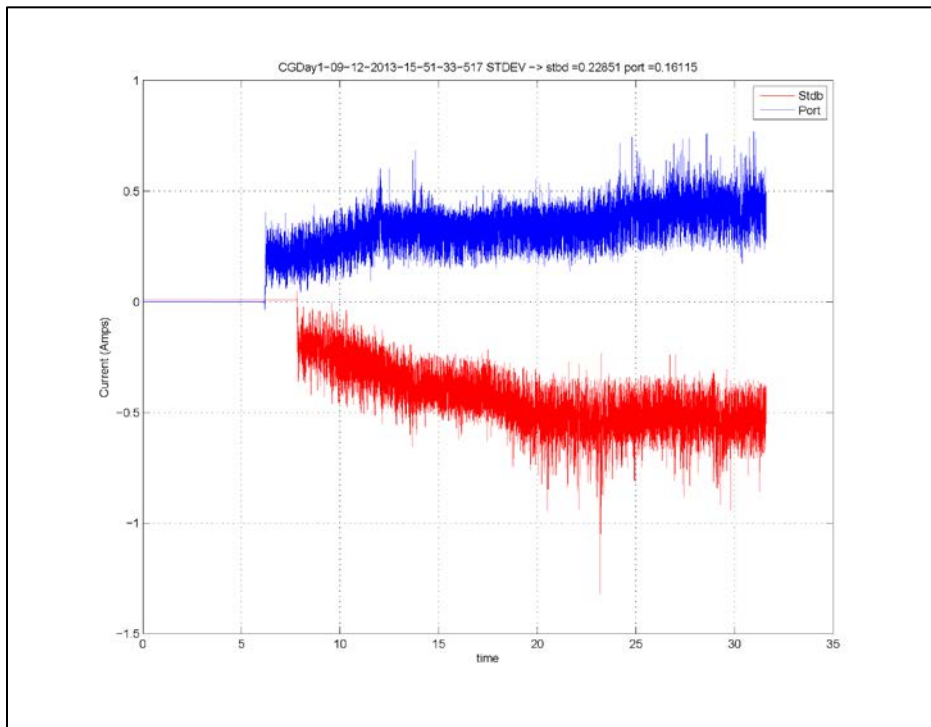
152 mm-thick ice field, carriage speed of 0.8 ms⁻¹
Current (Grams smoothing) vs. time (from 8 m to 18 m during constant carriage velocity)



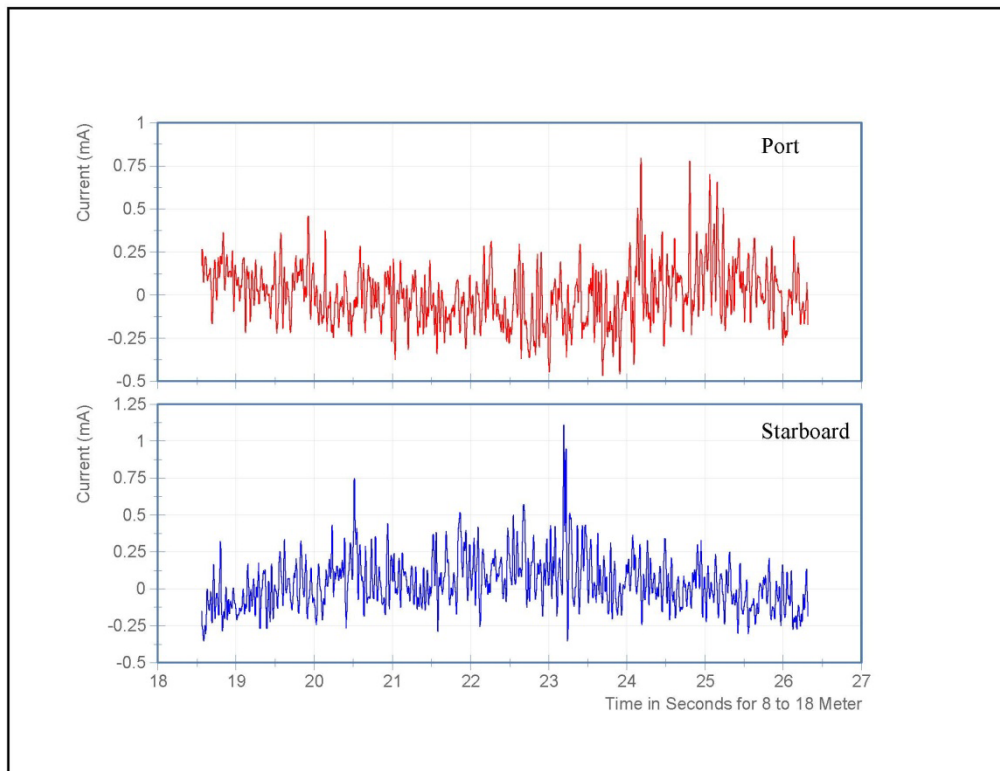
152 mm-thick ice field, carriage speed of 1.3 ms⁻¹
Speed and position plot vs. time



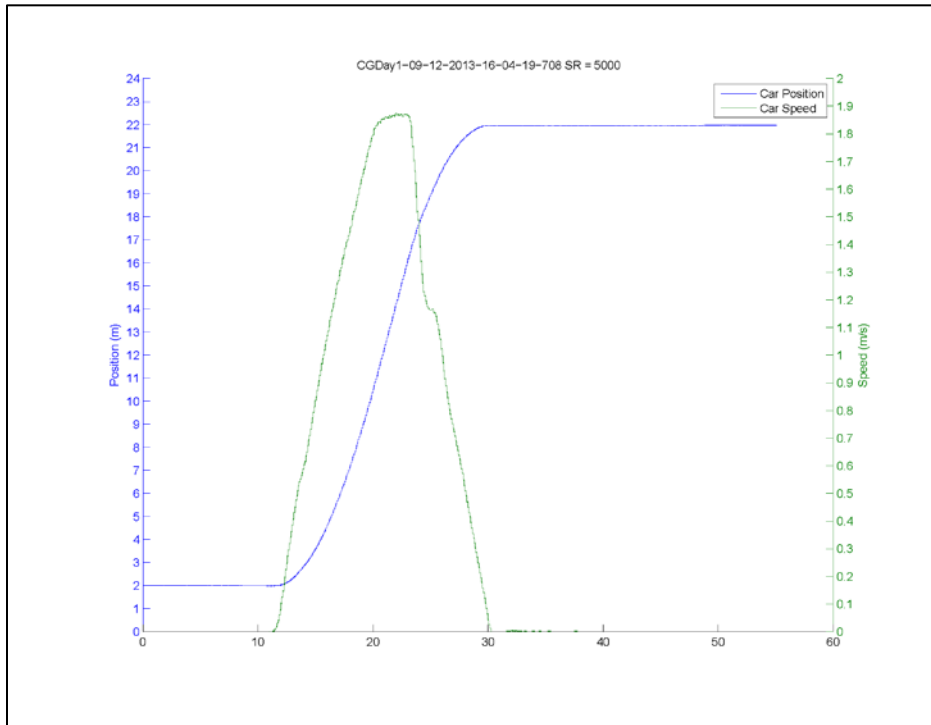
152 mm-thick ice field, carriage speed of 1.3 ms⁻¹
Current vs. time



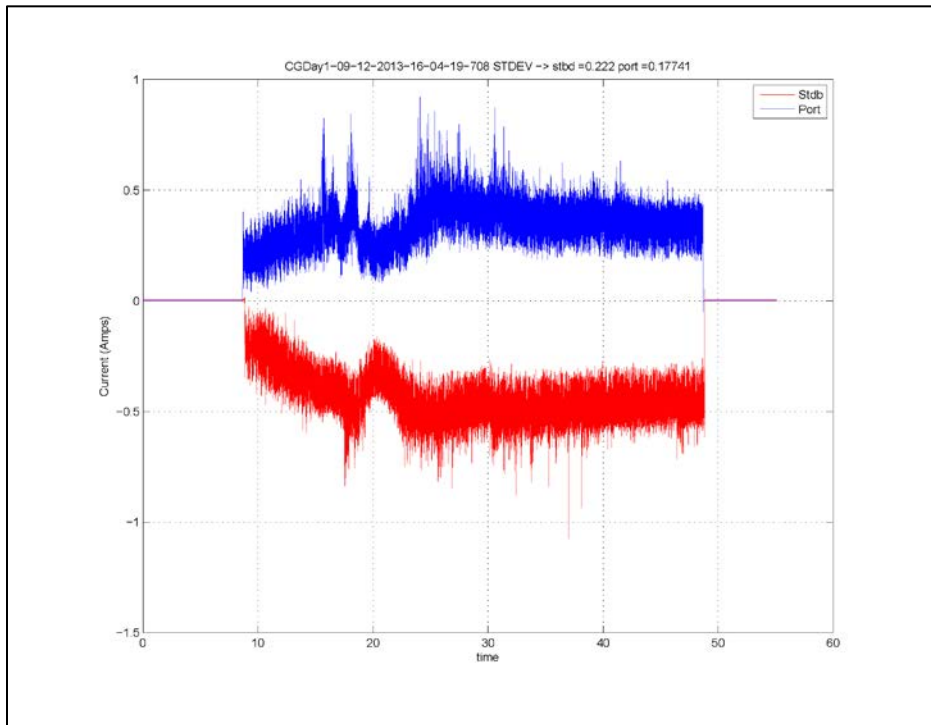
152 mm-thick ice field, carriage speed of 1.3 ms⁻¹
Current (Grams smoothing) vs. time (from 8 m to 18 m during constant carriage velocity)



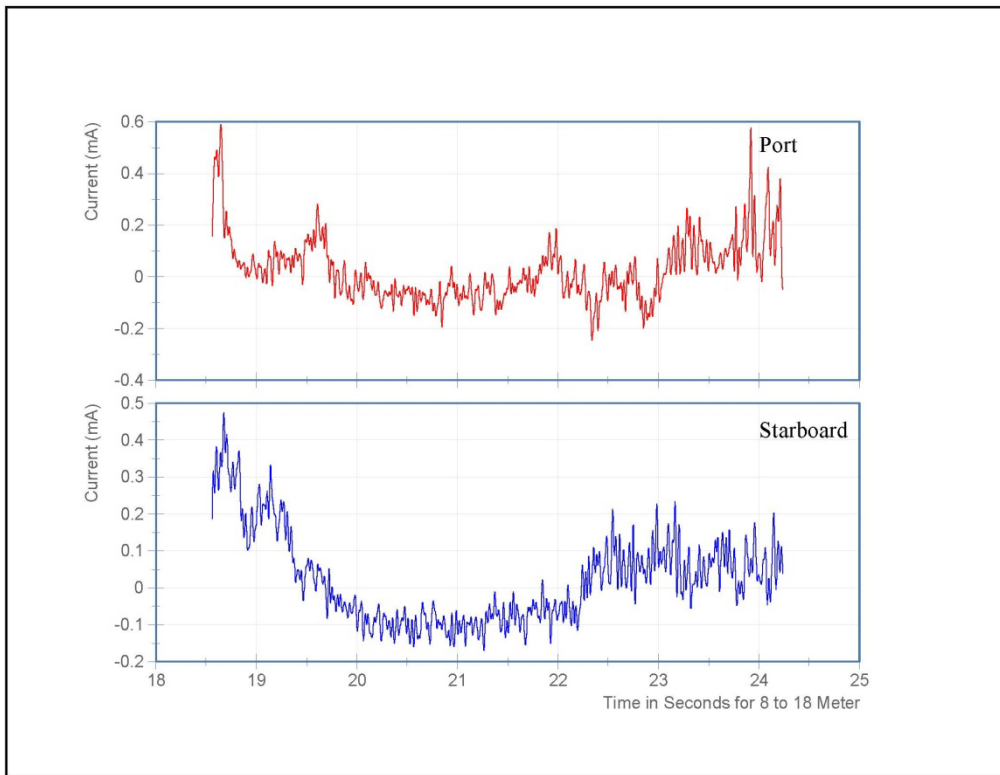
152 mm-thick ice field, carriage speed of 1.8 ms⁻¹
Speed and position plot vs. time



152 mm-thick ice field, carriage speed of 1.8 ms⁻¹
Current vs. time



152 mm-thick ice field, carriage speed of 1.8 ms⁻¹
Current (Grams smoothing) vs. time (from 8 m to 18 m during constant carriage velocity)



REPORT DOCUMENTATION PAGE

Form Approved
OMB No. 0704-0188

Public reporting burden for this collection of information is estimated to average 1 hour per response, including the time for reviewing instructions, searching existing data sources, gathering and maintaining the data needed, and completing and reviewing this collection of information. Send comments regarding this burden estimate or any other aspect of this collection of information, including suggestions for reducing this burden to Department of Defense, Washington Headquarters Services, Directorate for Information Operations and Reports (0704-0188), 1215 Jefferson Davis Highway, Suite 1204, Arlington, VA 22202-4302. Respondents should be aware that notwithstanding any other provision of law, no person shall be subject to any penalty for failing to comply with a collection of information if it does not display a currently valid OMB control number. **PLEASE DO NOT RETURN YOUR FORM TO THE ABOVE ADDRESS.**

1. REPORT DATE (DD-MM-YYYY) February 2014		2. REPORT TYPE TR Final		3. DATES COVERED (From - To)	
4. TITLE AND SUBTITLE Interaction between Brash Ice and Boat Propulsion Systems				5a. CONTRACT NUMBER	
				5b. GRANT NUMBER	
				5c. PROGRAM ELEMENT NUMBER	
6. AUTHOR(S) Leonard J. Zabilansky, Devinder Singh Sodhi, Jesse M. Stanley, Zoe R. Courville, Kevin L. Haskins, Jason M. Story				5d. PROJECT NUMBER 6204, Arctic Craft Project	
				5e. TASK NUMBER	
				5f. WORK UNIT NUMBER	
7. PERFORMING ORGANIZATION NAME(S) AND ADDRESS(ES) Cold Regions Research and Engineering Laboratory US Army Engineer Research and Development Center 72 Lyme Road Hanover, NH 03755				8. PERFORMING ORGANIZATION REPORT NUMBER ERDC TR-14-1	
9. SPONSORING / MONITORING AGENCY NAME(S) AND ADDRESS(ES) US Coast Guard Research and Development Center New London, CT 06320				10. SPONSOR/MONITOR'S ACRONYM(S)	
				11. SPONSOR/MONITOR'S REPORT NUMBER(S)	
12. DISTRIBUTION / AVAILABILITY STATEMENT Approved for public release; distribution is unlimited.					
13. SUPPLEMENTARY NOTES					
14. ABSTRACT Increased interest and ship traffic in ice-covered Arctic waters necessitates the determination of the range of conditions in which current, small non-ice-hardened vessels can operate and the best operating procedures in ice-covered conditions. A series of tests in varying brash ice thickness conditions were conducted at a range of speeds in the CRREL test basin using a model craft with shrouded and open propellers as well as an intake pumping propulsion system. Results from the testing indicate that boats operating in brash ice fields should operate at slow speeds (5 knots) to prevent increased strain on the outboard motors and possible damage to the propulsion system. Waterjet impellers appear to have greater protection from brash ice than an outboard propulsion system. It was thought that the shrouds would protect the propellers from ice impacts, which they may have done, but a secondary effect was that the brash ice caught inside the shroud area could not be forced away by the propellers as could be done in the open-propeller tests. This could mean that shrouds may still offer protection to the propellers but in a different configuration than the one tested.					
15. SUBJECT TERMS Arctic Brash ice			Propeller Propulsion Waterjet		
16. SECURITY CLASSIFICATION OF:			17. LIMITATION OF ABSTRACT	18. NUMBER OF PAGES	19a. NAME OF RESPONSIBLE PERSON Kevin L. Haskins
a. REPORT Unclassified	b. ABSTRACT Unclassified	c. THIS PAGE Unclassified			None